NTNU – Trondheim
Norwegian University of
Science and Technology

Catalytic Hydrodeoxygenation of Bio-oils with Supported MoP-Catalysts

Sindre Asphaug

Chemical Engineering and Biotechnology
Submission date: June 2013
Supervisor: Edd Anders Blekkan, IKP
Co-supervisor: Rune Lødeng, IKP
Sara Boullosa Eiras, IKP

Norwegian University of Science and Technology
Department of Chemical Engineering

NTNU
Det skapende universitet

Catalytic Hydrodeoxygenation of Bio-oils with Supported MoP-Catalysts

Sindre Asphaug

Chemical Engineering
Handed in: June 2013
Main supervisor: Professor Edd Anders Blekkan

Faculty for Engineering Science and Technology
Department of Chemical Engineering
Norwegian University of Science and Technology (NTNU)

Preface

This thesis was part of the course TKP4900 during 20 weeks in the spring 2013. The work was carried out at the Department of Chemical Engineering, at the Norwegian University of Science and Technology (NTNU). This study is part of a collaborative research project between NTNU and SINTEF on catalytic hydrodexygenation of bio-oils. The project is funded by the Research Council of Norway.

I would like to give my sincere thanks to my supervisor Professor Edd A. Blekkan, and my co-supervisors Senior Researcher Rune Lødeng and Post Doc. Sara Boullosa Eiras for advice and guidance throughout the project. A special thanks to Sara for all help in the laboratory. I would also thank Karin Dragsten, Harry Brun and Julien Tolchard for all technical support.

I would like to thank my parents for proofreading my thesis, my friend John Erik for the front page photo and my friend Jin for all help with Latex. I would also thank my lunch and quiz friends for all the good lunch and coffee breaks during this semester. Finally I would like to thank all my friends in Trondheim and the student organization Høyskolens Chemikerforening for all the fantastic years I have had as a student at NTNU.

I declare that this in an independent work according to the exam regulations of the Norwegian University of Science and Technology

Trondheim, 07.06.2013

Sindre Asphaug

Sammendrag

Biomasse som energikilde har fått en økende interesse, grunnet økt etterspørsel for fornybare og CO_2-nøytrale energikilder. Biomasse som stammer fra rester av landbruksprodukter og energivekster, konkurrerer med matproduksjon, og det har derfor vært mye forskning på å utnytte energien fra biomasse som ikke er i konkurranse med matproduksjon, for eksempel skogrester og avfall fra byområder. Biomasse kan omdannes til bio-olje via pyrolyse i fravær av oksygen. Sammenlignet med petroleumsbasert olje, har pyrolyseolje dårlige kjemiske egenskaper, hovedsakelig på grunn av høyt vann- og oksygeninnhold. Det er dermed nødvendig med videre oppgradering av bio-olje før den kan brukes til energiproduksjon. I dette prosjektet blir oksygenet i bio-olje fjernet i en hydrogenbehandlingsmetode som kalles katalytisk hydrodeoksygenering (HDO).

Hovedformålet med denne oppgaven var å teste MoP-katalysatorene som ble framstilt i løpet av høsten 2012, i en HDO-reaksjon av fenol til benzen. Katalysatorene hadde et metallinnhold på 15 wt%, og bærerne som ble brukt var γ-Al_2O_3, SiO_2, TiO_2 og ZrO_2. Katalysatorene ble framstilt via impregnering, deretter kalsinering, redusering og passivering. Det ble framstilt nye prøver av de to katalysatorene som viste høyest aktivitet, MoP/Al_2O_3 og MoP/TiO_2. Disse ble karakterisert med N_2-adsorpsjon, kjemisorpsjon, TPR og XRD. Katalysatorene ble videre testet ved HDO-riggen ved ulike temperaturer, gjennomstrømningsmengde, trykk og H_2/olje-forhold.

Resultatene fra N_2-adsorpsjonsanalysene viste at overflatearealet til bærerne minket etter impregneringen og økte litt etter reduseringen. TPR-analysene bekreftet at MoO_3 reduseres til MoP i 3 trinn. Partikkelstørrelsen av MoP ble regnet ut fra resultatene av kjemisorpsjonsanalysen, og den lave partikkelstørrelsen ble bekreftet av XRD-analysene, hvor ingen refleksjonstopper som indikerte dannelse av MoP-partikler ble funnet.

Aktiviteten til katalysatorene økte i rekkefølgen: $MoP/SiO_2 < MoP/ZrO_2 < MoP/Al_2O_3 < MoP/TiO_2$. Dette var den motsatte rekkefølgen for mengde av metalldispersjon på overflaten. Aktiviteten til MoP/TiO_2 sank over tid, pga katalysatordeaktivering. Aktiviteten endret seg ikke betraktelig ved forskjellige trykk og H_2/olje-forhold. Den høye aktivitetsenergien som ble målt, indikerte at

overflatereaksjonen er det hastighetsbestemmende trinnet. Gjentakelsesforsøket av MoP/TiO_2 ga imidlertid betydelige forskjeller, som betyr at det finnes stor usikkerhet i resultatene. Små forskjeller i tørking- og røringshastighet under katalysatorframstillingen endret egenskapene til katalysatorene betraktelig. Utskifting av termoelement og oppvarmingselement kan også ha påvirket resultatene. Flere forsøk med katalysatorene er derfor nødvendig for å verifisere resultatene.

Abstract

Due to the increasing demand for renewable and CO_2-neutral energy sources, there has been a growing interest for biomass as an energy source. Biomass from agricultural residues and energy crops are food-competing, and there has therefore been much research in order to utilize the energy from non food-competing biomass feedstocks, such as forest residues and urban wastes. The biomass can be converted to bio-oils through a pyrolysis treatment in absence of oxygen. Pyrolysis bio-oils have, in comparison to petroleum-based fuels, poor chemical properties, due to high water and oxygen content. Further upgrading to remove water and oxygen is needed to improve the bio-oil properties. A hydrotreating reaction to remove oxygen from bio-oils, hydrodeoxygenation (HDO), is carried out in this thesis.

The goal of this thesis was to test the MoP catalysts which were made during autumn 2012, in a HDO reaction of phenol to benzene at a HDO rig. The catalysts were supported by γ-Al_2O_3, SiO_2, TiO_2 and ZrO_2, and they were prepared by impregnation, followed by calcination, reduction and passivation. New samples of the 2 catalysts which showed the highest activity, MoP/Al_2O_3 and MoP/TiO_2, were prepared. They were characterized with N_2-adsorption, chemisorption, TPR and XRD, and they were further tested at the HDO rig with varying temperature, flow rate, pressure and H_2/oil ratio.

The results from the N_2-adsorption showed that the surface area of the supports decreased during impregnation, and increased slightly during reduction. The TPR analyses confirmed the 3 stage reduction of MoO_3 to MoP. The low calculated particle size from the chemisorption was confirmed by the XRD analyses, where no peaks indicating formation of MoP was found.

The activity of the catalysts increased in the order: $MoP/SiO_2 < MoP/ZrO_2 < MoP/Al_2O_3 < MoP/TiO_2$, which was the opposite trend of the metal dispersion. The activity of the MoP/TiO_2 catalyst decreased over time due to catalyst deactivation, and the activity varied not significantly with different pressure and H_2/oil ratio. The high activation energy indicated that the rate determining step is the surface reaction. However, the varying results from the repeatability measurement of the MoP/TiO_2 catalyst showed that there are large uncertainties in the results. Small variations in the stirring and drying rate during catalyst preparation changed

the catalyst properties significantly. Replacement of the thermocouple and heating tape may also have influenced the results. More research is therefore needed to verify the results.

Contents

List of symbols

Latin letters

A	Surface area
A	Frequency factor in the Arrhenius equation
C	Constant in the BET-equation
D	Dispersion
d	Distance between two lattice planes in XRD
d	Particle diameter
d_v	Volume-weighted crystalline diameter
E_A	Activation energy
F	Number of surface atoms covered by one adsorbed molecule
f	Shape factor
K	Constant in the Scherrer equation
k	Rate constant
M_m	Molecular weight
m	Number of moles H_2 in HDO
N_A	Avogadro number
n	Order of reflection
n_i	Number of moles of i in the conversion and selectivity equation
P	Pressure
P_o	Saturation vapor pressure
P_R	Pressure of reactants in HDO equilibrium
P_P	Pressure of products in HDO equilibrium
q_1	Heat of adsorption in the first monolayer
q_L	Heat of condensation
R	Gas constant
r	Experimental reaction rate
S_m	Specific surface area
S_i	Selectivity of i
T	Temperature
t/day	Metric tons per day
V	Volume
V_m	Volume adsorbed at monolayer coverage in the BET-equation
V_m	Volume of 1 mole of ideal gas at 0^oC
V_{sp}	Specific volume
v_{ads}	Adsorption of gas by selective chemisorption
X_i	Mole fraction
x_A	Conversion of A
x_m	Weight fraction of metal

Greek letters

α	Conversion of hydrogenated products
β	Peak width in the Scherrer equation
θ	Angle between incoming X-rays and the normal to the reflecting lattice plane
λ	Wavelength of X-rays
ρ	Density
σ_M	Atomic cross-section area

List of abbrevations

AL MAS NMR	Aluminium-27 Magic Angle Spinning Nuclear Magnetic Resonance
BET	Brunauer, Emmet and Teller
BJH	Barret-Joyer-Halenda
CCP	Cubic Closed Packed
FCC	Fluid Catalytic Cracking
FID	Flame-Ionization Detector
HDM	Hydrodemetallization
HDN	Hydrodenitrogenation
HDO	Hydrodeoxygenation
HDS	Hydrodesulfurization
HYD	Hydrogenation
IEA	International Energy Agency
IPCC	Intergovernmental Panel on Climate Change
IUPAC	International Union of Pure and Applied Chemistry
Mbbl/d	Million barrels per day
MS	Mass Spectroscopy
OPEC	Organization of the Petroleum Exporting Countries
OECD	Organization for Economic Co-operation and Development
STP	Standard Temperature and Pressure
TCD	Thermal Conductivity Detector
TPR	Temperature-programmed Reduction
TOF	Turnover Frequency
WC	Tungsten-carbide structure
WHSV	Weight Hourly Space Velocity
XRD	X-Ray Diffraction

1 Introduction

The world's energy demand has risen during the 20th century, mainly due to increased transportation demands.[1] This demand is projected to grow, particularly in Non-OECD countries, such as China and India. Due to this increased demand, the International Energy Agency (IEA) has projected that the overall crude oil demand will grow from 85 million barrels per day (Mbbl/d) in 2008 to 105 Mbbl/d in 2030.[2] Non-OPEC countries are now producing 60% of the total worldwide production, but the number and size of new discoveries in these countries are small. Two-thirds of the estimated oil reserves are located in the Middle East. However, the production capacity is not high enough to meet the growing demand.[3] Many of these countries suffer from civil unrest, which causes production uncertainty.

Today, the most used energy sources are liquid fuel, coal and natural gas,[4] and these constitute 80% of the world's energy production.[5] These fossil fuels lead to large CO_2 emissions in the atmosphere, and the UN's Intergovernmental Panel on Climate Change (IPCC) has concluded in several reports that man-made CO_2 and other green house gas emissions are the main reason for global warming.

These environmental reasons and a growing demand for new energy resources have led to an increased interest for biomass as an energy source, mainly because it is an inexpensive, renewable and a rich source of carbon.[6] The increase in the crude oil price in the last decade has also motivated the research for new energy sources, and the demand for biofuels is projected by the IEA to increase from 0.8 Mbbl/d in 2008 to 2.7 Mbbl/d in 2030.[2]

Biomass has a low energy density compared to fossil fuels because of high oxygen and water content and low carbon density.[1] There are several technologies available to increase the energy and reduce transportation costs, as shown in Figure 1.1. Gasification produces syngas (CO and H_2) which can be converted to alkanes in Fischer-Tropsch reactions. Fast pyrolysis is a method to make bio-oils, where biomass is heated to $450 - 550^oC$ in absence of oxygen and with a short contact time $(1 - 2s)$. Liquefaction is a method similar to pyrolysis, but occurs at higher pressure and lower temperatures $(250 - 325^oC)$.[6,7] The product is a mobile liquid which can be upgraded to liquid fuels.

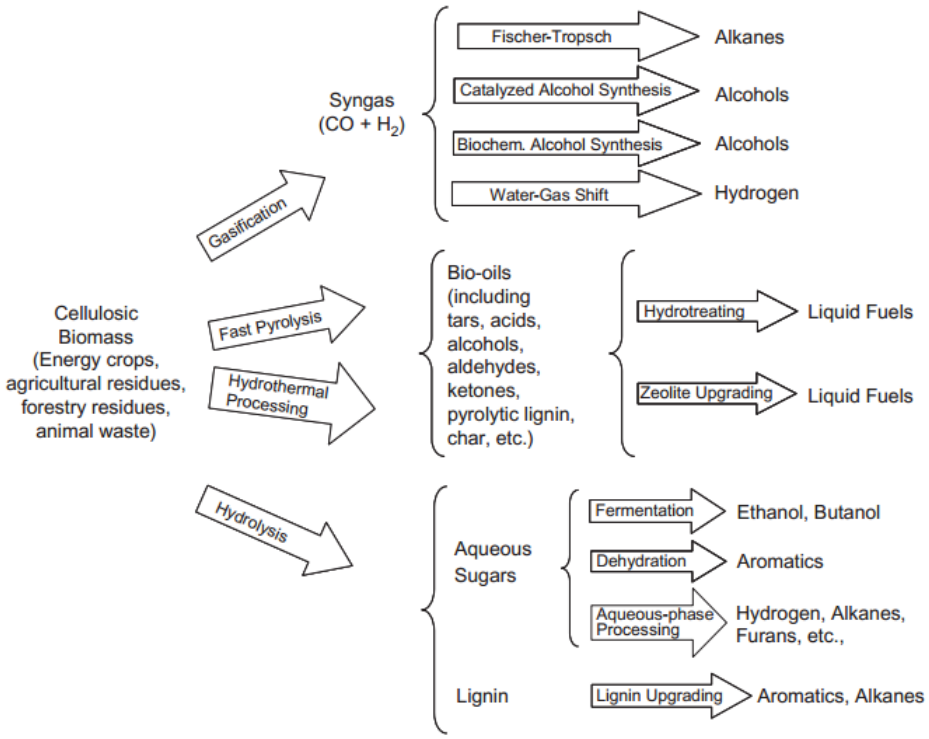

Figure 1.1: *Different pathways for cellulosic biomass to chemicals and liquid fuels through the upgrading processes gasification, fast pyrolysis, hydrothermal processing and hydrolysis, from Crocker (2010)* [1]

Bio-oils or pyrolysis oils have smaller sulfur and nitrogen content than crude oil, but a significantly larger amount of oxygen. The high oxygen value is very undesirable because of its properties, such as high viscosity, nonvolatility, corrosiveness, immiscibility with fossil fuels, thermal instability and polymerization under exposure to air.[1] It is therefore important to remove oxygen in bio-oil upgrading.

During upgrading of bio-oils, hydrodeoxygenation (HDO) is one method of removing oxygen. Other methods to remove oxygen are cracking, zeolite upgrading and forming of emulsion with diesel fuel.[8] HDO is a hydrotreating process, but since crude oil, as already mentioned, has very low oxygen content, HDO is not an important process in a crude oil refinery. Other hydrotreating processes in a refinery are hydrodesulfurization (HDS), hydrodenitrogenation (HDN) and hydrodemetallization (HDM).[9] The reason why these hetero-atoms (S, N, O) are removed, is to protect

the downstream catalysts, stringent sulfur content regulations, avoid corrosion and to ensure environmental protection. Hydrotreating reactions use hydrogen gas in exothermic reactions to remove hetero-atoms as H_2S, NH_3 and H_2O in a fixed bed reactor at $350 - 430^oC$.[9] For heavier feedstock, a trickle bed reactor is needed.

Hydrotreating uses a sulfided CoMo or NiMo catalyst with γ-Al_2O_3 as support. These catalysts have also been tested for HDO of bio-oils.[1] However, for sulfur-free feedstocks such as bio-oils, the sulfided catalysts are unstable, and the feed needs to be added sulfur to compensate for the sulfur loss. Addition of sulfur is undesired because the product can be contaminated by sulfur-containing species.[1] There has therefore been research of using noble metals and other sulfur-free metals as HDO catalysts.

Oyama et al (2001) have tested molybdenum phosphide (MoP) catalysts on γ-Al_2O_3 in hydrotreating processes and found high activities in HDN of quinoline and HDS of dibenzothiophene.[10] Phillips et al (2001) have used silica-supported MoP/SiO_2 as a catalyst in HDS, and found higher activity for MoP/SiO_2 than for a sulfided Mo/SiO_2 catalyst.[11]

There has, however, been little research of the use of MoP-catalyst in HDO processes. In this project, MoP-catalysts on 4 different supports, γ-Al_2O_3, SiO_2, TiO_2 and ZrO_2, were tested on a HDO reaction of phenol to benzene. The catalysts on Al_2O_3 and TiO_2 supports showed the highest activity. New samples of these catalysts were prepared and characterized, and several analyses were made on these catalysts to determine the activation energy, deactivation and effect of H_2/oil ratio.

2 Theory and background

2.1 Biomass

2.1.1 Feedstocks

The main biofuels feedstocks are waste materials, forest products, energy and sugar crops and aquatic biomass.[6] The cheapest biofuel feedstocks are cellulosic biomass, however, the conversion technology of cellulosic biomass is expensive. Triglyceride-based biomass is expensive, but also cheap to convert into fuel.

Biomass is a rich carbon source and receives its carbon from the photosynthesis process, as shown in the following reaction.[1]

$$CO_2 + H_2O \xrightarrow{\text{Light}} CH_2O + O_2$$

This process creates 2 types of metabolites; primary and secondary. The main products are primary metabolites, and these are composed of different types of polymers, for example cellulose, hemicellulose, starch and lignin.[12] These primary metabolites can be converted to biofuels. Other products from the photosynthesis process are secondary metabolites, for example resins, alkaloids, sterols and plant acids. These secondary metabolites can be used to produce high value chemicals such as pharmaceutical and cosmeceutical products.[12]

Naik et al (2010) divide biomass into 2 different generation biofuels,[12] and a comparison between the different generations biofuel and petroleum-based fuel is illustrated in Figure 2.1. First generation biofuels consist of biodiesel, bioethanol and biogas. These fuels have been produced at a large scale world wide and are considered "established technologies". Biodiesel is produced through transesterification of vegetable oils and can be used as a substitute of conventional diesel. Bioethanol is produced through fermentation of sugar and starch, and can be used as a substitute for gasoline and feedstock to ethyl tertiary butyl ether. There are, however, controversies about 1st generation biofuels because they are competing with food crops, and it is uncertain how much they decrease the production of CO_2.[12] The 2nd generation does not compete with food crops and is carbon neutral. It uses cheap feedstock such as abundant plant waste, and it can utilize all parts of the plant, such as seeds, barks and leaves. Lignocellulosic materials from the

cell walls are used as feedstock in pyrolysis and liquefaction to produce bio-oil and in gasification to produce Fischer-Tropsch oil. The production of 2nd generation biofuels is, however, not yet cost effective due to many technological barriers.

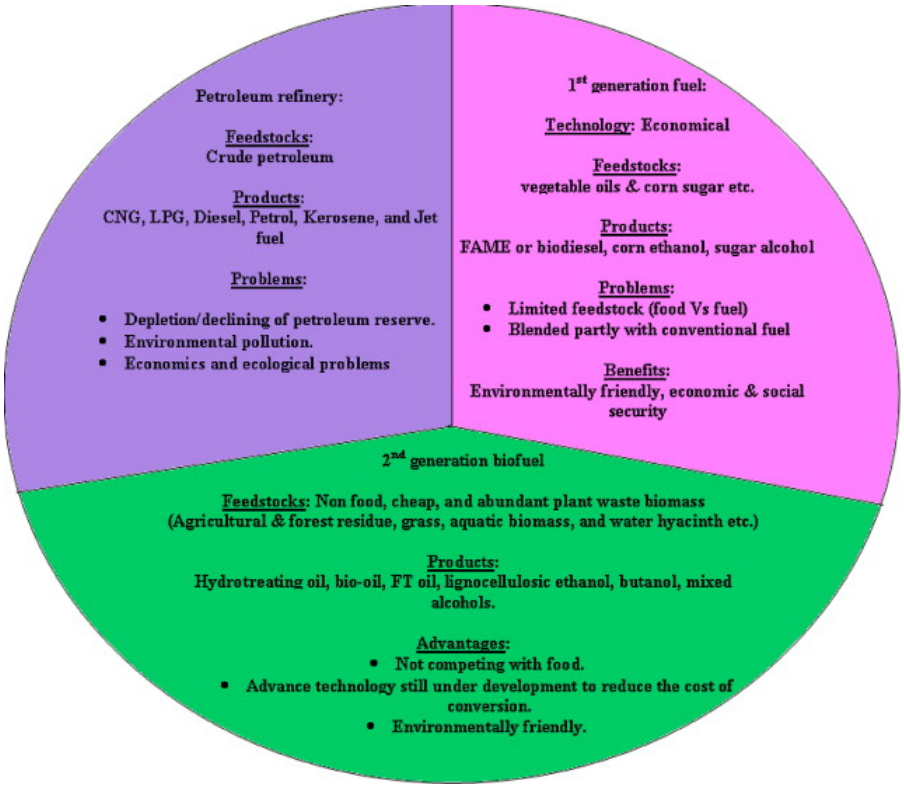

Figure 2.1: *Comparison between petroleum-based fuel and the different generations of biofuels, from Naik et al (2010)*[12]

2.1.2 Pyrolysis

As shown in Figure 1.1 in Section 1, there are several pathways to convert biomass into chemicals and liquid fuels. To produce bio-oils, pyrolysis or liquefaction processes are needed. The liquefaction process is a direct hydrothermal process of biomass, and it uses high pressure ($50 - 200$ atm), low temperatures ($250 - 450^oC$) and absence of O_2. H_2 and CO can be used as reducing gases. Several types of catalysts can be used, such as alkali, metals (zinc, copper, nickel) and heterogeneous catalysts (nickel and ruthenium).[8] The liquefaction products are water-insoluble bio-oils with lower oxygen content than pyrolysis oils. However, the high pressure

used in the process causes technical difficulties, and the capital cost of the liquefaction process is higher than for pyrolysis processes.[8]

The pyrolysis process is a thermal decomposition process of biomass, and it uses low pressure ($1-5$ atm), high temperature ($375-600^o$C) and absence of O_2.[8] There are 3 types of pyrolysis; fast, intermediate and slow pyrolysis. In fast pyrolysis, the temperature is carefully controlled to the desired temperature, and the vapor is rapidly cooled with a residence time less than 1 s. In intermediate pyrolysis, a low moderate temperature is reached and the vapor is cooled with a moderate residence time. Slow pyrolysis reaches a temperature at 400^oC and has a long vapor residence time up to 24 h[8]

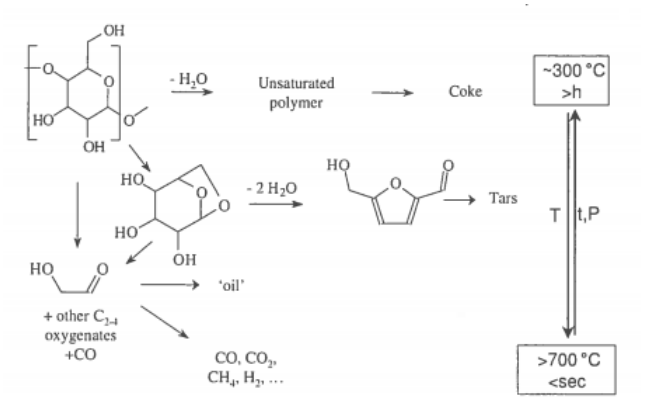

Figure 2.2: *Different reactions during pyrolysis from* 300^oC *to* 700^oC*, from Centi et al (2007)*[13]

Figure 2.2 shows some reactions that occur during pyrolysis. At around 300^oC, the carbohydrate polymers depolymerize and dehydrate into unsaturated species, which can later undergo oligomerization and elimination reactions to form unsaturated polymers and char.[13] At higher temperatures ($400-500^o$C), the depolymerization reactions can produce volatile species, such as glycol aldehydes, anhydro-sugars and furans. To avoid tar production, they need to be efficiently removed from the medium.[13] At 600^oC, the polysaccharides decompose due to C-C bond breaking. C_2-C_4 oxygenates, such as glycol aldehydes, acetic acid and hydroxyacetone are produced. These products can condensate into heavier oxygenates, oil and tars. At higher temperatures than 700^oC, the oxygenates are further decomposed to a mixed gas of CO, CO_2, CH_4 and H_2.[13]

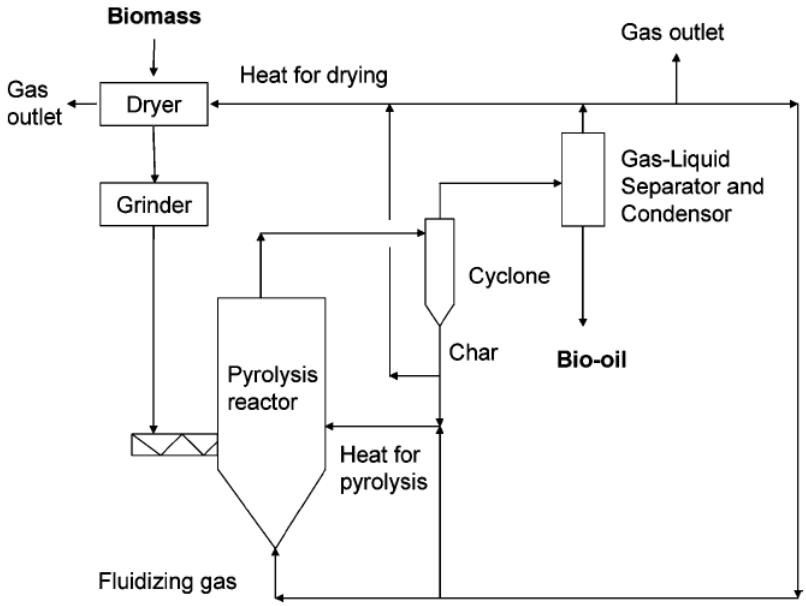

Figure 2.3: *Reactor system of a pyrolysis plant, from Huber et al (2006)*[8]

Today there are several fast pyrolysis plants operating on full scale, the largest being Ensyn Technologies (USA) which produces 50 t/day.[14] An example of a pyrolysis reactor system is given in Figure 2.3. The biomass must first be dried and ground to obtain the optimal heat transfer properties. The two most used reactor systems are bubbling and circulating fluidized bed. In addition, rotating plane reactor, vacuum pyrolyzer and auger reactor can also be used. After the reactor, a cyclone separates the solid char products, which can cause further downstream processing problems. The liquid product is separated from the gas and rapidly cooled to prevent cracking.[8] The liquid product from pyrolysis and liquefaction has a dark brown color and a distinctive smoky odor,[14] It is a mixture containing up to 400 different compounds, such as acids, esters, alcohols, aldehydes, sugars, furans, phenols, guaiacols and syringols.[6]

Normally, pyrolysis processes are non-catalytic. However, it is possible to use a circulating fluid bed with FCC catalysts such as USY-zeolite type and ZSM-5 additive, which is described by Lappas et al (2002).[15] The process is run at $400 - 500^oC$ and the liquid product is less corrosive and more stable than non-catalytic pyrolysis oil. On the other hand, the coke and gas formation (mostly CO and CO_2) is increased.[15]

2.2 Hydrotreating and dexoygenation of bio-oils

Table 2.1 shows the property differences between pyrolysis (wood-based) bio-oil and heavy fuel oil. Bio-oils contain more acids and water than heavy fuel oil, which causes lower energy density and corrosion problems. The high oxygen content in pyrolysis oil is caused by the oxygen content in cellulose, hemicellulose and lignin, and is present in bio-oils as phenols, naphthols, furans and ethers, see Figure 2.4. This can cause high viscosity, corrosiveness, nonvolatility and thermal instability.[1] The high water and oxygen content causes a lower heating value (15-19 MJ/kJ) compared to petroleum based oil (40 MJ/kJ).[16] Bio-oils can over time polymerize and condensate upon exposure to oxygen and UV, and this can cause transportation and storage problems.[6] Hydrodeoxygenation (HDO) is therefore needed to remove oxygen as H_2O from the oil. HDO has not received as much attention as HDN and HDS, as these processes are more important for hydrotreating of petroleum-based oils. There has, however, been an increase in the research of HDO in the last 25 years, due to the increasing interest for using biomass as an energy source.[7]

Table 2.1: *Properties of liquefaction oil, pyrolysis oil and hydrotreated bio-oil, from Huber et al (2006)*[8]

Property	**HP liquefaction**	**Flash pyrolysis**	**HDO bio-oil**
Carbon (wt%)	72.6	43.5	85.3-89.2
Hydrogen (wt%)	8.0	7.3	10.5-14.1
Oxygen (wt%)	16.3	49.2	0.0-0.7
Sulfur (wt%)	<45	29.0	0.005
H/C-ratio (dry)	1.21	1.23	1.40-1.97
Density (g/mL)	1.15	24.8	0.796-0.926
Moisture (wt%)	5.1	24.8	0.001-0.008
Higher heating value (MJ/kg)	35.7	22.6	42.3-45.3
Viscosity (cP)	15000 (61^{o}C)	59 (40^{o}C)	1.0-4-6 (23^{o}C)
Aromatic/aliphatic carbon	-	-	38/62-22/78
RON	-	-	77
Distillation range (wt%)			
IBP - 225^{o}C	8	44	97-36
225 - 350^{o}C	32	coked	0-41

After the HDO process, the products are oxygen free and high quality fuel, as shown in Table 2.1, and they are able to blend with petroleum-based fuel. It is more expensive to hydrotreat pyrolysis oil than liquefaction oil, as pyrolysis oil has higher oxygen content, even though liquefaction oil has higher content of acid, such as formic acid and acetic acid, and higher density due to lower water content.[17]

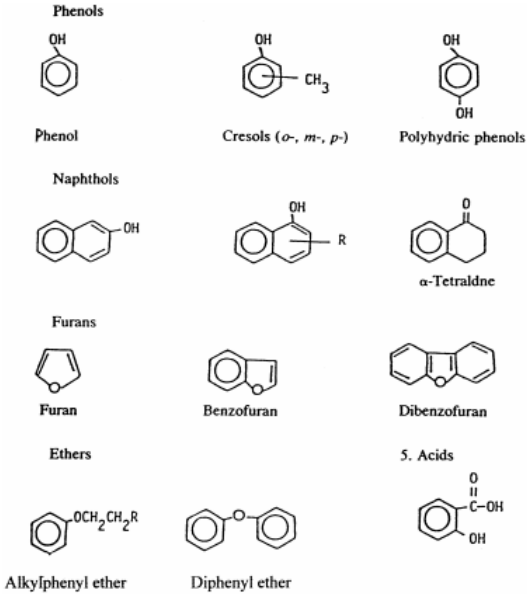

Figure 2.4: *Oxygen-containing compounds in pyrolysis oil, from Furimsky (2000)*[18]

According to Choudhary et al (2011), pyrolysis oil has a tendency for coke formation during mild hydrotreating conditions, because it contains highly reactive species such as guaiacol and alkoxyphenols.[17] The oxygen-containing compounds can also polymerize during hydrotreating. Choudhary et al (2011) therefore recommend a low-temperature stabilization step prior to the upgrading.[17] Elliot et al (1991) suggested a low-temperature step at 270^{o}C and 136 atm H_2 prior to the second higher-temperature step at 400^{o}C and 136 atm H_2.[19] 20-30% of the carbon was converted to gas-phase carbon. However, gum formation in the lines was considered a major uncertainty. Conti et al (1997) suggested non-isothermal conditions and used temperature of 140^{o}C at the inlet and 280^{o}C at the outlet, and received a yield of 72% with respect to dry bio-oil feed.[20]

2.2.1 Hydrotreating of phenols

In this project the hydrotreating of phenol is studied. During the HDO, H_2 reacts with oxygen and forms water and saturated C-C bonds,[6] as shown in Figure 2.5.[9] The reaction is exothermic and has a formation enthalpy of $-62\ kJ\ mol^{-1}$.

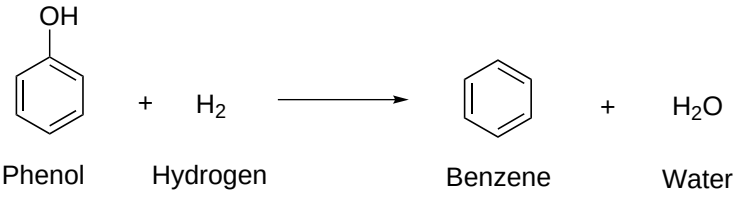

Figure 2.5: *The exothermic hydrodeoxygenation reaction of phenol to benzene, from Moulijn (2008)*[9]

Hydrotreating of phenol is a simple model used to study the reactivity of the bond between oxygen and aromatic carbon.[1] It is more difficult to break the oxygen-carbon bond in phenols than in alcohols and in aliphatic ethers, as the bond strength is 86 $kJ\ mol^{-1}$ greater.[18] Furimsky (2000) has estimated the equilibrium correlations in HDO, and it is given in Equation 2.1.[18]

$$\log K_p = \log\left(\frac{\alpha}{1-\alpha}\right) - m \log P \quad where \quad \frac{\alpha}{1-\alpha} = \frac{P_P}{P_R} \tag{2.1}$$

where P, P_P and P_R are the pressures of H_2, product and reactant respectively, α is the conversion to hydrogenated products and m is the number of moles of H_2.

In kinetic studies, both trickle bed and batch reactors have been used to find the reaction pathways for HDO of phenols.[18] Two main parallel routes were suggested in early studies. One route is a hydrogenolysis reaction of phenol to benzene, and another route is a combined hydrogenation-hydrogenolysis reaction via cyclohexanon and cyclohexene to cyclohexane. These routes are shown in Figure 2.6.

By using different catalysts and reaction conditions, the reaction routes can vary and cause different intermediate and end products. Senol et al (2007) used a plug-flow reactor for the gas phase and a batch reactor for the liquid phase.[21] They discovered that cyclohexene and cyclohexane were the main products with the use of sulfided NiMo, and benzene was the end product with the use of CoMo.[21] Cyclohexanone was detected as an intermediate, but not as an end product. Ryymin et al (2010) detected with a sulfided NiMo, small amounts of cyclohexyl cyclohexane, and this reaction pathway is also shown in Figure 2.6.[22]

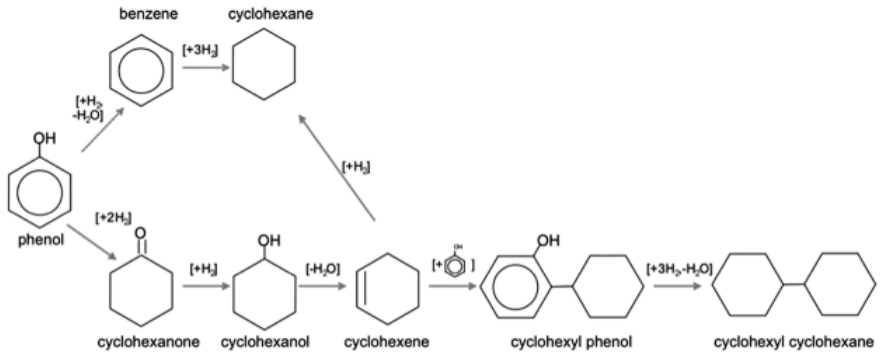

Figure 2.6: *Different reaction pathways for phenol to cyclohexane via a benzene and cyclohexene route, from Crocker (2010)*[1]

Wildschut et al (2010) used a Ru/C catalyst on a HDO reaction of phenol and discovered no benzene in the product. Instead, they proposed a reaction pathway via cyclohexanol to cyclohexane.[23]

Gevert et al (1987) used a batch reactor with a sulfided CoMo catalyst[24] and proposed a similar route for methyl substituted phenols, as seen in Figure 2.7.

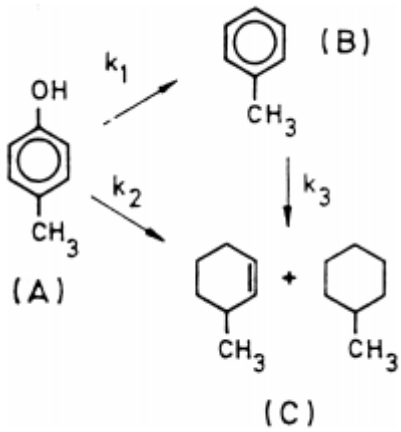

Figure 2.7: *Reaction pathways for methyl phenol to methyl cyclohexene and methyl cyclohexane via a toluene route, from Gevert et al (1987)*[24]

They derived the following equations for mole fractions of phenol (X_A), aromatics (X_B) and cyclohexane/cyclohexene (X_C) with 1st order rate constants.

$$X_B = \frac{k_1}{k_1 + k_2}(1 - x_A) \quad and \quad X_C = \frac{k_2}{k_1} X_B \tag{2.2}$$

In this project, no cyclohexanone, cyclohexanol or cyclohexyl phenol was detected in the product. A simplified reaction pathway from phenol to cyclohexane is therefore presented in the following figure.

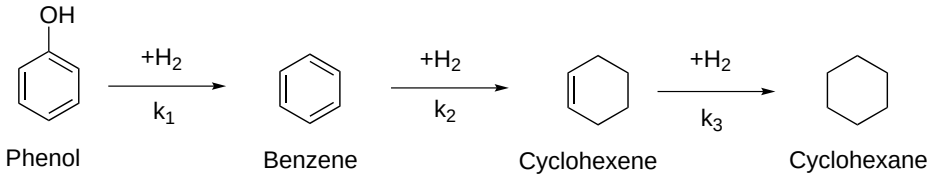

Figure 2.8: *Simplified reaction pathway from phenol to cyclohexane.*

A proposed reaction mechanism of phenol to benzene is given in Figure 2.9. The hydroxyl group makes a nucleophilic attack on the activated hydrogen atom. Benzene is formed as the hydrogen and oxygen atoms leave the phenol molecule as water.

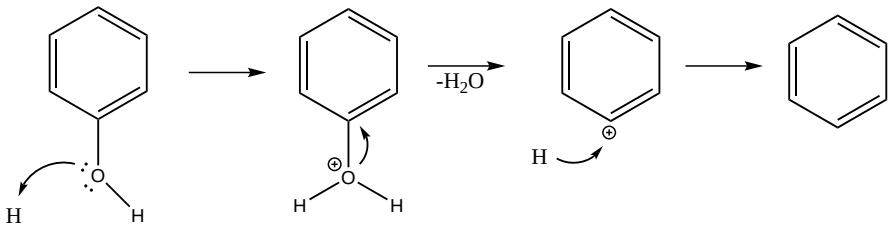

Figure 2.9: *Proposed reaction mechanism for the HDO reaction of phenol to benzene.*

2.3 Catalysts in this project

The catalysts used in this project are molybdenum phosphide (MoP) on different supports, such as γ-alumina (Al_2O_3), silica (SiO_2), titania (TiO_2) and zirconia (ZrO_2). As sulfided NiMo and CoMo catalysts are mainly used in industrial hydrotreatment of petroleum-based oils, these catalysts have also been widely studied in HDO of bio-oils. However, recent environmental regulations in many countries allow less sulfur in transportation fuels.[11] In the future, the heavier petroleum feedstocks with poor quality need to be processed, and there is a general consensus that sulfide-based catalysts will not be sufficient. There has therefore been research in alternative sulfur-free noble metal catalysts as HDO catalysts. Several molybdenum-based catalysts have been tested, and Mo_2C, Mo_2N and MoP have all shown higher activities in HDS and HDN reactions and HDO of guaiacol than sulfided molybdenum-based catalysts.[11,25]

Phosphide promoted catalysts have also been tested in hydroprocessing reactions. Oyama et al (2009) has reported that activity of different phosphide promoted catalysts in HDS of dibenzothiophene and HDN of quinoline increases in the order Fe_2P < CoP < MoP < WP < Ni_2P.[26] The high Ni_2P activity is also reported in HDO reactions by Whiffen et al (2012).[27] They reported that unsupported Ni_2P had 3.2 times higher mass based activity than MoP in a HDO reaction of 4-methylphenol. Other catalysts which have been tested are Pt, Rh, Pd, Ru, Fe-based and Ni-based catalysts.[28]

There has been much research in literature of HDS of dibenzothiophene and HDN of quinoline, due to the high content of these components in crude oil. It is, however, important to emphasize that these reactions are different hydrotreatment reactions than HDO of phenol, as the molecular structures are not similar. An effective catalyst for HDS of dibenzothiophene may not necessarily be an effective catalyst for HDO of phenol. Another HDS reaction which is more similar to HDO of phenol, is the HDS reaction of mercaptan. However, as mercaptan is not present to the same extent in crude oil as dibenzothiophene, there has been less research of HDS of mercaptan in literature.

2.3.1 Molybdenum phosphide

The MoP structure is according to Clark et al (2003) a tungsten-carbide (WC)-structure, with a lattice parameter $a_0 = 332\ pm$ and $c_0 = 319\ pm$.[29] A figure of a WC-structure type with MoP is given in Figure 2.10. 6 P-atoms trigonal-prismatically coordinate each Mo-atom in this WC-structure.[30] The bondings of P-atoms are ranging from P^{3+} (ionic) to P^0 (metallic or covalent).

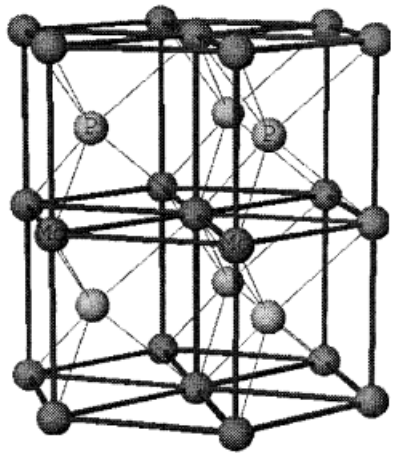

Figure 2.10: *Tungsten carbide (WC) crystall structure of MoP. Mo atoms are in lattice corners and P atoms are between the lattice, bulk lattice parameters* $a_o = 332\ pm$ *and* $c_o = 319\ pm$*, from Oyama et al (2001)*[10]

Several studies have been made on MoP catalysts in hydroprocessing reactions. Montesinos-Castellanos et al (2007) studied the effect of the P/Mo ratio in a HDS reaction of dibenzothiophene.[30] They discovered that the reactivity was highest for the ratios 1:1 and 1.1:1, as can be seen in Figure 2.11. They also tested the reactivity of MoS_2-γ-Al_2O_3, and discovered that MoP had a higher reactivity.

Oyama et al (2001) compared MoP catalyst on γ-Al_2O_3 to sulfided NiMo catalysts, and the results are shown in Table 2.2.[10] The study was made by HDN of quinoline and HDS of dibenzothiophene. Hydrogenation (HYD) refers to the conversion of quinoline to saturated N-containing hydrocarbons.

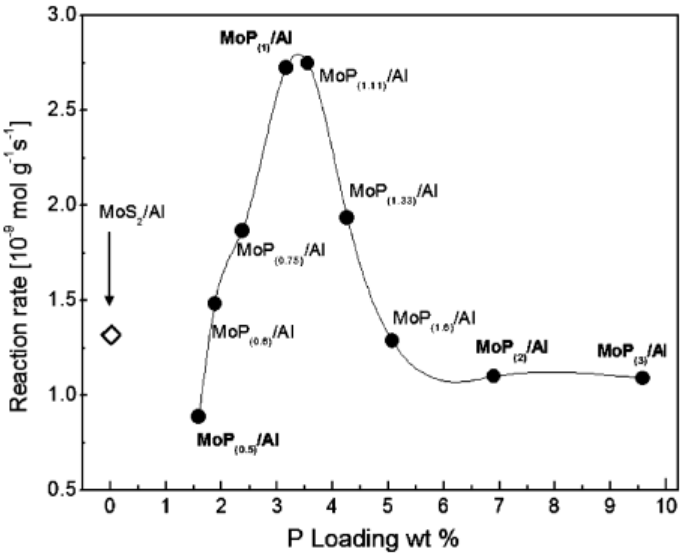

Figure 2.11: *The effect of P/Mo-ratio in a HDS reaction of dibenzothiophene (DBT), the feed was adjusted to get a conversion below 15%, $T = 553\ K$ and $P_{H_2} = 3.4\ MPa$, from Montesinos-Castellanos et al (2007)*[30]

The use of metal on the support had little effect in HYD, as can be seen from Table 2.2. There were small differences of the activity of the two catalysts in HDS, but the MoP catalysts showed higher activity than the sulfided catalyst in HDN.

Table 2.2: *Comparison of hydrotreat reactions for different molybdenum catalysts, from Oyama et al (2001)*[10]

Sample	**% HDN**	**% HYD**	**%HDS**
Al_2O_3	2.4	32	1.1
6.8% MoP/Al_2O_3	54	31	51
13% MoP/Al_2O_3	52	33	57
MoP	54	34	24
NiMo−S/Al_2O_3	22	29	54

Other studies by Stinner et al (2000) showed that MoP had six times higher activity in a HDN reaction of orthopropylaniline than MoS_2.[31] Phillips et al (2002) showed that MoP/SiO_2 had four times higher activity in a HDS reaction of dibenzothiophene than sulfided Mo/SiO_2.[11] However, as explained in the previous section, studies of HDS of dibenzothiophene can only give indications of which catalysts are effective for HDO of phenol.

2.3.2 Supports

The supports used in this project are γ-Al_2O_3, SiO_2, TiO_2 and ZrO_2. The supports are used to avoid sintering and instability of the metal particles. The metal particles are therefore placed in the pores of these inert supports.

Alumina (Al_2O_3) is the most widely used support because of its excellent thermal and mechanical stability. Alumina can exist in several structures, and the 3 most used are crystallographically ordered α-Al_2O_3 and the porous amorphous η- and γ-Al_2O_3. α-Al_2O_3 is used in high temperature processes, such as steam reforming, and where low surface areas are desired. γ-Al_2O_3 can be used as a catalyst without metal particles in the Claus process (production of elemental sulfur from H_2S), alkylation of phenol and dehydration of formic acid.[32] It has high surface areas, $50 - 300\ m^2g^{-1}$, mesopores between 5 and 15 nm and pore volumes of 0.6 cm^3g^{-1}. γ-Al_2O_3 can also be shaped into mechanically stable extrudates and pellets.[32]

Silica (SiO_2) is mainly used in processes below 300^oC, such as hydrogenations, polymerizations and oxidations.[32] SiO_2 has a relatively low thermal stability, and at higher temperatures, silica can form volatile hydroxides. It is easy to adjust the properties of SiO_2, such as pore size, particle size and surface area. SiO_2 supports are amorphous, but can still exhibit some local order similar to the mineral β-crystoballite.[32] The surface area can range up to 300 m^2g^{-1}, the pore diameter 7 nm and above and does not contain micropores.

Titania (TiO_2) is in some processes the most efficient catalyst, such as Claus process and Friedel-Craft acylation. However, in many other catalytic reactions, titania shows low activity and selectivity.[33] TiO_2 is relatively cheap, inert and has good mechanical properties. It can also interact with the active phase on the surface. There are 3 different types of titania; anatase, rutile and brookite. The latter is not used because it has low stability. Anatase is mostly used. It is thermodynamically stable to 800^oC, and at higher temperatures, anatase is transformed to rutile. The lattice structure of both anatase and rutile are tetragonal, the coordination number of titanium is 6 and for oxygen 3.

Zirconia (ZrO_2) has high thermal stability with both acid and base properties.[34] It is also stable under reduced pressure and reducing atmosphere. The surface

area varies with the calcinations temperature, and with calcination at 600^oC, the surface area ranges from $40 - 100\ m^2$. There are 3 stable crystalline modifications of zirconia. A monoclinic structure is stable up to 1200^oC, a tetragonal structure is stable up to 1800^oC and a cubic structure is stable above 1800^oC. A metastable tetragonal form is also known and is stable up to 650^oC.

2.4 Preparation of catalyst materials

To make MoP catalysts, several preparation methods are needed such as drying, calcination, incipient wetness method, reduction and passivation.

Incipient wetness or impregnation is a method to deposit metal on the support surface.[35] The pores are filled with a solution of metal salt, due to capillary forces. The method is therefore also known as capillary impregnation. The concentration of metal in the solution is controlled to give the desired metal loading on the support. The support is first dried or calcinated to remove pore moist, because this increases diffusion into the pores. The amount of metal solution added must be enough to fill the pores and wet the outside.[35] Every support has a wetness point, and if the amount of solution needed to obtain the desired metal loading is higher than the wetness point, the impregnation has to be done in two or several stages.

After the impregnation, drying is necessary to crystallize salt from the metal solution to the surface, and to remove the large amount of water. The drying rate influences the concentration distribution of salt on the surface. The goal of the drying is to obtain uniform deposits of metal. However, if the drying rate is too slow, the main deposits will be deep in the pores, and if the drying rate is too fast, most of the deposits will occur on the outside.

Calcination is a heat treatment method. The temperature increases slowly to the desired temperature, and after the calcination time, the temperature decreases slowly to room temperature.[35] Several processes can occur during calcination. Volatile fractions such as water, CO_2 and nitrates are removed from the samples. Salts are converted to oxides and metals, and it is therefore not possible for the salts to re-dissolve when exposed to moist environment. The mechanical properties are stabilized, and the pore size distribution and surface conditioning are changed. Phase transformation can occur, especially for Al_2O_3. At 450^oC, Al_2O_3 has a cubic closed packed (ccp) structure and is called γ-Al_2O_3. Al_2O_3 can undergo several structure changes up to 1200^oC, where Al_2O_3 has a hexagonal structure.[35] However, in this project, the calcination temperature is not above 500^oC.

Reduction or activation is a process where the metal oxide from the impregnation is reduced to active metal, normally with hydrogen as the reducing agent. By

using temperature controlled reduction (TPR), it is also possible to estimate which reactions occur during reduction. Clark et al (2003) studied the reactions during reduction of an alumina-supported MoP catalyst by using TPR.[29] They concluded that the following reactions take place during reduction.

$$\mathrm{MoO_3 + H_2 \rightarrow MoO_2 + H_2O}$$
$$\mathrm{MoO_2 + 2\,H_2 \rightarrow Mo + H_2O}$$
$$\mathrm{AlPO_4 + Mo \rightarrow Al_2O_3 + MoP}$$

After the reduction, the surface metal can be very pyrophoric and will burn in contact with air. Therefore, the catalysts need to be passivated, before they can be handled safely. This can be done by cooling the catalyst and removing the remaining hydrogen with an inert gas. This gas is normally 1% oxygen in an inert gas, such as argon. The gas is flowed slowly so the oxidation only takes place in the first layers, protecting the bulk. After this passivation, the catalysts can be handled safely.

2.5 Characterization methods

2.5.1 N_2-adsorption

The total surface area of support and metal can be determined using the BET (Brunauer, Emmett and Teller) Equation 2.3.[36]

$$\frac{P}{V(P_0 - P)} = \left[\frac{(C-1)}{V_m C}\right]\frac{P}{P_0} + \frac{1}{V_m C} \tag{2.3}$$

where P_0 is the saturation vapor pressure, V is the total volume adsorbed (STP) at pressure P, V_m is the volume adsorbed (STP) at monolayer coverage, and C is defined by Equation 2.4.

$$C = e^{\frac{q_1 - q_L}{RT}} \tag{2.4}$$

where q_1 is the heat of adsorption in the first monolayer and q_L is the heat of condensation of the adsorbate.

A plot of $\frac{P/P_0}{V(1-P/P_0)}$ against P_0/P gives a linear plot with a slope $\frac{C-1}{V_m C}$ and an intercept $\frac{1}{V_m C}$. When N_2 is used as an adsorbate, an assumption that $C \gg 1$ can be made, thus the slope $\approx \frac{1}{V_m}$. The specific surface area $\left(m^2 g^{-1}\right)$ can be calculated from Equation 2.5.

$$A\left[\frac{m^2}{g}\right] = V_m\left[\frac{cm^3 STP}{g}\right]\left[\frac{6.023 \cdot 10^{23}\ molecules}{21400\ cm^3 STP}\right]\left[\frac{cross-section, m^2}{molecule}\right] \tag{2.5}$$

The BET-equation derives from the Langmuir isotherm, which assumes constant heat of adsorption, monolayer and immobile adsorption and dynamical equilibrium between gas and adsorbed molecules. The BET-equation does not assume monolayer adsorption, but multilayer physical adsorption. Each adsorbed molecule in the 1st layer serves as a site for the 2nd layer and so on for higher layers. The adsorption energy for molecules in the 2nd and higher levels is the same as the condensation energy and the multilayer grows to infinite thickness at saturation

pressure ($P = P_0$).[32]

The isotherms obtained can be categorized into 6 different types, which are given in Figure 2.12.[37]

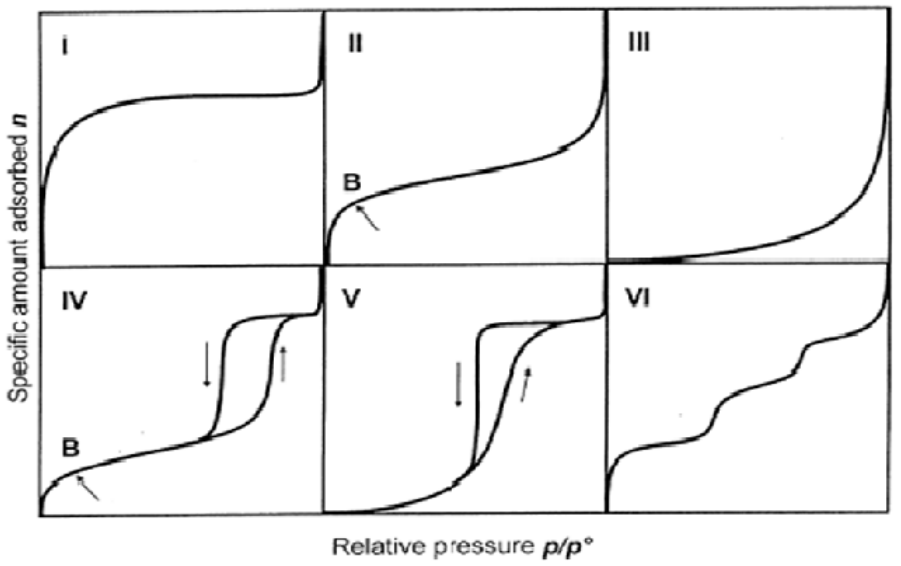

Figure 2.12: *Type I-VI isotherms defined by IUPAC, from Sing et al (1982)*[37]

These isotherms are by IUPAC called Type I-VI. For Type I, the microporous solids have relatively small external surfaces, and only monolayer is formed. This can be the case for activated carbon and molecular sieved zeolites. The Type II is the most common isotherm along with Type IV, and in both isotherms, monolayer is formed. Type II is normal for non-porous and macroporous adsorbents. Type III is a rare isotherm. It appears in water-vapor adsorption, non-porous carbon, and the interactions between adsorbate and surface. The Type IV is similar to Type II and is common for mesoporous adsorbents. It has a hysteresis loop which is caused by capillary condensation in the mesopores. Type V is uncommon and similar to type IV, except that the absorbent-adsorbate interaction is weak for Type V. In Type VI, a stepwise multilayer adsorption occurs on a non-porous surface. Examples of Type VI isotherms are argon and krypton on graphitized carbon blacks at liquid nitrogen temperatures.

2.5.2 XRD

X-ray Diffraction (XRD) is a characterization method used to identify crystalline phases inside the catalyst and to give an approximation of the particle size. XRD uses X-ray photons, which are scattered elastic in a periodic lattice. The Bragg relation is given in Equation 2.6 and can be used to determine the lattice spacing. [38]

$$n\lambda = 2d\sin\theta; \quad n = 1, 2.. \tag{2.6}$$

where λ is the wavelength of the X-rays, d is the distance between two lattice planes, n is the order of the reflection and θ is the angle between incoming X-rays and the normal to the reflecting lattice plane.

The crystalline diameter can be obtained by using the Scherrer equation:

$$d_v = \frac{K\lambda}{\beta\cos\theta} \tag{2.7}$$

where d_v is the volume-weighted crystalline diameter, K is a constant usually set to $0.9 - 1$ and β is the peak width.

A limitation of XRD is that particles, which are either too small or amorphous, cannot be detected. There can therefore exist other phases than the ones detected by the XRD. [32,39]

2.5.3 TPR

TPR (Temperature programmed reduction) is a method where the catalyst is reduced by a monitored chemical reaction while the temperature increases with time. Similar methods are temperature-programmed oxidation and sulfidation. The catalyst is placed inside a reactor, and a processor heats the reactor at a rate of typically 0.1^{o}C to 20^{o}C min^{-1}, while H_2 is flowed through the reactor at a constant rate. A mass spectrometer measures the H_2 content of the outlet flow. A plot of partial pressure of H_2 against the temperature gives different peaks, which can give an indication of the reduction reactions, and how well the metals are mixed on the

support surface. The total amount of H_2 used can be measured by calculating the area under the curve.[32]

2.5.4 Volumetric chemisorption

Chemisorption is a method to determine the dispersion of the catalyst. IUPAC defines the dispersion as percentage exposed, and it is given in Equation 2.8.[36]

$$D = \frac{number\ of\ surface\ atoms\ in\ the\ metal}{number\ of\ metal\ atoms} \tag{2.8}$$

The gasses normally used in chemisorption are H_2, CO, N_2O and O_2. They are adsorbed on a catalyst sample with increasing pressure and constant temperature. The volume of adsorbed molecules can be determined by using the Langmuir isotherm. A plot of the volume of adsorbed molecules against the pressure will give a plot similar to Figure 2.13.

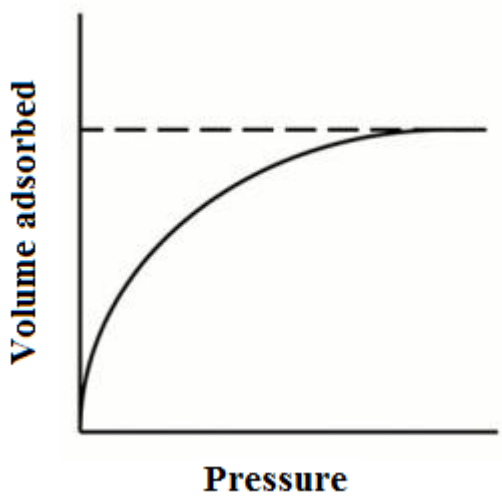

Figure 2.13: *Example plot of the Langmuir isotherm, volume of adsorbed molecules against pressure, from Goldberg et al (2007)*[40]

The amount of adsorbed molecules can be determined by extrapolating to zero, and the dispersion can be calculated by using Equation 2.9.

$$D = \frac{v_{ads} M_m F}{x_m} \tag{2.9}$$

where M_m is the molecular weight of the metal $[g/mol]$, F is the number of surface atoms covered by one adsorbed molecule, x_m is the weight fraction of metal in the catalyst and v_{ads} is the adsorption of gas by selective chemisorption $[mol/g]$ and can be determined by Equation 2.10.

$$v_{ads} = \frac{V}{V_m} \tag{2.10}$$

where V is the volume of gas determined from the plot $\left[cm^3/g\right]$ and V_m is the volume of 1 mole of ideal gas at 0°C $\left[22414\ cm^3/g\right]$.

Although the Langmuir isotherm is widely used, there are also some limitations, because very few chemisorption processes actually follow the Langmuir isotherm. The reasons being that the real surfaces are heterogeneous and not homogenous as assumed by the isotherm. There are also repulsing forces between neighboring molecules and several types of bonds between the adsorbed molecules and the surface.

2.5.5 Gas chromatography

Chromatography is a separation method used to identify and quantify different species in a mixture. This is done by separation of the species in two phases, mobile and stationary phases. In this study, gas is used as the mobile phase, hence the name *gas chromatography*. The gasses used in gas chromatography are N_2, He and H_2. Helium is expensive and H_2 can be dangerous and demands certain precautions. N_2 is therefore mostly used because it is relative cheap, and it needs a purity of 99.99%.[41,42]

The principle of chromatography is to separate the species through a column. The species mix with the phases differently according to their volatility and affinity to the stationary phase. The specie which mostly mixes with the mobile phase will

pass fastest through the tube, and those which mix with the stationary phase will pass more slowly. The velocities of the species depend on the composition of the mobile and stationary phases and the temperature.

At the end of the tube there is a detector which registers the species as they pass through. These detectors are mostly TCD (Thermal conductivity detector) and FID (Flame-ionization detector). The TCD can be used for both inorganic and organic compounds and is the oldest detector used in gas chromatography. The carrier gas flows through a heated filament, and the gas cools the filament by absorbing heat. The filament is set to a temperature, and the temperature difference over the filament is measured as electrical resistance by the detector. A problem with using the TCD is low sensitivity.

The FID is mostly used for organic compounds. The carrier gas is mixed with H_2 and is burned with excess of air. There is an electric voltage between the flame and the collector. During the burning, ions and free electrons are formed, and the current in the detector is proportional to the amount of gas burned.

During quantitative analyses, an internal or external standard is often used to compensate for variations in the amount of injected sample.[41] A known amount of the standard is added to the sample. The ratio of added and measured amount of the standard is used to adjust the measured amount of the other species in the sample. The specie used as a standard has to be stable and not previously present in the sample. It also needs to be pure and have a retention time which is close to the other species in the sample.[41]

2.6 Definitions

In the results, the particle size, conversion, selectivity, reaction rate, turnover frequency (TOF) and activation energy have to be calculated. The definitions and equations needed are given in this chapter.

The particle size can be estimated from the XRD by the Scherrer equation, Equation 2.7 in Section 2.5.2, or by the data from the chemisorption.[36] The particle size is given Equation 2.11.

$$d = \frac{f \cdot V_{sp} \cdot M_{Mo}}{\sigma_M \cdot N_A \cdot D} \tag{2.11}$$

where f is a factor which describes the shape of the particle. The factor f is set to 6 by assuming spherical particles,[36] $\sigma_M[cm^2]$ is the atomic cross-section area of the metal, N_A is the Avogadro number, D is the dispersion calculated from Equation 2.9 and M_M is the molecular weight of the metal [g/mol]. The specific volume V_{sp} $[cm^3/g]$ can be calculated by Equation 2.12.

$$V_{sp} = \frac{1}{\rho_{Mo}} \tag{2.12}$$

When assuming spherical shaped particles, the particle diameter d can be approximated to[36]

$$d[nm] \approx \frac{0.9}{D} \tag{2.13}$$

The conversion x_A is defined as

$$x_A = \frac{n_{in} - n_{out}}{n_{in}} \tag{2.14}$$

where n_{in} is the number of moles into the reactor and n_{out} is the number of moles out of the reactor.[36]

The selectivity S_i of species i is defined as

$$S_i = \frac{n_{i(in)}}{n_{in} - n_{out}} \tag{2.15}$$

where $n_{i(in)}$ is the number of moles of product i out of the reactor, and n_{in} and n_{out} are the total number of moles in and out of the reactor.[36]

The weight hourly space velocity (WHSV) is defined by Equation 2.16.[43]

$$WHSV = \frac{q_{feed}}{m_{cat}} \tag{2.16}$$

where q_{feed} is the flow rate of feed into the reactor and m_{cat} is the mass weight of the catalyst.

The turnover frequency (TOF) or specific catalyst activity is defined by Equation 2.17.

$$TOF = \frac{r \cdot M_m}{x_m \cdot D} \tag{2.17}$$

where r is the experimental reaction rate, M_m is the molecular weight of the metal, x_m is the weight fraction of metal and D is the dispersion calculated from Equation 2.9.[36]

The activation energy can be calculated from the Arrhenius equation.[44]

$$k = Ae^{-E_A/RT} \tag{2.18}$$

where k is the rate constant, A is the frequency factor and E_A is the activation energy. The Arrhenius equation can be linearized by taking the natural logarithm of each side.[44]

$$\ln k = -\frac{E_A}{R}\left(\frac{1}{T}\right) + \ln A \tag{2.19}$$

This equation gives a linear equation with the slope $m = -E_A/R$ and an intercept $b = \ln k$.[44]

3 Experimental

3.1 Preparation of catalysts

2 MoP supported catalysts were prepared with different supports; alumina (Al_2O_3) and titania (TiO_2). During autumn 2012, these catalysts were made in addition with the supports silica (SiO_2) and zirconia (ZrO_2). These two catalysts were prepared in the same way as described for the MoP/TiO_2 in this section.

The TiO_2 support was crushed and sieved ($100 - 200\ mc$), and was in the same way as γ-Al_2O_3, calcinated at 500^oC for 5 hours at a rate of 3^oC/min prior to use.

Loadings of 15 wt% MoP was obtained by the incipient wetness method. Equimolar Mo and P was achieved by using the precursors ammonium molybdate tetrahydrate ($(NH_4)_6Mo_7O_{24} \cdot 4\,H_2O$) and ammonium phosphate ($(NH_4)_2HPO_4$). The calculations of the amount precursor needed are given in Appendix B.1 and the procedure for incipient wetness impregnation is given in Appendix B.2.

After the precursors were mixed with the supports, the impregnates were dried at room temperature and further dried at 110^oC overnight. The dried impregnates were calcinated in flowing air at 500^oC for 5 hours, at a rate of 3^oC/min prior to use.

Finally the impregnated TiO_2 catalyst was reduced in flowing H_2 at 700^oC, and Al_2O_3 at 850^oC. H_2 was prior to the reduction flowed through the samples for 1 h at 150 mL/min in room temperature. The temperature was increased with a rate of 5^oC/min until the reduction temperature was reached. The samples were then quickly cooled to room temperature in 60 mL/min He-flow. Afterwards, the samples were passivated in 1% O_2 in Ar at 20 mL/min for 2 h.

3.2 Characterization methods

The samples were characterized by different characterization methods. Pure supports and calcinated impregnates were characterized by N_2-adsorption and TPR. Reduced catalysts were characterized by N_2-adsorption, XRD and chemisorption. The catalysts made during spring 2013 were characterized by all the methods, and the catalysts made during autumn 2012 were only characterized by chemisorption. The other characterization results for these catalysts are given in the specialization project. [45]

3.2.1 N_2-adsorption

Samples of calcinated supports, calcinated impregnates and reduced catalysts were characterized with N_2-adsorption. The samples were degassed at 200^oC overnight before the analysis. The measurements were done at -196^oC. The N_2-adsorption apparatus used was a Micromeritics TrisStar II, and the apparatus used for degassing was a Micromeritics VacPrep 061. A detailed procedure of the BET experiment is given in Appendix C.1.

3.2.2 XRD

Samples of reduced catalysts were characterized by XRD. The XRD-apparatus used was a Bruker AXS D8 Focus, with CuKα radiation. The samples were measured between $5^o < 2\theta < 90^o$. The step size was set to 0.019^o with a time step of 0.27 s. The total number of steps were 4253, and the slit was 0.2 mm. A detailed procedure of the XRD experiment is given in Appendix C.2.

3.2.3 TPR

Samples of calcinated support and calcinated impregnates were characterized with TPR. The samples were heated to 300^oC in flowing Ar-gas prior to the analysis to remove water from the samples. The samples were reduced with 3-4 mL/min 7% H_2 in Ar during heating to 800^oC at 10^oC/min. The apparatus used was a Quantachrome Chembet-3000. A detailed procedure of the TPR experiment is given in Appendix C.3.

3.2.4 Chemisorption

Samples of reduced catalysts were characterized with CO-chemisorption. A U-tube shaped reactor was filled with quartz wool and the catalysts. The samples were evacuated with He at 120^{o}C at a rate of 10^{o}C/min for 30 min and followed by a leak test. They were further reduced with H_2 at 500^{o}C for 50 min and afterwards evacuated with He at 500^{o}C for 50 min and 40^{o}C for 30 min. The analysis was done with CO at 40^{o}C at a pressure range between 20-500 mmHg. The chemisorption apparatus used was a Micromeritics ASAP 2020. A detailed procedure of the chemisorption experiment is given in Appendix C.5.

3.3 Activity testing

The activity of the supported MoP catalysts was tested in a HDO reaction of phenol to benzene in a fixed bed reactor. The reactor was filled with two types of silicon carbide (SiC I16, 1092 microns and SiC I60, 254 microns) and quartz wool in addition to the catalyst, according to Figure 3.1. Detailed descriptions of the reactor preparation and the activity measurement are given in Appendix E.1.

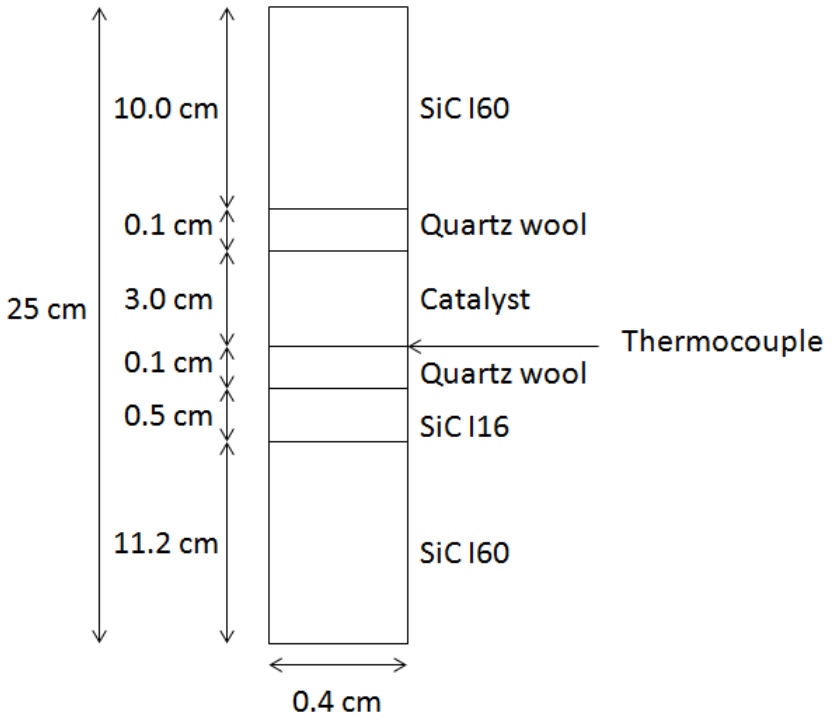

Figure 3.1: *Fixed bed reactor used in the activity measurement*

The activity measurement was carried out at the HDO rig in Chemistry Hall 4 at the Department of Chemical Engineering. Figure 3.2 shows a process flow diagram of the rig. The gas chromatography apparatuses used are Agilent Technologies 6890N for the gas GC and Agilent Technologies 6850 for the liquid GC. The feed was prepared by dissolving 1 vol% phenol in n-decane. The catalyst was activated *in situ* for 2h in flowing H_2 (100 mL/min) and N_2 (32 mL/min) at 450^{o}C. The gas product was analysed in the on-line GC, at 50^{o}C, 25 bar and with He as carrier gas. The calibration table used in the GC is given in Appendix E.5.

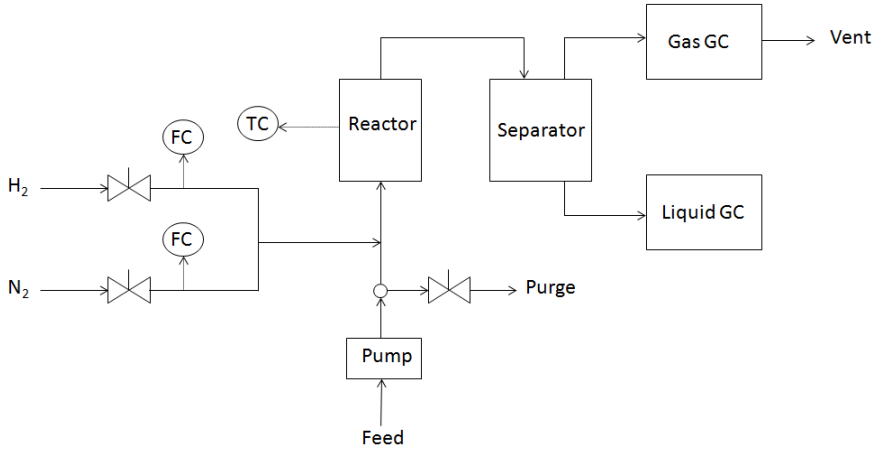

Figure 3.2: *Process flow diagram of the HDO rig, FC = Flow Controller, TC = Temperature Controller*

The liquid product was taken out in 6 samples at varying pressure (10 bar - 50 bar), temperature (330^{o}C - 450^{o}C), liquid flow rate (0.2 mL/min - 0.4 mL/min) and H_2 flow rate (40 mL/min - 100 mL/min). The liquid product was further analyzed quantitatively in the liquid GC. Each sample and the feed was mixed with 10 mL pentan-1-ol as external standard prior to the analysis. 5 injections were made for each sample, and the average measured amount of each specie was corrected by the ratio of known and measured amount of pentan-1-ol. The calculations of the quantitative analyses are given in Appendix E.2.

4 Results and discussion

4.1 Characterization

In this section, the results of the catalyst characterizations are given. Additional results are given in Appendix D. The characterized catalysts are made during spring 2013. The N_2-adsorption, XRD and TPR results for the catalysts made during autumn 2012 are given in the specialization project,[45] and the chemisorption results are given in Section 4.1.4.

4.1.1 N_2-adsorption

The surface area, pore volume and pore size measurement of calcinated supports, calcinated impregnates and reduced catalysts, obtained by the N_2-adsorption analysis, are given in Table 4.1. The isotherm plots and pore volume distribution plots are given in Appendix D.1.

The results from the N_2-adsorption analyses show that the BET surface area of the calcinated supports were higher for Al_2O_3 than TiO_2. The BET surface area of Al_2O_3 was in the surface range described by Chorkendorff (2007) in Section 3.2.1,[32] and the BET surface area of TiO_2 also corresponded with the results in literature.[46] The pore volume of calcinated supports were also higher for Al_2O_3 for TiO_2, and the pore size measurement showed an opposite trend than for the BET surface area. The results were also very similar to the samples made in autumn 2012, so the repeatability of the samples was good.[45]

After impregnation, the BET surface area and pore volume decreased. This trend is also reported in literature.[10,11,29] Clark et al (2003) studied the effect of different loadings, and Montesinos-Castellanos et al (2007) studied the effect of the stochiometric ratio between molybdenum and phosphide.[29,30] They discovered that the BET surface area decreased with increased loading of MoP and with increased P/Mo-ratio. An assumption that phosphide metal particles block the pores and therefore decrease the surface area and pore volume can be made. As the BET surface area and pore volume decreased, the pore size increased after impregnation, and the pore size increased the most for MoP/TiO_2. This trend is expected when the pore volume decreases.

After the reduction, all samples showed an increase in BET surface area and pore volume. This trend was also found in the master's thesis of Christina Carlsen [47] and in the specialization project in autumn 2012. [45] A reason for this may be that the MoP particles are smaller than the metal oxide particles such as MoO_3 and MoO_2 which are present after the impregnation. When the particles become smaller, the pores are less blocked, thus increasing the surface area and pore volume.

Table 4.1: *Results from the N_2-adsorption analyses. The samples were first degassed at 200^oC overnight, and the measurements were done at -196^oC.[1] BET surface area, [2] BJH desorption, [3] BJH desorption.*

Sample	**Surface area** $[m^2/g]$[1]	**Pore Volume** $[cm^3/g]$[2]	**Pore size** [Å][3]
Calcinated supports, run 1			
Al_2O_3	187.98	0.41	61.38
TiO_2	92.23	0.28	102.38
Calcinated supports, run 2			
Al_2O_3	198.16	0.42	61.36
TiO_2	91.32	0.28	101.19
Impregnated 15 wt% MoP			
MoP/Al_2O_3	102.91	0.20	59.22
MoP/TiO_2	17.51	0.06	177.36
Impregnated, run 2 15 wt% MoP			
MoP/Al_2O_3	100.52	0.20	59.19
MoP/TiO_2	18.16	0.06	198.40
Reduced 15 wt% MoP			
MoP/Al_2O_3	109.88	0.21	58.31
MoP/TiO_2	20.72	0.08	135.12
Reduced, run 2 15 wt% MoP			
MoP/Al_2O_3	110.33	0.21	58.18
MoP/TiO_2	23.06	0.08	129.77

All samples were tested twice to investigate how the results change with different analyses, and the results had very small differences. Calcinated and impregnated MoP/Al_2O_3 samples gave a Type IV isotherm, and the MoP/TiO_2 sample gave an isotherm similar to Type II and III, however, with a hysteresis loop.[37] The pore volume distribution plots show that most pores are mesopores, in the range of 20-500 Å[32] and that the largest pores are found for MoP/TiO_2.

4.1.2 XRD

The XRD results of the reduced catalysts are given in Figures 4.1-4.2.

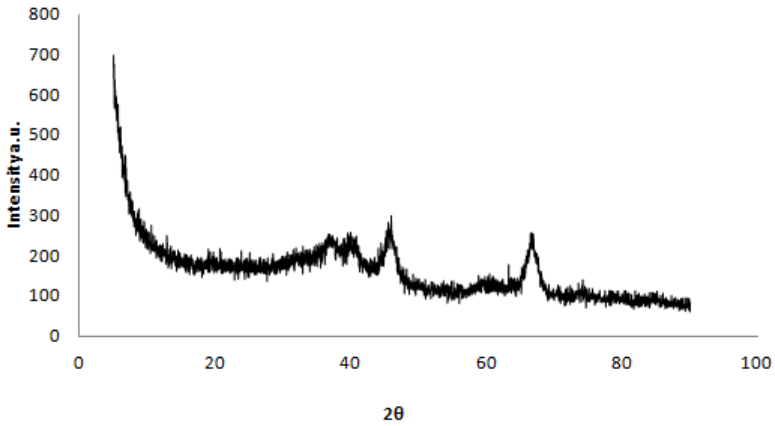

Figure 4.1: *XRD-plot for reduced 15 wt% MoP/Al_2O_3 with a step size set to* 0.019^o*, time step of 0.27, total number of steps of 4253 and the slit was 0.2 nm.*

All samples were analyzed with the same procedure, described in Section 2.5.2. The total number of steps used was 4253, and the time step was 0.27 s. By using these parameters, the analyses were a little slower and more precise, than the analyses which were done during autumn 2012.[45] However, there were no significant changes in the result with an increased number of steps and time step. Similar to the result from autumn 2012, the result for MoP/Al_2O_3 gave a rough plot, and the result for MoP/TiO_2 gave a smooth plot.

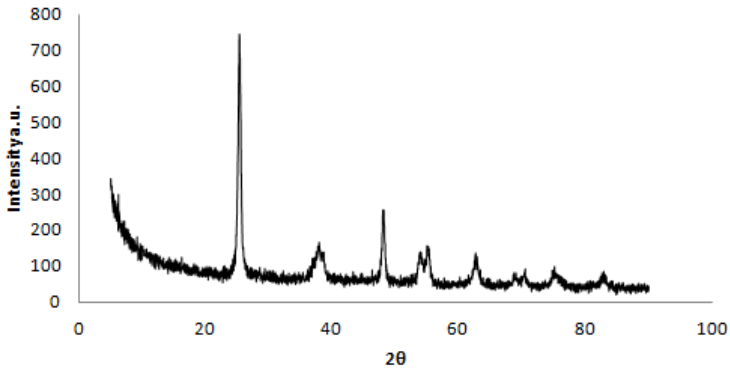

Figure 4.2: *XRD-plot for reduced 15 wt% MoP/TiO_2 with a step size set to* 0.019^o*, time step of 0.27, total number of steps of 4253 and the slit was 0.2 nm.*

The XRD plot for reduced MoP/Al_2O_3 is shown in Figure 4.1. It shows peaks at $2\theta = 45$ and $2\theta = 67$, which were also present in the result from autumn 2012.[45] In addition, 2 small peaks at around $2\theta = 40$ are visible. Whiffen et al (2010) made an XRD-analysis of unsupported MoP, with used and unused catalysts.[48] They discovered a large peak at angle $2\theta = 45$, medium peaks at angles $2\theta = 28$ and 31, and some small peaks at $2\theta = 56, 64, 66$ and 73. MoO_3 and MoO_2 show large peaks at angle $2\theta = 25$.[48] As Figure 4.1 does not show peaks at this angle, an assumption that most of MoO_3 and MoO_2 have been reduced to Mo during the reduction, can be made.

Oyama et al (2001) analyzed pure MoP, pure Al_2O_3 and different metal loadings of MoP on Al_2O_3.[10] The result of pure MoP was very similar to the findings of Whiffen et al (2010),[48] as mentioned above. The results of pure Al_2O_3 showed peaks at $2\theta = 45$ and 67, and some small peaks between 33 and 40. For 13 *wt*% MoP/Al_2O_3 sample, peaks were found corresponding to both pure MoP and Al_2O_3.[10] The XRD-plot in Figure 4.1 also shows peaks at $2\theta = 45$ and 67, corresponding well to pure Al_2O_3. As MoP also shows peaks at $2\theta = 45$, it is difficult to determine if the peak in Figure 4.1 derives from MoP or pure Al_2O_3. However, as the peaks at around $2\theta = 40$ in Figure 4.1 correspond to the peaks between 33 and 40 of pure Al_2O_3, it is reasonable to assume that all the peaks in Figure 4.1 correspond to pure Al_2O_3.

The XRD-plot for reduced MoP/TiO_2 is shown in Figure 4.2. Schacht et al (2003) analyzed pure TiO_2 in addition to CoMo on La-doped TiO_2 support.[49] On the pure TiO_2, they discovered a large peak at $2\theta = 25$, and other peaks at $2\theta = 38, 48, 55$ and 63. These peaks are also found in Figure 4.2. Similar results are found by Zhang et al (2000), who analyzed nanocrystals of anatase TiO_2.[50] However, no peaks at $2\theta = 45$ and 67 were found, which correspond to MoP. There are few reports of MoP/TiO_2 in literature, so comparison with other experiments is difficult. Christina Carlsen analyzed the 15 $wt\%$ MoP/TiO_2 and the XRD results for this sample were very similar to Figure 4.2, which also showed no peaks corresponding to MoP.[47] The same conclusion was made in the specialization project during autumn 2012.[45]

No peaks corresponding to MoP particles were observed for the two catalysts. This probably means that the metal particles are well dispersed on the catalyst.[11] As the XRD plots are very similar for the supports and the reduced catalyst, the H_2 reduction does not influence the XRD results.

4.1.3 TPR

The TPR-profiles for calcinated supports and calcinated impregnates made during autumn 2012 are given in Figures 4.3-4.6. The TPR profiles for the calcinated support and calcinated impregnates for the 15 wt% MoP/TiO_2 made in spring 2013 are given in Figure 4.7.

The calcinated supports and impregnates were also characterized by TPR during autumn 2012, which is described in the specialization project.[45] These samples were, however, characterized by TPR one more time, because the analyses for the samples on TiO_2 and ZrO_2 gave bad results. All samples were therefore characterized by another TPR-apparatus.

The plot for MoP/Al_2O_3 in Figure 4.3 shows a large peak at 500^oC, a small peak at around 750^oC, and a starting peak at 800^oC. This corresponds well to the results from autumn 2012.[45] These peaks can be compared with the plots obtained by Clark et al (2003) and Montesinos-Castellanos et al (2007).[29,30] Clark et al (2003) measured the TPR-profiles of MoP/Al_2O_3 with different metal loading. They concluded that the reduction occurred at 3 different peaks, which they labelled β, γ and δ-peaks, which occurred at 450^oC, 550^oC, and 850^oC respectively. MoO_3 was reduced

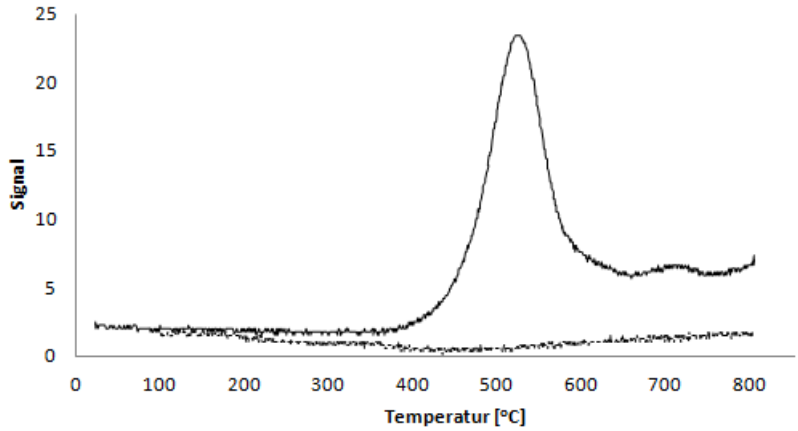

Figure 4.3: *TPR-plot for 15 wt% MoP/Al_2O_3 made during autumn 2012, – calcinated impregnates, ··· calcinated supports, reduced with 3-4 mL/min 7% H_2 in Ar during heating to 800^oC at $10^oC/min$.*

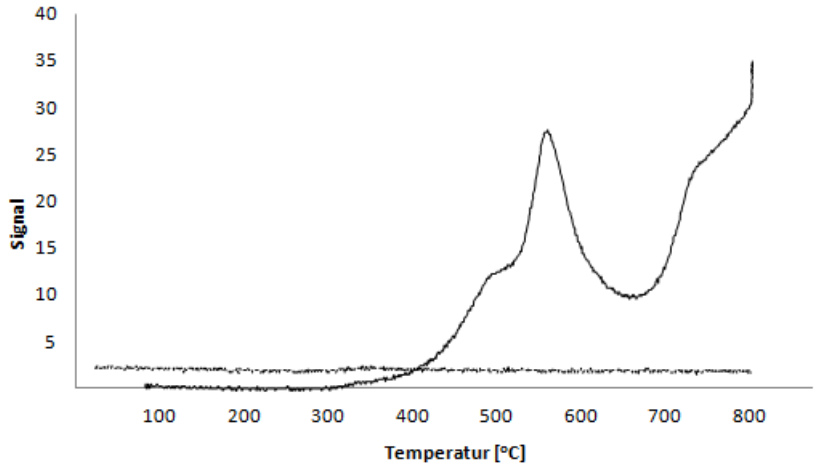

Figure 4.4: *TPR-plot for 15 wt% MoP/SiO_2 made during autumn 2012, – calcinated impregnates, ··· calcinated supports, reduced with 3-4 mL/min 7% H_2 in Ar during heating to 800^oC at $10^oC/min$.*

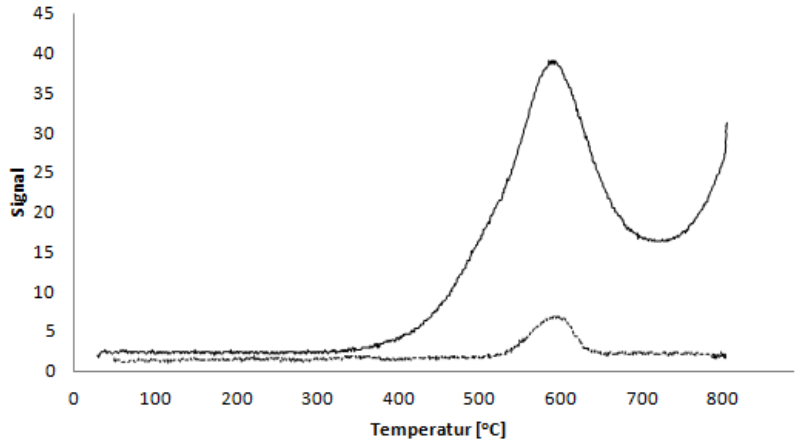

Figure 4.5: *TPR-plot for 15 wt% MoP/TiO_2 made during autumn 2012, — calcinated impregnates, ··· calcinated supports, reduced with 3-4 mL/min 7% H_2 in Ar during heating to 800^oC at $10^oC/min$.*

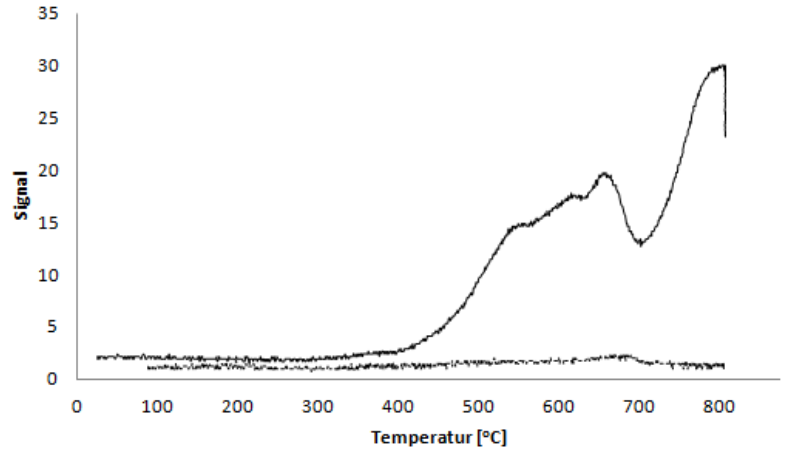

Figure 4.6: *TPR-plot for 15 wt% MoP/ZrO_2 made during autumn 2012, — calcinated impregnates, ··· calcinated supports, reduced with 3-4 mL/min 7% H_2 in Ar during heating to 800^oC at $10^oC/min$.*

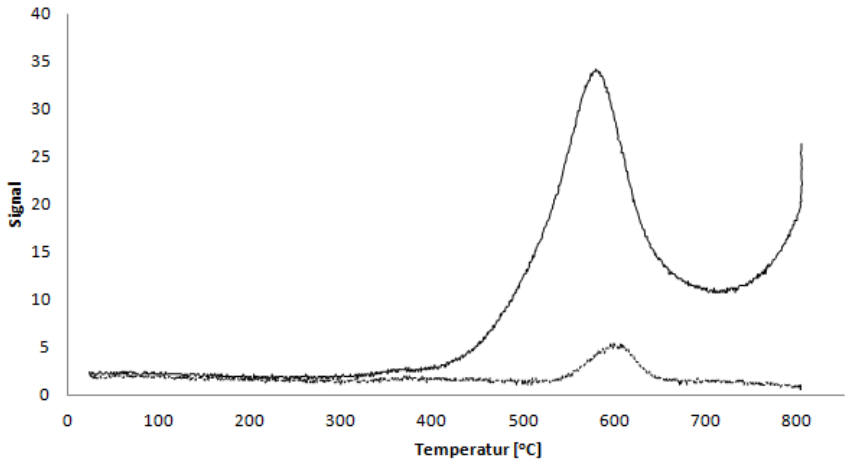

Figure 4.7: *TPR-plot for 15 wt% MoP/TiO_2 made during spring 2013, − calcinated impregnates, ··· calcinated supports, reduced with 3-4 mL/min 7% H_2 in Ar during heating to 800^oC at $10^oC/min$.*

at the β-peak, MoO_2 at the γ-peak and MoP was formed during the δ-peak.[29] They supported the conclusions with XRD-measurements of the samples from the intermediate temperatures. The peaks in Figure 4.3 correspond well to the β, γ and δ-peaks, as they fit with the reduction temperature intervals reported by Clark et at (2003).[29]

Montesinos-Castellanos et al (2007) tested bulk MoP in addition to MoP/Al_2O_3. For the bulk sample, they found a reduction peak of MoO_3 at 680^oC and reduction of MoO_2 at 850^oC.[30] For the supported samples, they also found 3 reduction peaks, but these peaks were discovered at higher temperatures than those of Clark et al (2003).[29] The results were supported by using AL MAS NMR (Aluminium-27 Magic Angle Spinning Nuclear Magnetic Resonance) spectroscopy. However, in this experiment, no analysis of the intermediate species was done, and it is therefore difficult to determine exactly which reactions took place. For the pure calcinated Al_2O_3 sample in Figure 4.3, no signals from the MS-apparatus were detected, indicating that no gas phase products were formed.

The TPR-plot for MoP/SiO_2 in Figure 4.4, shows peaks at 550^oC and a beginning peak at 800^oC, indicating dehydration peaks and that MoP is starting to form at

800^{o}C. This result also corresponds well to the results from autumn 2012.[45] Teng et al (2009) tested MoO_3 and MoP on MCM-41, a mesoporous silica support.[51] They got peaks at 500^{o}C and 850^{o}C, which corresponds well to this result. As for the Al_2O_3 sample, no gas phase products were detected with the pure calcinated SiO_2 sample.

The TPR-plots for MoP/TiO_2 and MoP/ZrO_2 in Figure 4.5-4.6, respectively, show large peaks at 550^{o}C and beginning peaks at 800^{o}C, similar to the sample with MoP/SiO_2. However, the sample with MoP/ZrO_2 shows several small peaks and not smooth lines, indicating that the reduction take place through more steps than the other samples. No gas phase product was detected for the pure ZrO_2 sample, and for the TiO_2 sample, a small peak was detected at 600^{o}C. This peak also appeared in the other TPR-apparatus in autumn 2012,[45] indicating that a reaction takes place in the pure TiO_2 sample. This reaction may be caused by traces of iron in the TiO_2 pellets.

The TPR-plot for the MoP/TiO_2 made during spring 2013 is shown in Figure 4.7, and it is very similar to the sample made during autumn 2012, in Figure 4.5. However, the reduction peak at 550^{o}C for the spring 2013 sample was lower than for the autumn 2012 sample. This difference may be due to difference in H_2 flow rate or temperature control.

By using the *cut and weigh* method, the relative H_2-consumption at the first β peak could be compared for each support. The relative H_2-consumptions are given in Table 4.2. Calculations and procedures for the *cut and weigh* method are given in Appendix C.4.

Table 4.2: *Relative H_2-consumption at the β-peak, calculated by the "cut and weigh" method.*

Catalyst	**Relative H_2-consumption (Area curve [mV·C])**
MoP/Al_2O_3	2415
MoP/SiO_2	3380
MoP/TiO_2	6256
MoP/ZrO_2	3162

Table 4.2 shows that the H_2 consumption was the largest for the MoP/TiO_2 sample and the lowest for the MoP/Al_2O_3 sample. The MoP/SiO_2 and MoP/ZrO_2 samples had almost equal H_2 consumption. The reduction goes much deeper in the MoP/TiO_2 sample than in the MoP/Al_2O_3 sample, as the H_2 consumption was almost three times higher. The choice of support has therefore a large influence of the how the metal oxides are reduced. However, all samples showed β peaks at around 500^oC, independent of the support used. Therefore, the β peak is characteristic for MoP particles.

4.1.4 Chemisorption

The dispersion and particle size of the reduced catalysts made in autumn 2012 and spring 2013 are given in Table 4.3. The line fit plots, used to calculate the dispersion and particle size, are given in Appendix D.2. The plots were adjusted in the chemisorption software, so the extrapolating of the plot started at 150 mmHg. An example calculation of the dispersion and particle size is given in Appendix C.6.

The plots in Appendix D.2 gave good and smooth isotherm lines. The results from Table 4.3 show that the dispersion and CO-uptake, based on the first isotherm plot, increases in the order $MoP/TiO_2 < MoP/Al_2O_3 < MoP/ZrO_2 < MoP/SiO_2$. The particle size, calculated by Equation 2.11, increased in the opposite order. By using the approximated particle diameter from Equation 2.13, the order did not change, however, the particle size decreased slightly. The low particle diameter for MoP/SiO_2 confirms the result from the XRD-analysis in the specialization project, [45] that the metal particles are well dispersed on the surface. Similar results are also reported in literature. [11,29] The CO-uptake of 13 wt% MoP/Al_2O_3 is reported to be 71 μmol/g [29] and 134 μmol/g for 15 wt% MoP/SiO_2. [11,52] The results therefore correspond well with the results in literature. The CO-uptake of pure Al_2O_3 and SiO_2 is negligible. [53] As MoP/ZrO_2 and MoP/TiO_2 have been little investigated in literature, comparison with other experiments is difficult.

The assumptions made in this analysis are that the CO molecules are adsorbed on Mo particles and not MoP, that the particles are spherical shaped and that one active site adsorbs one CO molecule. In the XRD analysis in Section 4.1.2, no peaks indicating that MoP was present on the surface was detected. It is therefore a good assumption that that the active sites are Mo particles and not MoP. This

assumption has also been made in literature.[11,52]

Table 4.3: *Results from the chemisorption analysis; dispersion, particle size and quantity adsorbed.*

Sample	**Dispersion**[%]	**Particle size**[nm]	**Quantity adsorbed**[$\mu mol/g$]
Total			
Autumn 2012			
MoP/Al_2O_3	5.1	24.9	79
MoP/SiO_2	7.9	16.1	123
MoP/TiO_2	4.9	26.2	75
MoP/ZrO_2	7.1	18.1	109
Spring 2013			
MoP/Al_2O_3	5.1	25.3	78
MoP/TiO_2	4.0	31.7	62
Difference			
Autumn 2012			
MoP/Al_2O_3	0.6	209.2	9
MoP/SiO_2	4.5	28.1	70
MoP/TiO_2	2.0	63.5	31
MoP/ZrO_2	4.1	31.1	63
Spring 2013			
MoP/Al_2O_3	0.6	199.5	10
MoP/TiO_2	1.9	65.1	30

The results from the catalysts made during spring 2013 were almost identical to the autumn 2012 sample for the MoP/Al_2O_3 catalyst. The MoP/TiO_2 had lower dispersion and larger particle size. This may be due to small differences in the stirring and drying rate during the impregnation.

Clark et al (2003) made a comparison of the CO-uptake between freshly reduced catalysts and passivated catalysts.[29] They discovered that the CO-uptake was 55% higher for the fresh reduced than the passivated catalyst. This result means that only small portions of the active sites lost during passivation are recovered during re-reduction.

In Table 4.3, the difference dispersions are based on the second isotherm plot in Appendix D.2. This isotherm shows how much of the adsorbed molecules remain on the active sites after evacuation. For the MoP/SiO_2, MoP/TiO_2 and MoP/ZrO_2 samples, the dispersion is reduced by 43% - 59%. However, for the MoP/Al_2O_3 sample, the dispersion was reduced by 88%. This large reduction in dispersion for the MoP/Al_2O_3 sample means that very few molecules remain on the active site after evacuation, and that the metal particles are more loosely bonded on Al_2O_3 supports than on the other supports.

4.2 Activity

In this section, the results from all activity measurements are given. In Section 4.2.1, the activity influence of the different supports are compared. Deactivation studies of the MoP/TiO_2 catalyst were done in Section 4.2.2. In Section 4.2.3-4.2.5, the MoP/Al_2O_3 and MoP/TiO_2 catalysts which showed the highest activity, are tested with various conditions, such as different pressures, H_2/oil ratio and flow rates. 2 different MoP/TiO_2 catalysts were tested to investigate the repeatability of the results in Section 4.2.6, and in Section 4.2.7, a reactor filled with support and inert SiC was tested.

The conversion of phenol, selectivity to benzene and turnover frequency were calculated by the data obtained by the off-line liquid GC. The average concentrations from the GC were corrected by using pentanol as an internal standard. Example calculations are given in Appendix E.2, and additional results are given in Appendix E.4.

4.2.1 Effect of the support

The HDO reaction of phenol to benzene was tested with 15 wt% MoP on the different supports, in order to investigate the effect of the different supports used in the project. The flow rate was varied between 0.2-0.3 mL/min and temperature between 350-450^{o}C. The pressure was set to 25 bar and the H_2 flow rate to 100 mL/min. The conversions and reaction rates for each support are given in Table 4.4, the turnover frequencies are given in Table 4.5 and the selectivities to each product are given in Table 4.6. Example calculations are given in Appendix E.2 and additional results are given in Tables E.3-E.10 in Appendix E.4.1.

Table 4.4 shows the conversion of phenol and the reaction rates for each catalyst. At the lowest temperature, 350^{o}C, MoP/Al_2O_3 and MoP/TiO_2 had the highest conversion of phenol, and MoP/SiO_2 and MoP/ZrO_2 had the lowest conversion. When the temperature was increased to 400^{o}C, the MoP/TiO_2 catalyst showed much higher activity than the MoP/Al_2O_3 catalyst. At the highest temperature, 450^{o}C, almost full conversion of phenol was achieved for MoP/Al_2O_3 and MoP/TiO_2 catalyst. The MoP/SiO_2 had the lowest activity at 400^{o}C and 450^c. However, at 450^{o}C, the liquid GC also detected unidentified products, which were either formed by phenol or the solvent, n-decane. The results at 450^{o}C are therefore unreliable, and it is

better to use the results at 350^{o}C to compare the catalysts.

As the flow rate was decreased from the 0.3 mL/min to 0.2 mL/min, the conversion mostly increased due to increased contact time. However, for the MoP/Al_2O_3 at 350^{o}C, the conversion was steady. One possible reason for this is fast deactivation of the catalyst. When almost full conversion was reached, the effect of the increased contact time was low. As the temperature was increased from 350^{o}C to 400^{o}C, the conversion increased with 400-500%. A rule of thumb is that the conversion doubles every 10^{o}C, so the results follow this rule.

Table 4.4: *Comparison of the conversion of phenol for the different supports. Temperature varied between 350^{o}C and 450^{o}C and flow rate between 0.2 and 0.3 mL/min. The pressure was set to 25 bar and H_2 flow rate to 100 mL/min.*

		Conversions [%]				**Reaction rates** $[mol/g_{cat} \cdot s]$			
Temperature [C]	**Flowrate [mL/min]**	**Al_2O_3**	**SiO_2**	**TiO_2**	**ZrO_2**	**Al_2O_3**	**SiO_2**	**TiO_2**	**ZrO_2**
350	0.3	6.4	0.5	3.6	0.6	$8.3 \cdot 10^{-8}$	$9.2 \cdot 10^{-9}$	$5.3 \cdot 10^{-8}$	$6.9 \cdot 10{-}9$
350	0.2	6.3	0.2	6.8	1.2	$5.4 \cdot 10^{-8}$	$2.1 \cdot 10^{-9}$	$6.6 \cdot 10^{-8}$	$9.8 \cdot 10{-}9$
400	0.2	27.5	5.6	74.7	23.1	$2.4 \cdot 10^{-7}$	$6.5 \cdot 10^{-8}$	$7.3 \cdot 10^{-7}$	$1.8 \cdot 10{-}7$
400	0.3	20.7	2.9	48.0	13.2	$2.7 \cdot 10^{-7}$	$5.2 \cdot 10^{-8}$	$7.0 \cdot 10^{-7}$	$1.6 \cdot 10{-}7$
450	0.3	92.5	20.8	95.2	56.6	$1.2 \cdot 10^{-6}$	$3.6 \cdot 10^{-7}$	$1.4 \cdot 10^{-6}$	$7.0 \cdot 10{-}7$
450	0.2	96.0	24.7	93.1	69.7	$8.4 \cdot 10^{-7}$	$2.9 \cdot 10^{-7}$	$9.1 \cdot 10^{-7}$	$5.8 \cdot 10{-}7$

Table 4.5: *Comparison of the turnover frequencies for the different supports. Temperature varied between 350^{o}C and 450^{o}C and flow rate between 0.2 and 0.3 mL/min. The pressure was set to 25 bar and H_2 flow rate to 100 mL/min.*

		TOF $[s^{-1}]$			
Temperature [C]	**Flowrate [mL/min]**	**Al_2O_3**	**SiO_2**	**TiO_2**	**ZrO_2**
350	0.3	$1.05 \cdot 10^{-3}$	$7.34 \cdot 10^{-5}$	$6.94 \cdot 10^{-4}$	$6.19 \cdot 10^{-5}$
350	0.2	$6.83 \cdot 10^{-4}$	$1.64 \cdot 10^{-5}$	$8.63 \cdot 10^{-4}$	$8.83 \cdot 10^{-5}$
400	0.2	$2.99 \cdot 10^{-3}$	$5.22 \cdot 10^{-4}$	$9.53 \cdot 10^{-3}$	$1.80 \cdot 10^{-3}$
400	0.3	$3.37 \cdot 10^{-3}$	$4.11 \cdot 10^{-4}$	$9.18 \cdot 10^{-3}$	$1.48 \cdot 10^{-3}$
450	0.3	$1.51 \cdot 10^{-2}$	$2.91 \cdot 10^{-3}$	$1.82 \cdot 10^{-2}$	$6.34 \cdot 10^{-3}$
450	0.2	$1.04 \cdot 10^{-2}$	$2.31 \cdot 10^{-3}$	$1.19 \cdot 10^{-2}$	$5.20 \cdot 10^{-3}$

Table 4.6: *Comparison of the selectivities to benzene for the different supports. Temperature varied between 350^oC and 450^oC and flow rate between 0.2 and 0.3 mL/min. The pressure was set to 25 bar and H_2 flow rate to 100 mL/min.*

		Selectivity to benzene [%]			
Temperature [C]	**Flowrate [mL/min]**	**Al_2O_3**	**SiO_2**	**TiO_2**	**ZrO_2**
350	0.3	93.8	100	100	100
350	0.2	90.1	100	89.2	100
400	0.2	93.7	100	91.4	96.5
400	0.3	93.1	100	93.2	97.3
450	0.3	94.3	100	90.5	95.4
450	0.2	90.9	99.4	88.8	93.2

By comparing the TOF and reaction rates in Table 4.5 with dispersions in Table 4.3, it can be seen that there is an almost inverse trend between activity and CO-uptake. This has also been reported in literature.[52,54,55] Sun et al (2004) measured the activity of different metal phosphides on SiO_2 support in a HDS reaction of dibenzothiophene.[52] They discovered that MoP/SiO_2 had higher CO-uptake and lower activity than Ni_2P/SiO_2. Oyama (2003) obtained similar results of the same reaction.[54] As the dispersion increases and the particle size increases, the surface structure may change enough to influence the activity. However, there is still some uncertainty about the chemistry and behavior of MoP particles, and some of the assumptions made in the chemisorption analysis may be wrong. The reaction rate $[mol/g_{cat} \cdot s]$ is therefore better to compare the activity of the catalysts than TOF.

Table 4.6 shows the selectivity to benzene, and the selectivity to the other products are given in Tables E.4, E.6, E.8 and E.10 in Appendix E.4. A comparison between conversion and selectivity to the different products are given in Figure 4.8. The selectivity to benzene showed the opposite trend than the conversion of phenol for several catalysts. MoP/SiO_2 had low conversion and high selectivity to benzene, while MoP/TiO_2 had high conversion and low selectivity to benzene. The selectivity to benzene of the MoP/Al_2O_3 catalyst was independent of the conversion. It was a general trend that the selectivity to cyclohexene increased with increased conversion. When the conversion was very high, more cyclohexane and methyl cyclopentane was formed. This can also be seen in Figure 4.8. This means that the reaction pathway

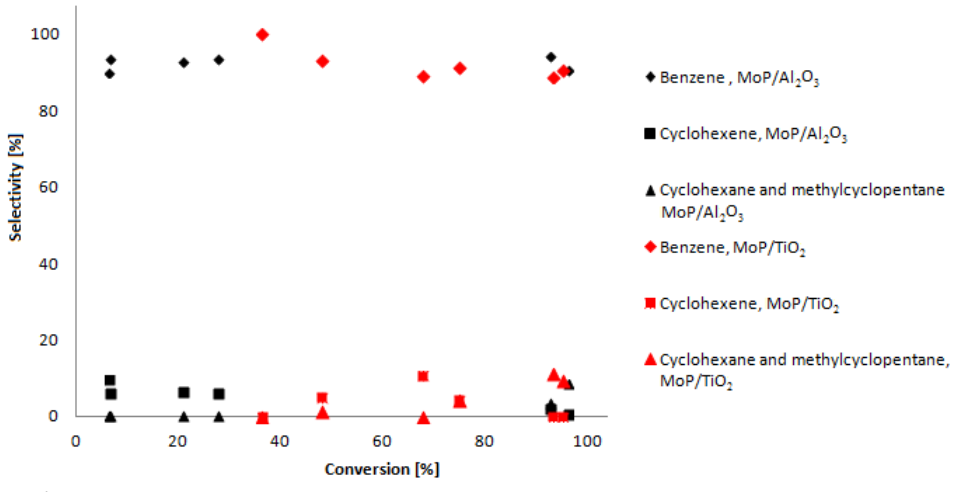

Figure 4.8: *Comparison of selectivity to the different products for the MoP/Al_2O_3 and MoP/TiO_2 catalysts.*

in Figure 2.8 is more favored to cyclohexane with increased temperature. As the selectivity to benzene was very high at all temperatures, it can be ascertained that benzene is the primary product. Even though the liquid GC sometimes showed no formation of the other products, some may still have been formed. However, the amount was too low to be detected by the GC.

The equation for calculation of selectivity is given in Equation 2.15. The assumed products from the HDO reaction of phenol were benzene, cyclohexene, cyclohexane and methyl cyclopentane. However, the results from the liquid GC showed other unidentified peaks, which increased with increased temperature. To avoid selectivites above 100%, the denominator in Equation 2.15 was modified to the sum of the formation of only assumed products.

The MoP/Al_2O_3 and MoP/SiO_2 catalysts have been studied in many reactions, such as HDS of dibenzothiophene and HDO of guaiacol.[11,29,30,53] Clark et al (2003) compared MoP/Al_2O_3 and MoP/SiO_2 in several reactions and discovered that MoP/Al_2O_3 had higher activity than MoP/SiO_2 in HDN and HYD of quinoline[29] and in HDS of dibenzothiophene. As discussed in Section 2.3, HDS of dibenzothiophene is a very different reaction than HDO of phenol. However, the catalysts seem

to behave similarly in both of the hydrotreatment reactions.

As little research of MoP/TiO_2 and MoP/ZrO_2 has been done, it is difficult to compare the activity results of these catalysts with other experiments in literature. Ohta et al (2011) tested TiO_2 and ZrO_2 supported platinum catalysts on HDO reactions of 4-propylphenol, and the TiO_2 supported catalyst had higher activity than the ZrO_2 supported catalyst.[56]

In Table 4.2 in Section 4.1.3, the relative H_2 consumptions during TPR are given. MoP/TiO_2 had the highest activity and in addition almost twice as much H_2 consumption during reduction than the other catalysts. However, as the MoP/Al_2O_3 had the lowest H_2 consumption, the HDO activity is not dependent on the H_2 consumption.

4.2.2 Deactivation

To investigate how the catalysts deactivate over time, a sample of the MoP/TiO_2 catalyst was tested at the HDO rig with the same flow rate and temperature over time. 2 separate measurements with different flow rates were done. The results of the measurement with 0.2 mL/min flow are given in this section, and the results with 0.3 mL/min are given in Tables E.13-E.14 in Appendix E.4. The conversion, turnover frequency, reaction rate and selectivity to benzene of the measurement with 0.2 mL/min are given in Table 4.7. Further results, such as carbon balance, time on stream, WHSV and selectivity to the other products, are given in Tables E.11-E.12 in Appendix E.4.2.

It is reported in literature that MoP catalysts show low deactivation,[10,11,30] however, Zhao et al (2011) reported deactivation of the MoP/SiO_2 catalyst in HDO of guaiacol.[53] In these measurements of the MoP/TiO_2 catalysts, the conversion decreased over time for both measurements. The decrease was highest at the beginning and slowed down at the last samples. The turnover frequency and reaction rate followed the same trend.

As the feed was 99% pure, the pressure was kept steady and the temperature was

350^oC, the deactivation mechanisms were most likely not particle failure or poison. No traces of rust or white particles were detected in the used catalyst, indicating that no fouling or component volatization had occurred. When carbon is used as feed, there is always a possibility of coking, and this is a large problem in many hydrotreatment processes.[35] Acidity of the support also increases coke formation, and the surface acidity of TiO_2 is of the Lewis type.[57] At high temperatures, sintering of the support is also a possible deactivation mechanism,[35] however, calcination of the catalyst is done at a higher temperature than during the activation measurement.

Table 4.7: *Results from the deactivation measurement of the MoP/TiO_2 catalyst. The temperature was kept steady at 350^oC, flow rate at 0.2 mL/min, pressure at 25 bar and H_2 flow at 100 mL/min.*

Temperature [C]	**Flow rate [mL/min]**	**Conversion [%]**	**TOF** $[s^{-1}]$	**Reaction rate** $[mol/g_{cat} \cdot s]$	**Selectivity to benzene [%]**
350	0.3	11.4	$2.99 \cdot 10^{-3}$	$1.9 \cdot 10^{-7}$	71.9
350	0.2	9.4	$1.63 \cdot 10^{-3}$	$1.0 \cdot 10^{-8}$	79.1
350	0.2	7.1	$1.23 \cdot 10^{-3}$	$7.8 \cdot 10^{-8}$	78.9
350	0.2	6.4	$1.11 \cdot 10^{-3}$	$7.0 \cdot 10^{-8}$	80.9
350	0.2	5.7	$9.94 \cdot 10^{-4}$	$6.3 \cdot 10^{-8}$	80.0
350	0.2	5.0	$8.71 \cdot 10^{-4}$	$5.5 \cdot 10^{-8}$	79.4

In Section 4.2.1, it was found that the selectivity to benzene was almost independent of temperature and conversion, and Tables 4.7 and E.12 show that the selectivity to benzene is also independent of catalyst deactivation. The selectivity to cyclohexene increased with decreased conversion, while the selectivity to cyclohexane and methyl cyclopentane decreased. This means that the reaction in Figure 2.8 stops at the second step as the catalyst is deactivated.

4.2.3 Effect of H_2 flow

To investigate how the H_2/oil ratio effects the catalyst, 2 measurements were done with a MoP/TiO_2 catalyst where the H_2 flow was decreased from 100 mL/min to 40 mL/min. The liquid feed flow rate was set to 0.3 mL/min for the first measurement and 0.2 mL/min for the second. The H_2/oil ratio was decreased from 500 Nm^3/m^3 to 200 Nm^3/m^3, which is often used in industrial refineries.[58] The conversion, turnover frequency, reaction rate and selectivity to benzene of the measurement

with the flow rate of 0.2 mL/min are given in Table 4.8. Further results, such as carbon balance, time on stream, WHSV and selectivity to the other products, are given in Tables E.15-E.16 and the results for the measurement with 0.3 mL/min flow rate are given in Tables E.17-E.18 in Appendix E.4.3.

As can be seen from Table 4.8 and E.15, the conversion decreased with decreasing H_2/oil ratio. In the experiment with 0.2 mL/min feed flow, the H_2/oil ratio was varied up and down to investigate if the decrease was only caused by variation in the H_2/oil ratio or by deactivation. The H_2/oil ratio was set back to 500 Nm^3/m^3 3 times during the experiment, and the conversion and reaction rate had decreased every time.

Table 4.8: *Results from the measurement with varying H_2/oil ratio. The catalyst used was MoP/TiO_2. The temperature was kept steady at 370^oC, the flow rate at 0.2 mL/min, pressure at 25 bar and the H_2 flow rate varied between 40-100 mL/min.*

Temperature [C]	**Flow rate [mL/min]**	**H_2/oil ratio**	**Conversion [%]**	**TOF [s^{-1}]**	**Reaction rate [$mol/g_{cat} \cdot s$]**	**Selectivity to benzene [%]**
370	0.2	500	9.6	$1.39 \cdot 10^{-2}$	$8.7 \cdot 10^{-7}$	93.7
370	0.2	200	6.3	$9.07 \cdot 10^{-3}$	$5.7 \cdot 10^{-7}$	98.3
370	0.2	500	6.1	$8.90 \cdot 10^{-3}$	$5.6 \cdot 10^{-7}$	92.1
370	0.2	200	4.5	$6.51 \cdot 10^{-3}$	$4.1 \cdot 10^{-7}$	100
370	0.2	500	4.7	$6.84 \cdot 10^{-3}$	$4.3 \cdot 10^{-7}$	100
370	0.2	350	4.3	$6.23 \cdot 10^{-3}$	$3.9 \cdot 10^{-7}$	100

A correction for deactivation was made to investigate how the H_2/oil ratio influenced the conversion without contribution from deactivation. The procedure and calculations for the correction are given in Appendix E.2.8. One of the assumptions made was that the deactivation is linear with time on stream, this being a very rough assumption. Figure 4.9 shows the result from the deactivation correction.

As can be seen in Figure 4.9, the conversion did not decrease as much after the correction, nevertheless, a slight decrease is visible with decreasing H_2/oil ratio for the measurement at 370^{o}C. For the measurement at 350^{o}C, the conversion did not change with increased H_2/oil ratio. However, the H_2/oil ratio was decreased during the entire measurement, and it is therefore more difficult to do the correction for deactivation. The same linear deactivation plot for the measurement at 370^{o}C

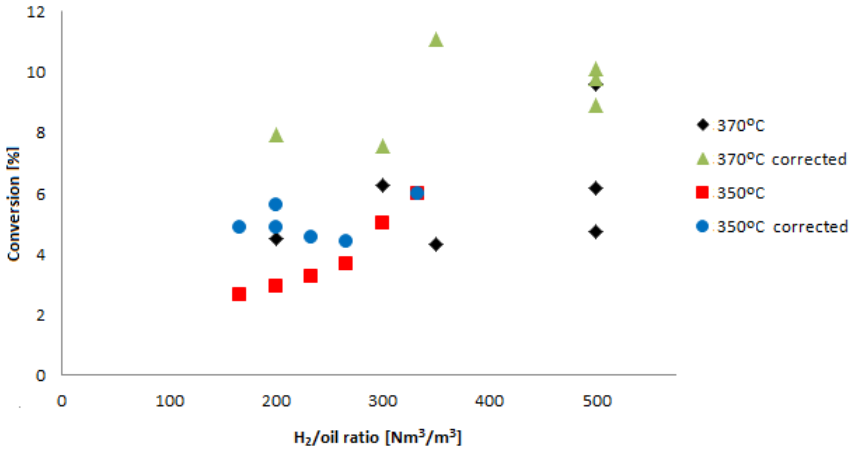

Figure 4.9: *Comparison of H_2/oil ratio against conversion for the MoP/TiO_2 catalyst at 350^oC and 370^oC before and after deactivation correction.*

was used for the measurement at 350^{o}C. This is a very rough assumption, as the deactivation normally is faster at higher temperatures. This is probably the reason why no decrease in conversion is visible for the corrected plot of the measurement at 350^{o}C.

Deactivation is a significant factor for the loss of activity in these experiments, however, the gas/oil ratio does have an influence of the activity as discussed above. One reason why the deactivation process is more significant may be that the amount of phenol in the feed mixture is only 1 vol%. In experiments with higher phenol concentrations, the gas/oil ratio would probably be more significant to the activity.

The selectivity to benzene was higher when the H_2/oil ratio was low. This result was expected, as lowering the amount of H_2 makes the reaction in Figure 2.8 stop at the first steps. The amount of cyclohexane and methyl cyclopentane was too low to be detected by the liquid GC.

4.2.4 Effect of pressure

To investigate how the partial pressure of H_2 effects the activity of the catalyst, a measurement was done where a MoP/TiO_2 catalyst was tested at 370^{o}C, 0.2 mL/min feed flow, 100 mL/min H_2 flow and pressure varying from 10-50 bar. The conversion, turnover frequency, reaction rate and selectivity to benzene are given in Table 4.9. Further results, such as carbon balance, time on stream, WHSV and selectivity to the other products, are given in Tables E.19-E.20 in Appendix E.4.4.

As seen in Table 4.9, the conversion decreased during the experiment, due to deactivation of the catalyst. The selectivity to benzene did not vary significantly. A deactivation correction was done to investigate how the pressure influences the activity without contribution from deactivation, with the same assumptions described in Section 4.2.3. The procedure and calculations for the correction are given in Appendix E.2.8. A comparison between the original and corrected conversions is given in Figure 4.10.

Table 4.9: *Results from the measurement with varying pressure. The catalyst used was MoP/Al_2O_3. The temperature was kept steady at 370^{o}C, the flow rate at 0.2 mL/min, H_2 flow rate at 100 mL/min and the pressure was varied between 10-50 bar.*

Temperature [C]	**Flow rate [mL/min]**	**Pressure** $[bar]$	**Conversion [%]**	**TOF** $[s^{-1}]$	**Reaction rate** $[mol/g_{cat} \cdot s]$	**Selectivity to benzene [%]**
370	0.2	25	16.7	$2.19 \cdot 10^{-3}$	$1.7 \cdot 10^{-7}$	93.0
370	0.2	35	13.3	$1.74 \cdot 10^{-3}$	$1.4 \cdot 10^{-7}$	90.8
370	0.2	50	14.6	$1.92 \cdot 10^{-3}$	$1.5 \cdot 10^{-7}$	88.7
370	0.2	25	11.0	$1.44 \cdot 10^{-3}$	$1.1 \cdot 10^{-7}$	90.3
370	0.2	10	11.8	$1.55 \cdot 10^{-3}$	$1.2 \cdot 10^{-7}$	93.6
370	0.2	25	7.8	$1.03 \cdot 10^{-3}$	$8.1 \cdot 10^{-8}$	88.4

As seen in Figure 4.10, the conversion was more steady after the correction. The few inequalities in the conversion are probably due to the rough assumptions made in the deactivation correction. This shows that the partial pressure of H_2 has little effect on the activity of the catalyst. The same conclusion was made by Su-Ping (2003), who studied HDO of raw bio-oils.[59] In Section 4.2.5, it is discussed that the surface reaction is the rate determining step. This shows that the proposed surface reaction mechanism in Figure 2.9 is independent of the partial pressure of H_2.

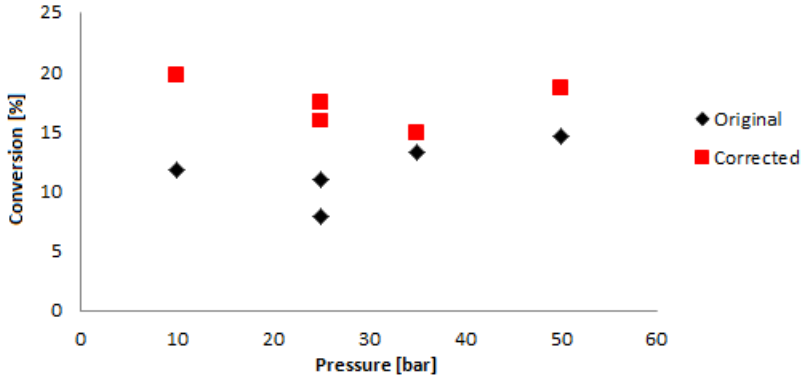

Figure 4.10: *Comparison of pressure against conversion for the MoP/Al_2O_3 catalyst at 370^oC before and after deactivation correction.*

In the industry, the pressures used in hydrotreating range from 10-40 bar for naphtha and 40-100 bar for gas oil.[9,58] The different pressures used in this experiment are therefore within the applied pressures for naphtha. A high pressure is often used to increase the solubility of H_2 in the oil. This causes a larger concentration of H_2 close to the active spots in the surface and decreases coking of the reactor.[60]

4.2.5 Activation energy

The MoP/TiO_2 catalyst was tested in a measurement around 350^{o}C and the MoP/Al_2O_3 catalyst was tested in 2 measurements around 350^{o}C and 370^{o}C, in order to determine the activation energy and the reaction constants for the mechanism illustrated in Figure 2.8. Table 4.10 shows the results for the MoP/TiO_2, and Table 4.11 shows the results for the MoP/Al_2O_3 measurement around 370^{o}C. The flow rate varied between 0.2-0.4 mL/min, the H_2 flow rate was 100 mL/min and the pressure was 25 bar. Further results, such as carbon balance, time on stream, WHSV, selectivity to the other products and the results for the measurement the MoP/Al_2O_3 catalyst around 350^{o}C are given in Tables E.21-E.26 in Appendix E.4.5.

As seen in the Tables 4.10 and 4.11, the conversion increased with increasing temperature. The selectivity to benzene increased with increased conversion for

MoP/Al_2O_3, and for MoP/TiO_2, the conversion to other products was too low to be detected by the GC analysis.

The activation energy was calculated for each measurement. The activation energy was calculated by the linearized Arrhenius equation, given in Equation 2.19. The procedure and example calculations are given in Appendix E.2.7. The results are given in Table 4.12.

Table 4.10: *Results from the measurement with the MoP/TiO_2 catalyst between 330^oC-370^oC. The flow rate varied between 0.2-0.4 mL/min, the H_2 flow rate was set to 100 mL/min and the pressure was 25 bar.*

Temperature [C]	**Flow rate [mL/min]**	**Conversion [%]**	**TOF** $[s^{-1}]$	**Reaction rate** $[mol/g_{cat} \cdot s]$	**Selectivity to benzene [%]**
330	0.2	1.7	$2.48 \cdot 10^{-4}$	$1.6 \cdot 10^{-8}$	100
340	0.25	1.8	$3.35 \cdot 10^{-4}$	$2.1 \cdot 10^{-8}$	100
350	0.3	2.2	$4.84 \cdot 10^{-4}$	$3.1 \cdot 10^{-8}$	100
360	0.35	2.7	$6.83 \cdot 10^{-3}$	$4.3 \cdot 10^{-8}$	100
370	0.4	3.7	$1.09 \cdot 10^{-3}$	$6.9 \cdot 10^{-8}$	100
350	0.3	1.6	$3.41 \cdot 10^{-4}$	$2.2 \cdot 10^{-7}$	100

Table 4.11: *Results from the measurement with the MoP/Al_2O_3 catalyst between 350^oC-390^oC. The flow rate varied between 0.2-0.4 mL/min, the H_2 flow rate was set to 100 mL/min and the pressure was 25 bar.*

Temperature [C]	**Flow rate [mL/min]**	**Conversion [%]**	**TOF** $[s^{-1}]$	**Reaction rate** $[mol/g_{cat} \cdot s]$	**Selectivity to benzene [%]**
350	0.2	4.3	$6.08 \cdot 10^{-4}$	$4.8 \cdot 10^{-8}$	88.4
360	0.25	4.5	$8.04 \cdot 10^{-4}$	$6.4 \cdot 10^{-8}$	87.2
370	0.3	5.6	$1.20 \cdot 10^{-3}$	$9.5 \cdot 10^{-8}$	90.1
380	0.35	8.6	$2.13 \cdot 10^{-3}$	$1.7 \cdot 10^{-7}$	91.8
390	0.4	14.5	$4.11 \cdot 10^{-3}$	$3.3 \cdot 10^{-7}$	93.0
370	0.3	6.9	$1.47 \cdot 10^{-3}$	$1.2 \cdot 10^{-7}$	90.1

As seen in Table 4.12, the activation energy varies with support, and MoP/Al_2O_3 has higher activation energy than MoP/TiO_2. As the activation energy for MoP/Al_2O_3 was higher in both measurements, the reason for the difference is not due to standard deviation. The supports showed no activity in the HDO reaction, as discussed in Section 4.2.7. In Section 4.1.4, it was discovered that MoP/Al_2O_3 had higher

Table 4.12: *Calculated activation energy for the measurements with MoP/Al_2O_3 and MoP/TiO_2 at 350^oC and 370^oC.*

Catalyst	**Temperature [C]**	**Activation energy [kJ/mol]**
MoP/TiO_2	350	116
MoP/Al_2O_3	350	151
MoP/Al_2O_3	370	164

dispersion than MoP/TiO_2. An opposite trend for dispersion and activation energy is reported by Reuel et al (1984), who characterized and tested Al_2O_3 and TiO_2 supported Co catalysts in a hydrogenation reaction.[55] As discussed in Section 4.1.4 and 4.2.1, there are uncertainties about the chemisorption result. In Section 4.2.6, the uncertainties about the activity measurements are also discussed. Furher work is therefore needed to confirm the relationship between metal dispersion and activation energy.

A comparison of the activation energies with other reports in literature may vary significantly even though the same catalysts are used. This is due to differences in feed stock, reactor system and operating conditions. However, in these measurements, the same feed stock, reactor system and operating conditions are used. The choice of support therefore has a large influence of the activation energy of the catalyst, as reported in literature.[55]

Due to the high activation energy, the surface reaction is most likely the rate determining step. It was discovered in Section 4.1.3 that the reduction of the MoP/TiO_2 catalyst was deeper than the reduction of the MoP/Al_2O_3 catalyst. As the rate determining step is the surface reaction, the depth of the reduction is not significant. This explains why the activity of the catalysts is similar even though the H_2 consumption during the reduction was different.

4.2.6 Repeatability

To investigate the repeatability of the results of the HDO reaction, 2 different MoP/TiO_2 catalysts were tested with the same conditions. The catalysts were made during autumn 2012 and spring 2013 with the same procedure and metal

loading. The conditions were the same as for the measurements in Section 4.2.1. The temperature varied between 350^{o}C and 450^{o}C and the flow rate between 0.2 and 0.3 mL/min. The pressure was set to 25 bar and H_2 flow rate to 100 mL/min. The conversion, turnover frequency, reaction rate and selectivity to benzene for both catalysts are given in Tables 4.13 and 4.14. Further results, such as carbon balance, time on stream, WHSV and selectivity to the other products, are given in Tables E.7-E.8 in Appendix E.4.1 for the catalyst from autumn 2012, and in Tables E.27-E.28 in Appendix E.4.6 for the catalyst from spring 2013.

Table 4.13: *Results from the repeatability measurement with the MoP/TiO_2 catalyst made during autumn 2012. The temperature varied between 350^{o}C-450^{o}C, flow rate was set to 0.2 and 0.3 mL/min, pressure was 25 bar and the H_2 flow rate was 100 mL/min.*

Temperature [C]	**Flow rate [mL/min]**	**Conversion [%]**	**TOF** $[s^{-1}]$	**Reaction rate** $[mol/g_{cat} \cdot s]$	**Selectivity to benzene [%]**
350	0.3	3.62	$6.94 \cdot 10^{-4}$	$5.3 \cdot 10^{-8}$	100
350	0.2	6.76	$8.63 \cdot 10^{-4}$	$6.6 \cdot 10^{-8}$	89.2
400	0.2	74.65	$9.53 \cdot 10^{-3}$	$7.3 \cdot 10^{-7}$	91.3
400	0.3	47.97	$9.18 \cdot 10^{-3}$	$7.0 \cdot 10^{-7}$	93.2
450	0.3	95.15	$1.82 \cdot 10^{-2}$	$1.4 \cdot 10^{-6}$	90.5
450	0.2	93.11	$1.19 \cdot 10^{-2}$	$9.1 \cdot 10^{-7}$	88.8

Table 4.14: *Results from the repeatability measurement with the MoP/TiO_2 catalyst made during spring 2013. The temperature varied between 350^{o}C-450^{o}C, flow rate was set to 0.2 and 0.3 mL/min, pressure was 25 bar and the H_2 flow rate was 100 mL/min.*

Temperature [C]	**Flow rate [mL/min]**	**Conversion [%]**	**TOF** $[s^{-1}]$	**Reaction rate** $[mol/g_{cat} \cdot s]$	**Selectivity to benzene [%]**
350	0.3	3.05	$6.05 \cdot 10^{-4}$	$3.8 \cdot 10^{-8}$	80.0
350	0.2	3.39	$4.49 \cdot 10^{-4}$	$2.8 \cdot 10^{-8}$	81.3
400	0.2	19.20	$2.54 \cdot 10^{-3}$	$1.6 \cdot 10^{-7}$	95.4
400	0.3	12.55	$2.49 \cdot 10^{-3}$	$1.6 \cdot 10^{-7}$	95.5
450	0.3	55.57	$1.10 \cdot 10^{-2}$	$6.9 \cdot 10^{-7}$	99.0
450	0.2	66.19	$8.75 \cdot 10^{-3}$	$5.5 \cdot 10^{-7}$	98.1

As seen in Tables 4.13 and 4.14, the conversion was higher for the catalyst made during autumn 2012 than during spring 2013, even though they had the same metal loading and were made by the same procedure. The characterization results from

Section 4.1 showed very similar results for both catalysts, but the dispersion was higher for the catalyst made in 2012. In Section 4.2.1 it was discussed that higher dispersion caused lower activity, however, this was not the trend in this experiment. Possible sources of error in this experiment are differences in the packing and isolation of the reactor and variations in catalyst particle size distribution. Between the experiments, the heating tape and the thermocouple, which measured the temperature inside the reactor, were changed. This could have caused different reaction temperatures and therefore different activities.

A third experiment was also done with another MoP/TiO_2 catalyst, which was made during spring 2013. Even though the catalyst was made with the same metal loading and procedure as the other catalysts, the catalyst showed almost no activity in the HDO reaction. This means that the repeatability is not good, and there are high uncertainties in the results. The characterization results showed that this catalyst had lower surface area and metal dispersion than the other catalysts. The same procedure was used. However, there could have been variations in the stirring and drying rate during impregnation and variations in the heating rates during calcination and reduction. Small changes in the catalyst preparation procedure can therefore change the catalyst properties and activity significantly.

4.2.7 Blank run

To investigate the influence of the support and inert in the reactor, one measurement was done with pure calcinated TiO_2 support and another measurement was done with inert SiC. The reaction conditions were set similar to the measurements from Section 4.2.1, where MoP catalysts with different supports were compared with each other. The temperature varied from 350^{o}C to 450^{o}C, the flow rate was set to 0.2 mL/min, H_2 flow rate was 100 mL/min and the pressure was 25 bar. The conversion, WHSV and carbon balance are given in Table 4.15.

The measurements without catalyst showed no activity and no products were formed. This means that only the MoP particles are active in this reaction. In Section 4.1 and 4.2.1, it was discovered that the choice of support had large influence on the characterization and activity of the catalysts. However, the supports themselves and the inert SiC are not active in the reaction.

Table 4.15: *Results from the blank run. The reactor was filled with inert SiC and pure calcinated TiO_2 support. The temperature varied between 350^oC to 450^oC, the flow rate at 0.2 mL/min, H_2 flow rate at 100 mL/min and the pressure was 25 bar.*

Temperature [**C**]	**Flow rate** [**mL/min**]	**Reactor fill**	**Conversion** [%]	**WHSV** [$g_{fenol}/g_{cat} \cdot h$]	**Carbon balance** [%]
350	0.2	TiO_2	0	0.31	21.9
400	0.2	TiO_2	0	0.31	7.4
450	0.2	TiO_2	0	0.31	3.7
350	0.2	Inert SiC	0	0.31	1.0
400	0.2	Inert SiC	0	0.31	0.4
450	0.2	Inert SiC	0	0.31	-0.1

4.3 Suggestions for future work

The results from the repeatability measurement of the MoP/TiO_2 catalysts show that there are some uncertainties in the activity results. More measurements are therefore needed to discover various sources of error and to obtain good repeatability of the results.

In this project, only the MoP/TiO_2 catalyst was tested for deactivation. The other catalysts could also be tested in order to investigate if there are variations in the deactivation rate or mechanism.

The measurement with different H_2/oil ratio did not show significant changes in the catalyst activity, mainly due to the low amount of phenol in n-decane. It would be interesting to investigate the same measurement with more phenol in the feed solution.

As discussed in Section 4.2.5, increased activation energy with increased metal dispersion is the opposite trend than in literature.[55] Further work is therefore needed to confirm this trend.

Even though phenol is a good model for bio-oil, it is also necessary to investigate the well-functioning catalysts on real bio-oil. In the real oil, more reactions take place which all could influence the catalyst. It would also be interesting to compare the deactivation rate of real bio-oil with phenol.

It has been reported that Ni_2P has higher activity than MoP in HDS of dibenzothiophene and HDN of quinoline,[26] and that unsupported Ni_2P has higher activity than unsupported MoP in a HDO reaction of 4-methyl phenol.[27] However, there are no reports of a comparison of Ni_2P/Al_2O_3 and Ni_2P/TiO_2 with the catalysts in this project in a HDO reaction of phenol.

5 Conclusion

The main goal of this thesis was to test the supported MoP catalysts which were made during autumn 2012, in a HDO reaction of phenol to benzene. New samples of the 2 most active catalysts, MoP/Al_2O_3 and MoP/TiO_2, were successfully prepared, characterized with N_2-adsorption, chemisorption, XRD and TPR, and tested at the HDO rig with varying temperature, flow rate, pressure and H_2/oil ratio.

The results from the N_2-adsorption showed that the BET surface area of the calcinated supports was higher for Al_2O_3 than for TiO_2. The TPR plots of the samples showed reduction peaks which fitted the reduction intervals reported in literature, where MoO_3 is reduced with H_2 to MoP in 3 stages. By using the *cut and weigh* method, it was discovered that the MoP/TiO_2 catalyst had the highest H_2 consumption during the reduction and therefore had a deeper reduction than the MoP/Al_2O_3 catalyst. The metal dispersion of the catalysts increased in the order $MoP/TiO_2 < MoP/Al_2O_3 < MoP/ZrO_2 < MoP/SiO_2$. The calculated particle size was low, which was confirmed by the XRD analyses. No peaks indicating formation of MoP particles were visible, probably because the particles were too small to be detected.

The activity of the catalysts increased in the order $MoP/SiO_2 < MoP/ZrO_2 < MoP/Al_2O_3 < MoP/TiO_2$. The 2 last catalysts showed full conversion at the highest temperature, 450^oC. There was no influence from the support or the reactor, as the results with pure calcinated support and inert SiC showed no activity. There was an opposite trend between the metal dispersion and activity, which also has been reported in literature. Benzene is the primary product as the selectivity to benzene remained very high for all flow rates and temperatures. The conversion to cyclohexane was highest at the lowest temperatures. As the conversion increased, more cyclohexane and methyl cyclopentane was formed.

The MoP/TiO_2 catalyst deactivated over time, most likely due to coking and sintering of the catalyst. The H_2/oil ratios and pressures were set to industrial conditions. Variations in the H_2/oil ratio showed little effect of the activity, due to the low phenol content in the feed mixture. Variations in the pressure also showed little effect of the activity, which also is reported in literature. The calculated activation energy was high, indicating that the surface reaction is the rate determining step.

The repeatability measurements of the different MoP/TiO_2 catalyst showed that there are large uncertainties in the results. Even though the catalysts were made with the same procedure and tested with the same conditions, the differences in the results were significant. However, small variations in the stirring and drying rate during catalyst preparation could have changed the catalyst properties. Replacement of the thermocouple and heating tape may also have influenced the results. More research is therefore needed to obtain a good repeatability and to verify the results.

References

[1] Crocker, M. *Thermochemical conversion of biomass to liquid fuels and chemical*; RCS Publishing, 2010.

[2] International Energy Agency, *World Outlook*; 2009.

[3] Maloney, S. *Taylor and Francis* **2008**, *50*, 129–150.

[4] Energy Information Agency, *International Energy Outlook*; 2009.

[5] Fisher, K.; Beitler, C.; Rueter, C.; Rochelle, G.; Jassim, M. *Integration MEA regeneration with CO2 compression and peaking to reduce CO2 capture cost - final report*; 2005.

[6] Huber, G.; Corma, A. *Angewandte Chemie* **2007**, *46*, 7184–7201.

[7] Elliot, D. *Energy and Fuels* **2007**, *21*, 1792–1815.

[8] Huber, G.; Iborra, S.; Corma, A. *Chem. Rev.* **2006**, *106*, 4044–4098.

[9] Moulijn, J.; Makkee, M.; van Diepen, A. *Chemical process technology*; Wiley, 2008.

[10] Oyama, S.; Clark, P.; V.L.S., T.; Lede, E.; Requejo, F. *J. Phys. Chem.* **2001**, *105*, 4961–4966.

[11] Phillips, D.; Sawhill, S.; Self, R.; Bussell, M. *Journal of Catalysis* **2002**, *207*, 266–273.

[12] Naik, S.; Goud, V.; Rout, P.; Dalai, A. *Renewable and Suitable Energy Reviews* **2010**, *14*, 578–597.

[13] Centi, G.; van Santen, R. *Catalysis for Renewables*; Wiley-VCH, 2007.

[14] Czernik, S.; Brigdwater, A. *Energy and fuels* **2004**, *18*, 590–598.

[15] Lappas, A.; Samolada, M.; Iatridis, D.; Voutekakis, S.; Vasalos, I. *Fuel* **2002**, *81*, 2087–2095.

[16] Wildsschut, J.; Mahfud, F.; Venderbosch, R.; Heeres, H. *Industrial and Engineering Chemistry Research* **2009**, *48*, 10324–10334.

[17] Choudhary, T.; Phillips, C. *Applied catalysis A: General* **2011**, *397*, 1–12.

[18] Furimsky, E. *Applied catalysis A:General* **2000**, *199*, 147–190.

[19] Elliott, C., D; Oasmaa, A. *Energy and Fuels* **1991**, *5*, 102–109.

[20] Conti, L.; Scano, G.; Boufala, J.; Mascia, S. *Development in thermochemical biomass conversion*; Chapman and Hall, 1997.

[21] Senol, O.; Ryymin, E.; Viljava, A., T.R.and Krause *Journal of Molecular Catalysis A: Chemical* **2007**, *277*, 107–112.

[22] Ryymin, E.; Honkela, M.; Viljava, T.; Krause, A. *Applied Catalysis A:General* **2010**, *389*, 114–121.

[23] Wildschut, J.; Melian-Cabrera, I.; Heeres, H. *Applied Catalysis B: Environmental* **2010**, *99*, 298–306.

[24] Gevert, B.; Otterstedt, J.; Massoth, F. *Applied Catalysis* **1987**, *31*, 119–131.

[25] Ghampson, I.; Sepulveda, C.; Garcia, R.; Garcia-Fierro, J.; Escalona, N.; W.J., D. *Applied Catalysis A: General* **2012**, *435-436*, 51–60.

[26] Oyama, S.; Gott, T.; Zhao, H.; Lee, Y. *Catalysis Today* **2009**, *143*, 94–107.

[27] Whiffen, V.; Smith, K. *Topics in Catalysis* **2012**, *55*, 981–990.

[28] He, Z.; Wang, X. *Catalysis for sustainable energy* **2012**, *1*, 28–52.

[29] Clark, P.; Oyama, S. *Journal of Catalysis* **2003**, *218*, 78–87.

[30] Montesinos-Castellanos, A.; Zepeda, T.; Pawelec, B.; Fierro, J.; de los Reyes, J. *Chem. Mater.* **2007**, *19*, 5627–5636.

[31] Stinner, C.; Prins, R.; Weber, T. *Journal of Catalysis* **2000**, *191*, 438–444.

[32] Chorkendorff, I.; Niemantsverdriet, J. *Concepts of modern catalysis and kinetics*; Wiley, 2007.

[33] Hadjiivanov, K.; Klissurski, D. *Chemical Society Reviews* **1996**, *25*, 61.

[34] Yamaguchi, T. *Catalysis today* **1994**, *20*, 199–218.

[35] Richardson, J. *Principles of Catalyst Development*; Plenum Press, 1989.

[36] Holmen, A. *Hetrogen katalyse*; Institutt for kjemisk prosessteknologi, NTNU, 2002.

[37] Sing, K.; Everett, D.; Haul, R.; Moscou, L.; Pierotti, R.; J., R.; Siemieniewska, T. *Pure and applied chemistry* **1985**, *57*, 603–619.

[38] Vannice, A. *Kinetics and catalysis reactions*; Springer, 2005.

[39] Butt, H.; Graf, K.; Kappl, K. *Physics and chemistry of interfaces*; Wiley, 2006.

[40] Goldberg, S.; Criscenti, L.; Turner, D.; Davis, J.; Cantrell, J. *Vadose Zone Journal* **2007**, *6*, 407–435.

[41] Greibrokk, T.; Lundanes, E.; Rasmussen, K. *Kromatografi, Separasjon og deteksjon*; Universitetsforlaget, 2005.

[42] Ravindranath, B. *Principles and practice of chromatography*; Ellis Horwood Limited, 1989.

[43] Kaeding, W. *Journal of catalysis* **1985**, *95*, 512–519.

[44] Zumdahl, S. *Chemical principles*; Houghton Mifflin Company, 2005.

[45] Asphaug, S. *Catalytic hydrodeoxygenation of bio-oils woth supported MoP-catalysts*; Specialization project, TKP 4510, 2012.

[46] Vassilieva, E.; Hadjiivanov, K.; Stoychev, T.; Daiev, C. *Analyst* **2000**, *125*, 693–698.

[47] Carlsen, C. Hydrotreating of bio-oils over metal-phosphide catalyst. Master's thesis, Deparment of Chemical Engineering at Norwegian University of Science and Technology, 2012.

[48] Whiffen, V. M. L.; Smith, K. *Energy and fuels* **2010**, *24*, 4728–4737.

[49] Schacht, P.; Hernandez, G.; Cedeno, L.; Mendoza, J.; Ramirez, S.; Garcia, L.; Ancheyta, J. *Energy and fuels* **2003**, *17*, 81–86.

[50] Zhang, W.; He, Y.; Zhang, M.; Yin, Z.; Chen, Q. *Journal of Physics D: Applied Physics* **2000**, *33*, 912–916.

[51] Teng, Y.; Wang, A.; Li, X.; Xie, J.; Wang, Y.; Hu, Y. *Journal of Catalysis* **2009**, *266*, 369–379.

[52] Sun, F.; Wu, W.; Wu, Z.; Guo, J.; Wei, Z.; Yang, Y.; Jiang, Z.; Tian, F.; Li, C. *Journal of Catalysis* **2004**, *228*, 298–310.

[53] Zhao, H.; Li, D.; Bui, P.; Oyama, S. *Applied Catalysis A: General* **2011**, *391*, 305–310.

[54] Oyama, S. *Journal of catalysis* **2003**, *216*, 343–352.

[55] Reuel, R.; Bartholomew, C. *Journal of Catalysis* **1984**, *85*, 78–88.

[56] Ohta, H.; Kobayashi, H.; Hara, K.; Fukuoka, A. *Chemical communications* **2011**, *47*, 12209–12211.

[57] Papp, J.; Soled, S.; Dwight, K.; Wold, A. *Chemistry of materials* **1994**, *6*, 496–500.

[58] Hsu, C. S.; P.R., R. *Practical Advances in Petroleum Processing*; Springer, 2006.

[59] Su-Ping, Z. *Taylor and Francis* **2003**, *25*, 57–65.

[60] Mortensen, P.; Grunwaldt, J.; Jensen, P.; Knudsen, K.; Jensen, A. *Applied Catalysis A: General* **2011**, *407*, 1–19.

A List of chemicals

All chemicals used in this project are given in Table A.1.

Table A.1: *List of chemicals used in this project*

Chemical	**Chemical formula**	**State**	**Purpose**	**Supplier**	**Purity**
Ammonium hydrogen phosphate	$(NH_4)_2HPO_4$	s	Precursor	Alfa Aesar	98%
Ammonium molybdate (para)tetrahydrate	$(NH_4)_6Mo_7O_{24} \cdot 4\,H_2O$	s	Precursor	Alfa Aesar	81-83%
γ-Alumina	Al_2O_3	s	Support	Strem Chemicals	97%
Silicon oxide	SiO_2	s (pellets)	Support	Alfa Aesar	100%
Zirconium oxide	ZrO_2	s (pellets)	Support	Alfa Aesar	100%
Titanium(IV) oxide	TiO_2	s (pellets)	Support	Alfa Aesar	100%
Hydrogen in Argon	H_2 in Ar	g	TPR	YaraPraxiar	7%
Hydrogen	H_2	g	TGA, HDO feed	YaraPraxair	100%
Argon	Ar	g	TGA	YaraPraxair	100%
Nitrogen	N_2	l	N_2-adsorption	AGA	100%
Helium	He	g	Reduction, HDO	YaraPraxair	
Nitrogen	N_2	g	Inert in HDO	YaraPraxair	
Oxygen in Argon	O_2 in Ar	g	Passivation	YaraPraxair	1%
Phenol	C_6H_5OH	s	HDO feed	Alfa Aesar	99%
n-Decane	$CH_3(CH_2)_8CH_3$	l	HDO feed	Alfa Aesar	99%
Pentanol	$C_5H_{12}O$	l	Internal Standard	Merck	98%

B Catalysts preparation

B.1 Calculation of metal loading

In this section, the amount of precursor needed to obtain 15 wt% Mo-loading on the support is calculated. The desired Mo/P molar ratio was 1:1. The source of molybdenum was ammonium molybdate tetrahydrate $(NH_4)_6Mo_7O_{24} \cdot 4\,H_2O$ and of phosphorus was ammonium phosphate $(NH_4)_2HPO_4$. The properties of the precursors are given in Table B.1.

Table B.1: *Properties of catalyst precursor*

Molecule	**Molar Weight [g/mol]**	**Solubility [g/100 ml water]**
$(NH_4)_6Mo_7O_{24} \cdot 4\,H_2O$	1235.9	43.0
$(NH_4)_2HPO_4$	131.9	57.5
Mo	95.9	-
P	31.0	-

The loading was calculated to 10.0 g of catalyst.

$$m_{Mo15\%} = 1.5\ g \tag{B.1}$$

$$N_{Mo15\%} = \frac{m_{Mo15\%}}{M_{\mathrm{Mo}}} = \frac{1.5\ g}{95.9\ g/mol} = 0.016\ mol \tag{B.2}$$

From the Mo precursor, 7 mol Mo is obtained from 1 mol $(NH_4)_6Mo_7O_{24} \cdot 4\,H_2O$. The purity of the Mo precursor was 82%. The amount of Mo precursor needed is:

$$m_{(NH_4)_6Mo_7O_{24}\cdot 4\,H_2O} = \frac{N_{\mathrm{Mo}}}{7 \cdot 0.82} \cdot M_{(NH_4)_6Mo_7O_{24}\cdot 4\,H_2O} = \frac{0.016}{7 \cdot 0.82} \cdot 1235.9 = 3.4\ g \tag{B.3}$$

As the Mo/P-ratio = 1, $N_{\mathrm{Mo}} = N_{\mathrm{P}}$. From the P precursor, 1 mol P is obtained from 1 mol $(NH_4)_2HPO_4$. The purity of the P precursor was 98%. The amount of

P precursor needed is:

$$m_{(NH_4)_2HPO_4} = \frac{N_P}{1 \cdot 0.98} \cdot M_{(NH_4)_2HPO_4} = \frac{0.016}{1 \cdot 0.98} \cdot 131.9 = 2.2\ g \tag{B.4}$$

To calculate the amount of support needed, the weight of P in the precursor needs to be calculated.

$$m_{P15\%} = N_P \cdot M_P = 0.016 \cdot 31.0 = 0.5\ g \tag{B.5}$$

The amount of support needed to make 10 g of catalyst is:

$$m_{Support} = 10\ g - m_{Mo} - m_P = 10.0\ g - 1.5\ g - 0.5\ g = 8.0\ g \tag{B.6}$$

B.2 Incipient wetness method

In this section, the procedure for the incipient wetness method is described. The incipient wetness point for each support is listed in Table B.2, and the solubility of the precursors were given and are listed in Table B.1.

After the supports were crushed and sieved, they were calcinated at 500^oC for 5 h. The required amount of precursor needed to make 15 $wt\%$ MoP loadings are given in Appendix B.1. The precursors were dissolved in required amount of deionized water according to the solubility of the precursors in water. The amount of precursor, support and deionized water used is given in Table B.2. As 8 g support was used, the incipient wetness points for 8 g support are also given in Table B.2. In both cases, the water content in the precursor mixture was higher than the incipient wetness point. Therefore the impregnation was made twice for these supports. It was difficult to determine how much water was needed to reach the wetness level. As the metal filled the pores, the next impregnation required less solution than the first time.

Table B.2: *The amount precursor, support and deionized water used in the incipient wetness method*

Catalyst	**Incipient wetness point [g water/8g support]**	**Support [g]**	**$(NH_4)_6Mo_7O_{24} \cdot 4H_2O$ [g]**	**$(NH_4)_2HPO_4$**	**Deionized water [g]**
MoP/Al_2O_3	8.536	8.0163	3.3764	2.1027	11.4863
MoP/TiO_2	8.056	8.0588	3.3494	2.1196	11.4887

C Characterization methods

C.1 N_2-adsorption procedure

In this section, the procedure for the N_2-adsorption is described. A Micromeritics TriStar II was used for N_2-adsorption, and Micromeritics VacPrep 061 was used for degassing. The apparatus are located on 4th floor of Department of Chemical Engineering, NTNU.

The following steps were used in the BET-measurement.

1. Fill the tube with 100-200 mg of sample.
2. Insert the sample tube to the degassing apparatus.
3. Close the valve and turn the control knob to *vacuum*.
4. Slowly open the valve and place the sample tube at the heating station for degassing overnight.
5. After degassing, place the sample tube at the cooling station for one hour, close the valve, turn the control knob to *gas*, open the valve and weigh the sample.
6. Slide a jacket down the stem of the sample tube and attach it to the N_2-adsorption apparatus.
7. Fill the dewar with liquid nitrogen and place it on the elevator.
8. Start the BET-program.

C.2 XRD procedure

In this section, the procedure of the XRD analysis is described. A Bruker AXS D8 Focus with CuKα radiation was used. The apparatus is located on the 1st floor of the Department of Materials Science and Engineering, NTNU.

The following steps were used in the XRD analysis.

1. Wash the sample holders with ethanol and water.
2. Place the dried sample holder on aluminum foil. Pour the catalyst sample on the sample holder and cover it with another aluminum foil. Use another sample holder to evenly distribute the catalyst. Use a sheet of glass to obtain a smooth catalyst surface on the sample holder.
3. Insert the sample in the XRD apparatus and choose the desired slit size. Check that the door is properly closed.
4. Make a parameter file in the XRD Wizard software. Choose the desired angles, step size and the time step.
5. Open the XRD Analysis software. Press *Jobs* and *Create jobs*. Choose the parameter file and the destination of the raw result file.
6. Start the analysis.

C.3 TPR procedure

In this section, the procedure for TPR is described. The apparatus used in this project was a Quantachrome Chembet-3000, and it is located on 4th floor of the Department of Chemical Engineering, NTNU.

The following steps were used in the TPR-measurement.

1. Fill the U-shaped reactor with quartz wool and 100 mg of catalyst sample and attach the thermocouple in the opposite tube.

2. Turn on the calibration gas (Ar) and the reduction gas (7% H_2 in Ar). Adjust the calibration gas so the calibration vent blows gas through a water flask. Control that the selector valve of the reduction gas is set on position 2. Switch the path selector to *Sample cell by-pass*. Adjust the flow of the reduction gas to 40-70 (corresponds to 3-4 mL/min).

3. Attach the heating mantle to the sample cell, and turn on the calibration gas. Set the temperature to 300^oC and leave the sample there for 30 min.

4. After the heating, set the temperature to 0^oC, and attach the sample cell to the analysis station.

5. Rest the ceramic ring on top of the furnace and isolate it with quartz wool.

6. Switch the path selector to *Sample cell* and control that the flow does not decrease below 40.

7. Press the *DES* to choose TPR measurement. Adjust the detector to zero by switching the attenuation dial to infinity (∞) and use *Zero adjust* to adjust to zero.

8. Switch the attenuation dial to 32 and wait for the signal to stabilize.

9. Open the TPRwin program and select TPR from the Data Acquisition menu.

10. Set the furnace heating to 10^oC/min by pushing *UP* and *DOWN* simultaneously, and push *UP* until **glbl** appears. Press *mode* until **rate** appears and set the desired temperature rate. Push *display* to to set the desired temperature.

11. Press *Start Analysis* on the software.

After the experiment

1. Press *End Experiment* on the software.
2. Set the temperature to 20^{o}C.
3. Switch the path selector to *Sample cell by-pass* before removing the sample cell.
4. Turn off the reduction gas.

C.4 Cut and weigh method

In this section, the calculations and procedure of the cut and weigh method are given. The cut and weigh method is an effective method to determine the relative area under a plot, and in this case, the relative H_2-consumption at the first β peak. An assumption was made that the papers used were of such good quality so there were no density gradients on the paper. The plots used were Figures 4.3-4.6. The area interval was limited to where the signal begins to increase and the local minimum after the first β peak.

Following are the calculations of the MoP/Al_2O_3 sample. The total area of the plot was limited by $x = 656^oC$ and $y = 45\ mV$. The total area was calculated to

$$A_{plot} = 656^oC \cdot 45mV = 29520^oC \cdot mV$$

The area weighed $m_{plot} = 1.8529\ g$, and the area/g paper was calculated to

$$Area/g = \frac{29520}{1.8529}\ C \cdot mV/g = 15932C \cdot mV/g$$

The area under the curve weighed $m_{curve} = 0.1516\ g$, and the area under the curve was calculated to

$$A_{curve} = 0.1516\ g \cdot 15932C \cdot mV/g = 2415^oC \cdot mV$$

The results for all samples are given in Table C.1.

Table C.1: *Calculations of the relative H_2 consumption at the β-peak in the TPR analysis by using the cut and weigh method.*

Support	**Area plot [mV·C]**	**Weight plot [g]**	**Area/g paper**	**Weight curve [g]**	**Area curve [mV·C]**
Al_2O_3	29520	1.8529	15932	0.1516	2415
SiO_2	29655	1.9860	14932	0.2264	3380
TiO_2	32850	1.9964	16319	0.3834	6256
ZrO_2	31500	1.9631	16046	0.1971	3162

C.5 Chemisorption procedure

In this section, the procedure for chemisorption is described. The apparatus is a Micromeritics ASAP 2020, and it is located on the 4th floor of the Department of Chemical Engineering, NTNU.

The following steps were used in the chemisorption measurement.

1. Insert quartz wool and 200 mg of catalyst sample into the special-made reactor.
2. Attach the reactor to the apparatus and thermocouple.
3. Evacuate the sample by lowering the pressure to below 0.003 mmHg. Check for leaks by measuring that the pressure does not change more than 50 μmHg/min, 2 hours after the evacuation.
4. Raise the furnace.
5. Put in the data in the sample information analysis conditions and report options.
6. Start the analysis.

After the analysis:

1. Lower the furnace.
2. Check for atmospheric pressure in the reactor before moving it from the apparatus.
3. Weigh the sample and calculate the changes in the mass.

C.6 Calculation of dispersion and particle size

In this section, the dispersion and particle size of the 15 wt% MoP/TiO_2 catalyst is calculated.

The data given are:

M_{Mo}	$= 95.9\ g/mol$
N_A	$= 6.022 \cdot 10^{23}\ g/cm^3$
ρ_{Mo}	$= 10.2\ g/cm^3$
σ_{Mo}	$= 7.3 \cdot 10^{-16}\ cm^2$
V	$= 1.71 \cdot 10^{-6}\ m^3/g\ STP$
V_m	$= 2.24 \cdot 10^{-2} m^3/g$
F	$= 1$
f	$= 6$

The values of σ, ρ and V_m were given from the chemisorption software. The adsorption of gas by selective chemisorption v_{ads} is given in Equation 2.10.

$$v_{ads} = \frac{V}{V_m} = \frac{1.71 \cdot 10^{-6}\ m^3/g}{2.24 \cdot 10^{-2}} = 7.63 \cdot 10^{-5} \tag{C.1}$$

To calculate the dispersion, an assumption that one surface atom is covered by one adsorbed molecule is made ($F = 1$). The dispersion is given in Equation 2.9

$$D = \frac{v_{ads} \cdot M_m \cdot F}{x_m} = \frac{7.63 \cdot 10^{-5} \cdot 95.9 \cdot 1}{0.15} = 4.9\% \tag{C.2}$$

To calculate the particle diameter, the specific volume needs to be calculated. The specific volume is given by Equation 2.12.

$$V_{sp} = \frac{1}{\rho_{Mo}} = \frac{1}{10.2\ g/cm^3} = 9.8 \cdot 10^{-2} cm^3/g \tag{C.3}$$

The particle diameter is given by Equation 2.11. The factor f was set to 6 by assuming spherical particles.

$$d = \frac{f \cdot V_{sp} \cdot M_{Mo}}{\sigma_M \cdot N_A \cdot D} = \frac{6 \cdot 9.8 \cdot 10^{-2} \cdot 95.9}{7.3 \cdot 10^{-16} \cdot 6.022 \cdot 10^{23} \cdot 0.049} = 2.62 \cdot 10^{-6}\ cm = 26.2\ nm \tag{C.4}$$

D Additional results

D.1 Additional N_2-adsorption results

The isotherm plot and pore volume distribution plot for calcinated supports, calcinated impregnates and reduced catalysts are given in Figures D.1-D.2.

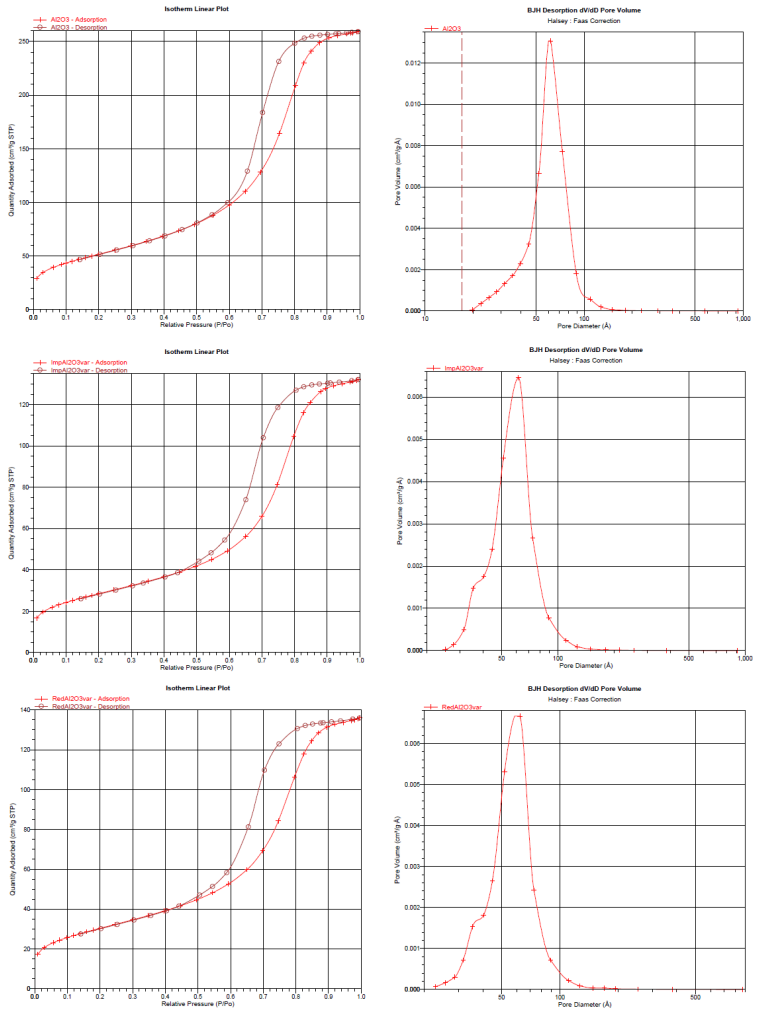

Figure D.1: *Isotherm plot and pore volume distribution plot for pure Al_2O_3, calcinated impregnates and reduced samples*

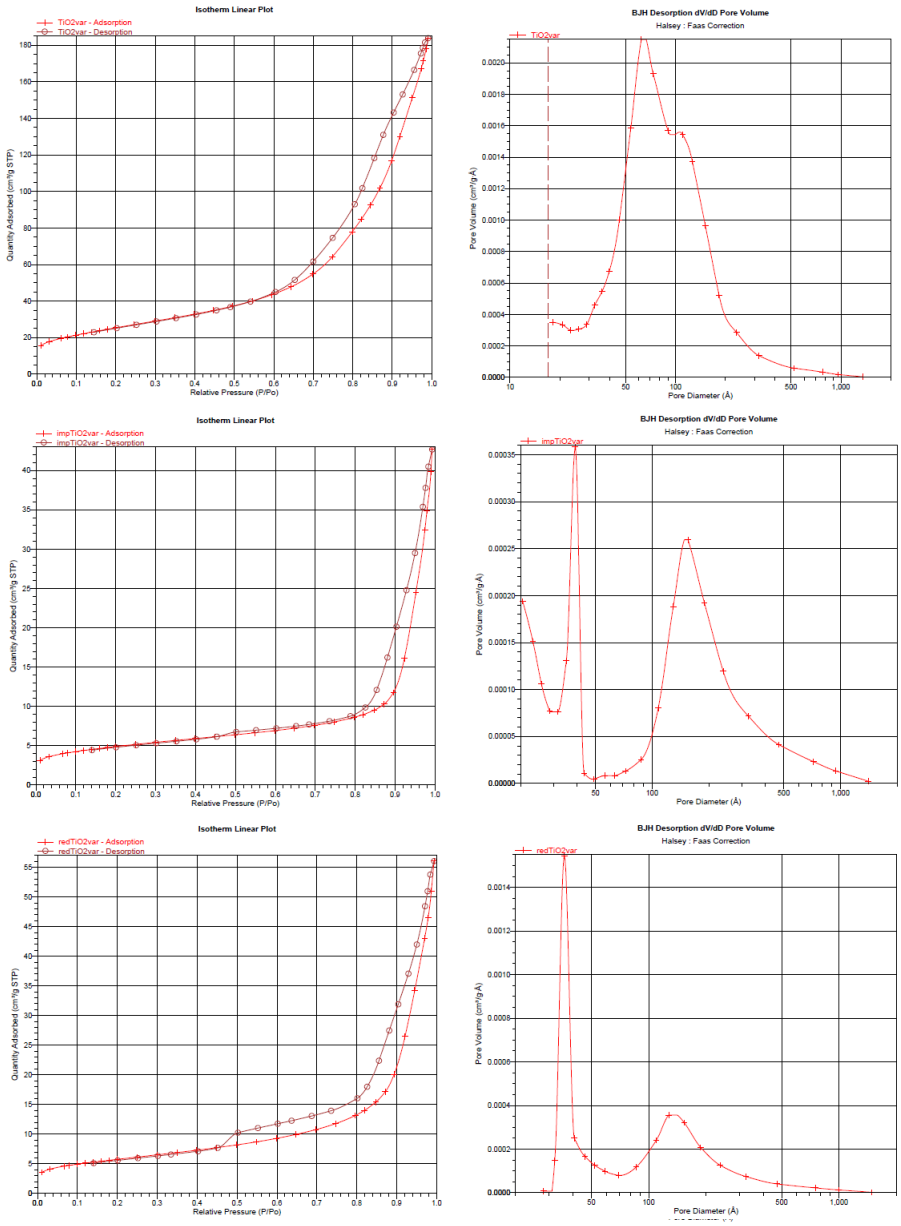

Figure D.2: *Isotherm plot and pore volume distribution plot for pure TiO_2, calcinated impregnates and reduced samples*

D.2 Additional chemisorption results

The line fit plots of the isotherm plots of the reduced catalysts are given in Figures D.3-D.8. The results for the catalysts made during autumn 2012 are given in Figures D.3-D.6, and the catalysts made during spring 2013 are given in Figures D.7-D.8. The plots were adjusted in the chemisorption software, so the extrapolating of the plot started at 150 mmHg.

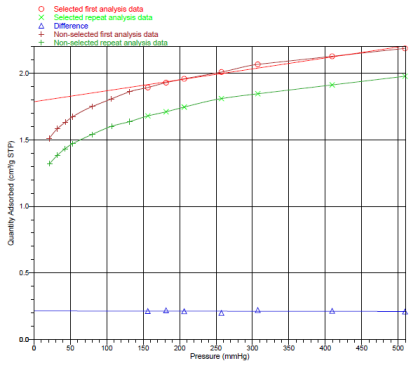

Figure D.3: *Line fit plot of the reduced MoP/Al_2O_3 catalyst, made during autumn 2012*

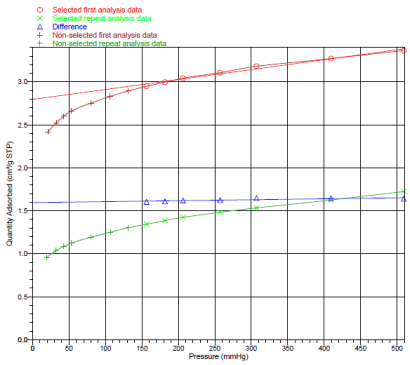

Figure D.4: *Line fit plot of the reduced MoP/SiO_2 catalyst, made during autumn 2012*

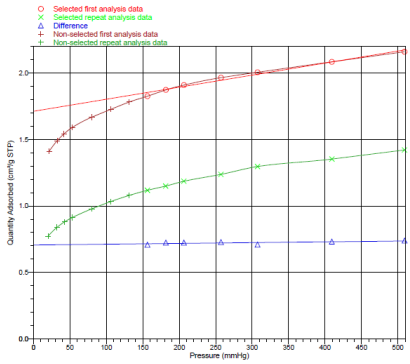

Figure D.5: *Line fit plot of the reduced MoP/TiO_2 catalyst, made during autumn 2012*

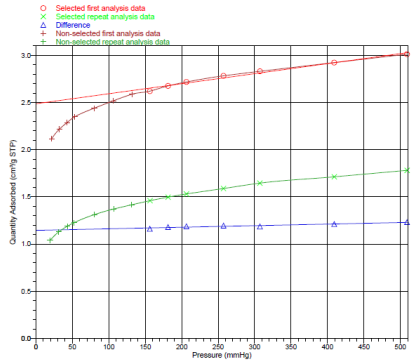

Figure D.6: *Line fit plot of the reduced MoP/ZrO_2 catalyst, made during autumn 2012*

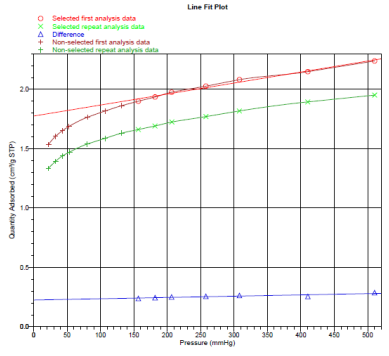

Figure D.7: *Line fit plot of the reduced MoP/Al_2O_3 catalyst, made during spring 2013*

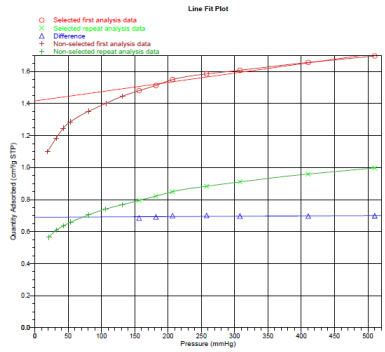

Figure D.8: *Line fit plot of the reduced MoP/TiO_2 catalyst, made during spring 2013*

E Activity measurement

E.1 Procedure

In this section, the procedure for activity measurement is described. The apparatuses and process rig used in this project are located in Chemistry Hall D at the Department of Chemical Engineering, NTNU. The gas chromatography apparatuses used are on-line Agilent Technologies 6890N and off-line Agilent Technologies 6850. The feed pump used is a Hewlett Packard 1050.

1st day - Reactor preparation

1. Check that the N_2, H_2 and air bottles contain enough gas for the measurement, and that the He gas for the GC analysis is connected to the rig.
2. Load the samples with silicon carbide, quartz wool and catalyst, as shown in Figure 3.1. Insert the thermocouple.
3. Attach the reactor to the rig. Tight another thermocouple on the outside of the reactor with an insulating tape.
4. Isolate the reactor with quartz wool and 3 turns of heating tape. Isolate the heating tape with more quartz wool and fasten it with insulating tape. Make sure that the heating tape does not overlap and come in contact with the reactor.
5. Turn on the N_2 flow and check for gas leakage from the reactor.
6. Turn on the H_2 flow and do another gas leak test.
7. Activate the catalyst by flowing H_2 (100 mL/min, 33% opening) and N_2 (40 mL/min, 10% opening) at 450^oC for 2 h.
8. After the activation, turn off the H_2 flow and let N_2 flow through the reactor overnight at 200^oC.
9. Turn the oven temperature in the on-line gas GC to 250^oC.

2nd day - Activity measurement

1. Decrease the oven temperature in the on-line gas GC to 50^{o}C. Open the gas flow to the gas GC to 25 bar (5 turns with the valve).

2. Prepare the feed by mixing 1 vol% phenol in 125 mL n-decane. Dissolve the phenol by using an ultrasonic bath at 35^{o}C for 1 h. Afterwards, connect the feed sample on the scale and attach it to the pump. Turn the reactor temperature to 350^{o}C.

3. Use the on-line gas GC software to choose the correct method and set a name for the experiment in *Sequence parameters* and *Sequence table*. Start the experiment by pushing *Sequence table* and *Run experiment*.

4. Open the purge valve, and set the pump to 5 mL/min to remove gas and old liquids from the pipes.

5. Set the pump to the desired flow rate, close the purge valve and open the valve to the reactor.

6. Take out the first waste sample after 15 min, note the temperature and weight of the sample. When taking out the sample, attach the sample bottle to the equipment and open the valve. Close the valve immediately after the liquid flow has ended.

7. Vary the flow rate, temperature, pressure and H_2 flow rate according to choice. If the temperature or pressure is changed, take out a waste sample after the desired temperature or pressure is achieved.

8. End the experiment by turning off the flow to the reactor, open valve to purge, turn off the pump and turn off the H_2 flow. Dry the reactor by flowing N_2 overnight at 200^{o}C and at atmospheric pressure.

9. Mix the samples and 9.9 mL of the feed with 10 mL pentanol. Run the samples in the off-line GC. Make sure there is enough n-decane and space for the waste.

E.2 Calculation of activity measurement

In this section, example calculations for the activity measurement are given. The catalyst used is 15 wt% MoP/ZrO_2. The calculations are done for the feed sample and sample 4 (0.2 mL/min and 400^{o}C). For the calculations of the activity energy, the 15 wt% MoP/TiO_2 is used.

E.2.1 Calculation of internal standard and correction

The data given are:

$$\begin{aligned}
\rho_{Phenol} &= 1.07\ g/mL \\
\rho_{n-Decane} &= 0.73\ g/mL \\
\rho_{Pentanol} &= 0.81\ g/mL \\
m_{phenol,feed} &= 1.4235\ g \\
m_{n-decane,feed} &= 89.5\ g \\
purity_{Pentanol} &= 98\%
\end{aligned}$$

	Flow [mL/min]	T [K]	Collected sample	Pentanol	Time [min]
Feed			6.9933	0.0694	
Sample 2	0.3	623	6.8500	0.0714	35
Sample 3	0.2	623	6.2818	0.0708	47
Sample 4	0.2	673	6.4930	0.0717	46
Sample 5	0.3	673	6.4119	0.0669	32
Sample 6	0.3	723	6.5740	0.0695	31
Sample 7	0.2	723	6.8584	0.0734	48

Pentanol is used as internal standard, thus the concentration of pentanol $C_{Pentanol}$ must be calculated in each sample.

In the feed

Total volume in the feed:

$$V_{feed,tot} = V_{phenol} + V_{n-decane} = \frac{1.4235\ g}{1.07\ g/mL} + \frac{89.5\ g}{0.73\ g/mL} = 123.9\ mL$$

Total volume in the feed sample:

$$V_{feed,sample} = \frac{m_{feed,sample} \cdot V_{feed,tot}}{m_{feed,tot}} + V_{pentanol} = \frac{6.9933\ g \cdot 123.9\ mL}{1.4235\ g + 89.5\ g} + \frac{0.0694\ g}{0.81\ g/mL}$$

$= 9.6\ mL$

The concentration of pentanol in the feed sample:

$$C_{pentanol} = \frac{m_{pentanol} \cdot Purity_{Pentanol}}{V_{feed,sample}} = \frac{0.0694\ g \cdot 0.98}{9.6\ mL} = 7.08 \cdot 10^{-3}\ g/mL$$

$= 7080\ ng/\mu L$

In sample 4

As seen from the table above, the sample consists mainly of n-decane. Therefore, an assumption that the total density of the sample is equal to the density of n-decane, is made.

Volume of sample:

$$V_{Sample\ 4} = \frac{m_{sample}}{\rho_{decane}} = \frac{6.4930\ g}{0.73\ g/mL} = 8.89\ mL$$

Concentration of pentanol in sample 4:

$$C_{Pentanol,sample4} = \frac{m_{pentanol} \cdot Purity_{Pentanol}}{V_{Sample\ 4}} = \frac{0.0717\ g \cdot 0.98}{8.89\ mL} = 7.90 \cdot 10^{-3}\ g/mL$$

$= 7900\ ng/\mu L$

Correction

An average concentration of each of the species in the sample is calculated based on the 5 different vial measurements. The average concentration is corrected based on the known concentration of pentanol in the samples.

The correction for phenol in sample 4:

$$\frac{C_{phenol,corr}}{C_{phenol,av}} = \frac{C_{pentanol,corr}}{C_{pentanol,av}}$$

$$C_{phenol,corr} = C_{phenol,av} \cdot \frac{C_{pentanol,corr}}{C_{pentanol,av}} = 11034 \cdot \frac{7900}{9141}\ ng/\mu L = 9536\ ng/\mu L$$

This gives the following results for the feed sample and sample 4, presented in Table E.1 and E.2 respectively.

Table E.1: *Calculation of corrected values in the feed sample, based on pentanol as internal standard*

Injection	**Pentanol [ng/μL]**	**Phenol [ng/μL]**	**n-Decane [ng/μL]**
1	9332	16982	1017070
2	9098	16506	978028
3	9083	16392	969156
4	8450	15087	890256
5	8733	15655	921483
Average	8939	16124	955199
Corrected	7080	12771	756534

Table E.2: *Calculation of corrected values in Sample 4, based on pentanol as internal standard*

Injection	**Methyl-cyclopentanol [ng/μL]**	**Benzene [ng/μL]**	**Cyclo-hexane [ng/μL]**	**Cyclo-hexene [ng/μL]**	**Pentanol [ng/μL]**	**Phenol [ng/μL]**	**n-Decane [ng/μL]**
1	0	2475	0	68	8543	10067	811450
2	0	2772	50	76	9505	11702	871652
3	0	2679	48	73	9218	11549	887008
4	0	2618	47	72	9045	10716	862415
5	0	2721	0	75	9397	11139	906175
Average	0	2653	29	73	9141	11034	867740
Corrected	0	2293	25	63	7900	9536	749877

E.2.2 Calculation of carbon balance

As all reactants and products contain 6 carbon atoms, the stoichiometric coefficient is not used in the calculations. It is assumed that phenol is the only reactant, and that methylcyclopentane, benzene, cyclohexane and cyclohexene are the only products.

Carbon into the reactor:

$$n_{C,in} = \frac{m_{phenol,in}}{M_{phenol}} = \frac{12.755 \cdot 10^{-3}\ g/mL}{94.1\ g/mol} = 1.35 \cdot 10^{-4}\ mol/mL$$

Carbon out of the reactor:

$$n_{C,out} = \frac{M_{phenol,out}}{M_{phenol}} + \frac{m_{methylcyclopentane}}{M_{methylcyclopentane}} + \frac{m_{benzene}}{M_{benzene}} + \frac{m_{cyclohexane}}{M_{cyclohexane}} + \frac{m_{cyclohexene}}{M_{cyclohexene}}$$

$$= \frac{9.536 \cdot 10^{-3}\ g/mL}{94.1\ g/mol} + \frac{0\ g/mL}{84.2\ g/mol} + \frac{2.293 \cdot 10^{-3}\ g/mL}{78.1\ g/mol} + \frac{0.025 \cdot 10^{-3}\ g/mL}{84.1\ g/mol} + \frac{0.063 \cdot 10^{-3}\ g/mL}{82.1\ g/mol}$$

$$= 1.32 \cdot 10^{-4}\ mol/mL$$

The difference between carbon in and out of the reactor:

$$Diff = \frac{n_{C,in} - n_{C,out}}{n_{C,in}} \cdot 100\% = \frac{1.35 \cdot 10^{-4}\ mol/L - 1.32 \cdot 10^{-4}\ mol/L}{1.35 \cdot 10^{-4}\ mol/L} \cdot 100\%$$

$$= 2.2\%$$

E.2.3 Calculation of conversion

The conversion of phenol is given by Equation 2.14. The conversion of phenol for sample 4 is:

$$x_{phenol} = \frac{n_{products}}{n_{phenol,out} + n_{products}}$$

$$= \frac{\frac{2.293 \cdot 10^{-3}\ g/mL}{78.1\ g/mol} + \frac{0.025 \cdot 10^{-3}\ g/mL}{84.1\ g/mol} + \frac{0.063 \cdot 10^{-3}\ g/mL}{82.1\ g/mol}}{\frac{9.536 \cdot 10^{-3}\ g/mL}{94.1\ g/mol} + \frac{2.293 \cdot 10^{-3}\ g/mL}{78.1\ g/mol} + \frac{0.025 \cdot 10^{-3}\ g/mL}{84.1\ g/mol} + \frac{0.063 \cdot 10^{-3}\ g/mL}{82.1\ g/mol}} \cdot 100\%$$

$$= 23.1\%$$

E.2.4 Calculation of selectivity

The selectivity to a product is given by Equation 2.15. The selectivity to benzene, methylcyclopentane, cyclohexane and cyclohexene are calculated. In this section,

the calculation for selectivity to benzene is presented.

$$S_{benzene} = \frac{n_{benzene}}{n_{benzene}+n_{methylcyclopentane}+n_{cyclohexane}+n_{cyclohexene}}$$

$$= \frac{\frac{2.293\cdot10^{-3}\ g/mL}{78.1\ g/mol}}{\frac{2.293\cdot10^{-3}\ g/mL}{78.1\ g/mol} + \frac{0\ g/mL}{78.1\ g/mol} + \frac{0.025\cdot10^{-3}\ g/mL}{84.1\ g/mol} + \frac{0.063\cdot10^{-3}\ g/mL}{82.1\ g/mol}} \cdot 100\%$$

$$= 96.5\%$$

E.2.5 Calculation of weight hourly space velocity (WHSV)

The WHSV is given by Equation 2.16. As the samples consist mainly of n-decane, an assumption is made that the total sample density is equal to the density of n-decane. The data given are:

$$\begin{aligned} \rho_{n-decane} &= 0.73\ g/mL \\ m_{cat} &= 0.4911\ g_{cat} \\ \upsilon_{tot} &= 0.2\ mL/min \end{aligned}$$

Amount of phenol in the feed:

$$X_{phenol} = \frac{m_{phenol}}{m_{phenol} + m_{n-decane}} = \frac{1.4235\ g}{1.4235\ g + 89.5\ g} = 0.016\ \frac{g_{phenol}}{g_{feed}}$$

Total flow in the reactor:

$$q_{tot} = \upsilon_{tot} \cdot \rho_{n-decane} = 0.2\ mL/min \cdot 0.73\ g/mL = 0.15\ g/min$$

Phenol in the total flow:

$$q_{phenol} = q_{tot} \cdot X_{phenol} = 0.146\ \frac{g_{feed}}{min} \cdot 0.016\ \frac{g_{phenol}}{g_{feed}} = 2.34 \cdot 10^{-3}\ g_{feed}/min$$

WHSV:

$$WHSV = \frac{q_{phenol}}{m_{cat}} = \frac{2.34 \cdot 10^{-3}\ g_{phenol}/min\ \cdot 60\ min/h}{0.4911\ g_{cat}} = 0.29\ \frac{g_{fenol}}{g_{cat} \cdot h}$$

E.2.6 Calculation of reaction rate and turnover frequency (TOF)

The TOF is given by Equation 2.17. 2 different TOFs based in total and differential dispersions are calculated. The data given are:

$$
\begin{aligned}
\upsilon_{sample4} &= 0.2\ mol/mL \\
m_{cat} &= 0.4911\ g_{cat} \\
x_{Mo} &= 0.15 \\
M_{Mo} &= 95.9\ g/mol \\
M_{phenol} &= 94.1\ g/mol \\
D_1 &= 0.065 \\
D_2 &= 0.019 \\
x_{phenol} &= 0.23
\end{aligned}
$$

Total volume in the feed:

$$V_{feed,tot} = V_{phenol} + V_{n-decane} = \frac{1.4235\ g}{1.07\ g/mL} + \frac{89.5\ g}{0.73\ g/mL} = 123.9\ mL$$

Concentration of phenol in the feed:

$$C_{phenol,feed} = \frac{m_{phenol}}{V_{feed}} = \frac{1.4235\ g}{123.9\ mL} = 0.011\ g/mL$$

Amount of phenol in the reactor, sample 4:

$$q_{phenol,sample4} = \frac{C_{phenol,feed} \cdot \upsilon_{sample4}}{M_{phenol}} = \frac{0.011\ g/mL \cdot 0.2\ mL/min}{94.11\ g/mol}$$

$$= 2.34 \cdot 10^{-5}\ mol/min$$

Amount of phenol out of the reactor (converted):

$$q_{phenol,out} = q_{phenol,in} \cdot x_{phenol} = 2.34 \cdot 10^{-5}\ mol/min \cdot 0.23 = 5.38 \cdot 10^{-6}\ mol/min$$

Reaction rate:

$$r = \frac{q_{phenol,out}}{m_{cat}} = \frac{5.38 \cdot 10^{-6}\ mol/min}{0.4911\ g_{cat} \cdot 60\ s/min} = 1.83 \cdot 10^{-7} \frac{mol}{g_{cat} \cdot s}$$

The TOF based on total dispersion, TOF1:

$$TOF_1 = \frac{r \cdot M_{Mo}}{x_{Mo} \cdot D_1} = \frac{1.83 \cdot 10^{-7} \frac{mol}{g_{cat} \cdot s} \cdot 95.9 g/mol}{0.15 \cdot 0.065} = 1.80 \cdot 10^{-3}\ s^{-1}$$

The TOF based in differential dispersion, TOF2:

$$TOF_2 = \frac{r \cdot M_{Mo}}{x_{Mo} \cdot D_2} = \frac{1.83 \cdot 10^{-7} \frac{mol}{g_{cat} \cdot s} \cdot 95.9 g/mol}{0.15 \cdot 0.019} = 6.16 \cdot 10^{-3}\ s^{-1}$$

E.2.7 Calculation of activation energy

In this section, the activation energy of the 15 wt% MoP/TiO_2 catalyst is calculated. The activation energy is calculated from the Equation 2.19. The experimental reaction rate r is used instead of the rate constant k. The data used in the calculations are from the measurement with conversion around 350^{o}C, and the raw data are given in Table E.23 in Appendix E.4.5.

The following data are used to make the plot in Figure E.2.7 of lnR against $1/T$.

Figure E.1: *Calculation of the activation energy of the 15 wt% MoP/TiO_2 catalyst. The linear regression was done in Excel*

$\ln R$	$1/T$
-17.97	$1.66 \cdot 10^{-3}$
-17.67	$1.63 \cdot 10^{-3}$
-17.30	$1.61 \cdot 10^{-3}$
-16.96	$1.58 \cdot 10^{-3}$
-16.49	$1.56 \cdot 10^{-3}$
-17.65	$1.61 \cdot 10^{-3}$

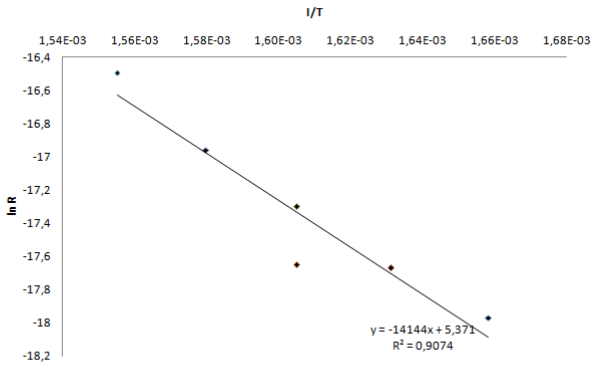

The slope in Figure E.2.7 was calculated by Excel to $m = -1.4 \cdot 10^{-4} K$. The activation energy is then determined to

$$E_A = -m \cdot R = -(-1.4 \cdot 10^{-4})\ K \cdot 8.314\ \frac{J}{K \cdot mol} = 1.16 \cdot 10^{-5}\ \frac{J}{mol}$$

.

E.2.8 Calculation of deactivation correction

In this section, the calculations of deactivation corrections for the measurements with varying pressure and H_2/oil ratio are given. The assumptions made are that the activity deactivation is linear with time on stream and that the first sample is not influenced by deactivation. As the conversion is low, another assumption made is that the conversion can be used in the calculations and not the reaction rate. A simple model for activity deactivation is

$$a = a_o \cdot d \rightarrow a_o = \frac{a}{d}$$

where d is the deactivation, a is the measured activity at time t and a_0 is the theoretical activity at time t without deactivation. By comparing a_0 for each sample, it is easier to analyse the influence of pressure or H_2/oil ratio.

The measurement with varying pressure is used as an example to calculate the deactivation correction. The 3 samples at 25 bar are used to make a linear regression between activity and time on stream. The data given are:

$$\begin{aligned}
t_{25bar,1} &= 1.23\ h \\
t_{25bar,2} &= 4.19\ h \\
t_{25bar,3} &= 6.53\ h \\
x_{25bar,1} &= 0.167 \\
x_{25bar,2} &= 0.110 \\
x_{25bar,3} &= 0.078 \\
x_{50bar} &= 0.146
\end{aligned}$$

Linear regression in Excel gives the following relation:

$$x = -0.0169t + 0.1857$$

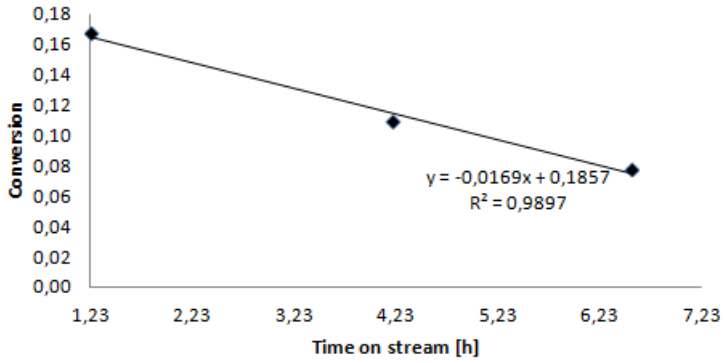

For the sample at 50 bar, which was analysed after 3.21 h, the calculated conversion is

$$x = -0.0169 \cdot 3.21 + 0.1857 = 0.131$$

The deactivation at this sample is calculated by comparison with the first sample.

$$D_{50bar} = \frac{x_{50bar}}{x_{25bar}} = \frac{0.131}{0.167} = 0.784$$

The theoretical conversion $x_{o,\ 50bar}$ without deactivation for the sample at 50 bar is

$$x_{o,\ 50bar} = \frac{x_{50bar}}{D_{50bar}} = \frac{0.146}{0.784} = 0.186$$

E.3 Original data from the off-line liquid GC

Figures E.2-E.8 show the original data from the off-line GC used to calculate the conversion, selectivity and turnover frequency for the 15 wt% MoP/ZrO_2 catalyst.

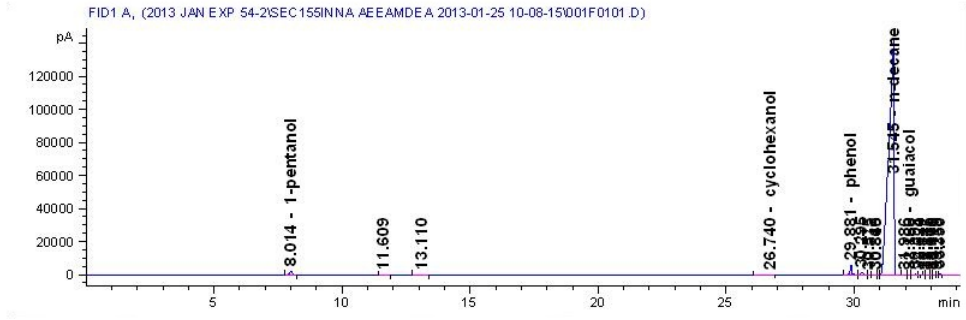

Figure E.2: *Data from the off-line GC for 15 wt% MoP/ZrO_2, feed sample, injection 1.*

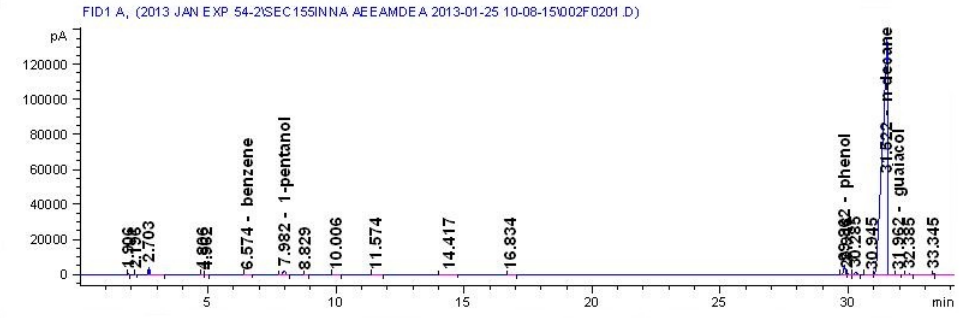

Figure E.3: *Data from the off-line GC for 15 wt% MoP/ZrO_2, 350^{o}C, 0.3 mL/min, injection 1.*

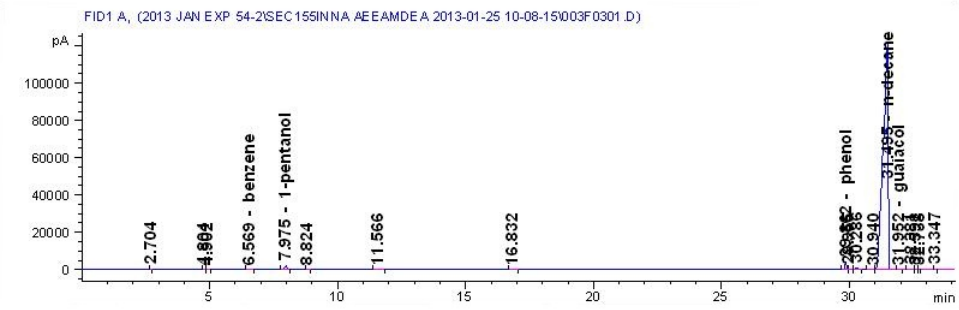

Figure E.4: *Data from the off-line GC for 15 wt% MoP/ZrO_2, 350^oC, 0.2 mL/min, injection 1.*

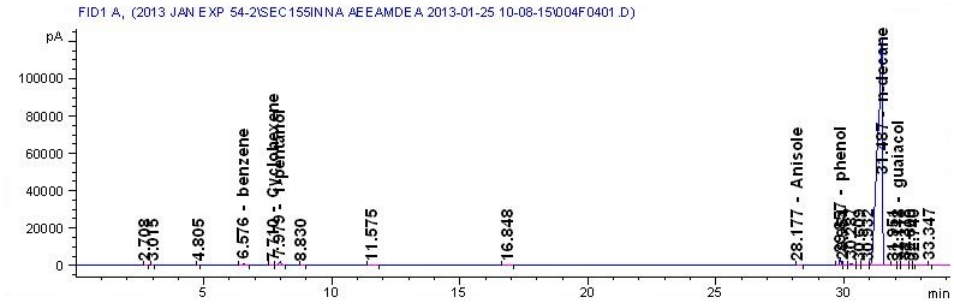

Figure E.5: *Data from the off-line GC for 15 wt% MoP/ZrO_2, 400^oC, 0.2 mL/min, injection 1.*

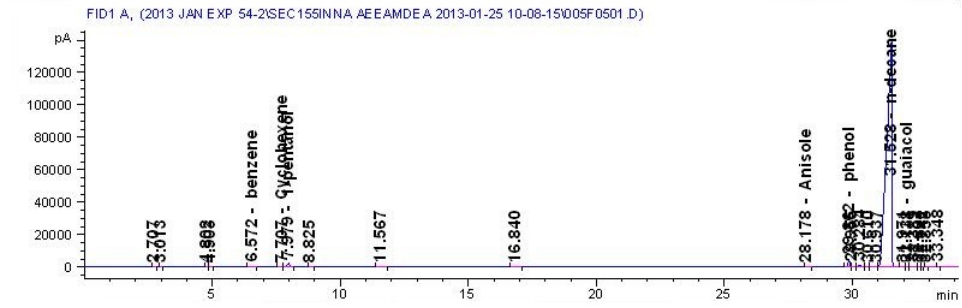

Figure E.6: *Data from the off-line GC for 15 wt% MoP/ZrO_2, 400^oC, 0.3 mL/min, injection 1.*

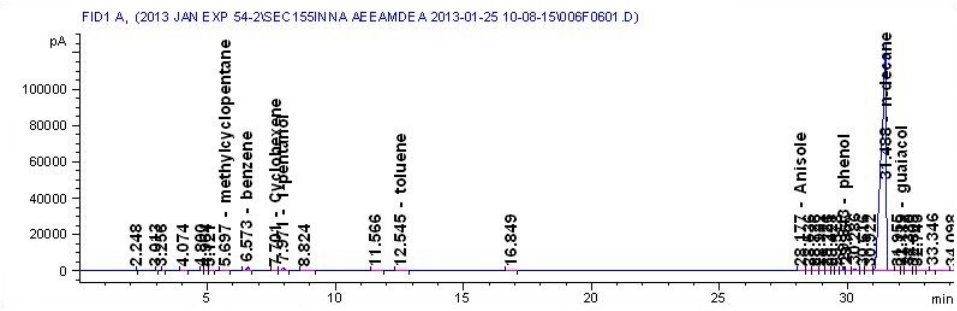

Figure E.7: *Data from the off-line GC for 15 wt% MoP/ZrO_2, 450^oC, 0.3 mL/min, injection 1.*

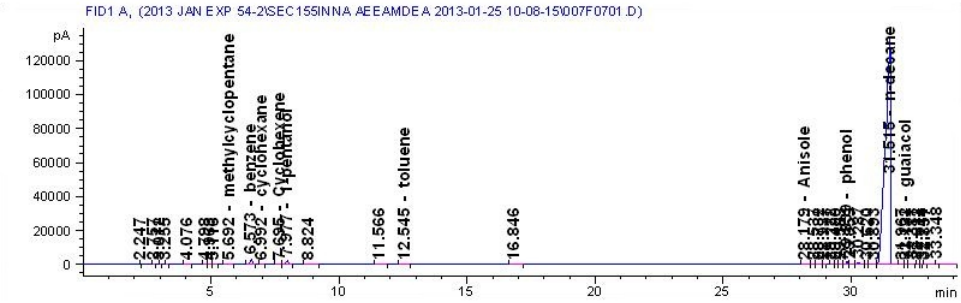

Figure E.8: *Data from the off-line GC for 15 wt% MoP/ZrO_2, 450^oC, 0.2 mL/min, injection 1.*

E.4 Additional results from the activity measurement

E.4.1 Additional results from different supports

MoP/Al_2O_3

Table E.3: *Results from the activity measurement of the MoP/Al_2O_3 catalyst. Temperature ranged between 350^oC and 450^oC, and flow rate between 0.2 and 0.3 mL/min. Pressure was set to 25 bar and H_2 flow to 100 mL/min. TOF is based on total dispersion.*

Temperature [C]	**Flow rate [mL/min]**	**Time on stream [h]**	**Conversion [%]**	**Carbon balance [%]**	**WHSV** $[g_{fenol}/g_{cat} \cdot h]$	**TOF** $[s^{-1}]$	**Reaction rate** $[mol/g_{cat} \cdot s]$
350	0.3	0.32	6.4	6.6	0.43	$1.05 \cdot 10^{-3}$	$8.28 \cdot 10^{-8}$
350	0.2	1.29	6.3	4.4	0.29	$6.83 \cdot 10^{-4}$	$5.40 \cdot 10^{-8}$
400	0.2	2.16	27.5	17.8	0.29	$2.99 \cdot 10^{-3}$	$2.36 \cdot 10^{-7}$
400	0.3	3.05	20.7	6.2	0.43	$3.37 \cdot 10^{-3}$	$2.67 \cdot 10^{-7}$
450	0.3	3.54	92.5	6.1	0.43	$1.51 \cdot 10^{-2}$	$1.19 \cdot 10^{-6}$
450	0.2	4.42	96.0	2.0	0.29	$1.04 \cdot 10^{-2}$	$8.24 \cdot 10^{-7}$

Table E.4: *Calculated selectivity to benzene, cyclohexane, cyclohexene and methylcyclopentane of the MoP/Al_2O_3 catalyst. Temperature ranged between 350^oC and 450^oC, and flow rate between 0.2 and 0.3 mL/min. Pressure was set to 25 bar and H_2 flow to 100 mL/min.*

		Selectivity to [%]			
Temperature [C]	**Flow rate [ml/min]**	**Benzene**	**Cyclohexane**	**Cyclohexene**	**Methylcyclopentane**
350	0.3	93.8	0	6.2	0
350	0.2	90.1	0	9.9	0
400	0.2	93.7	0	6.3	0
400	0.3	93.1	0	6.9	0
450	0.3	94.3	1.4	2.2	2.1
450	0.2	90.9	2.7	0.7	5.7

MoP/SiO_2

Table E.5: *Results from the activity measurement of the MoP/SiO_2 catalyst. Temperature ranged between 350^oC and 450^oC, and flow rate between 0.2 and 0.3 mL/min. Pressure was set to 25 bar and H_2 flow to 100 mL/min. TOF is based on total dispersion*

Temperature [C]	**Flow rate [mL/min]**	**Time on stream [h]**	**Conversion [%]**	**Carbon balance [%]**	**WHSV** $[g_{fenol}/g_{cat} \cdot h]$	**TOF** $[s^{-1}]$	**Reaction rate** $[mol/g_{cat} \cdot s]$
350	0.3	0.34	0.5	18.8	0.59	$7.34 \cdot 10^{-5}$	$9.16 \cdot 10^{-9}$
350	0.2	1.21	0.2	12.6	0.39	$1.64 \cdot 10^{-5}$	$2.05 \cdot 10^{-9}$
400	0.2	2.42	5.6	-10.4	0.39	$5.22 \cdot 10^{-4}$	$6.51 \cdot 10^{-8}$
400	0.3	3.15	2.9	7.9	0.59	$4.11 \cdot 10^{-4}$	$5.12 \cdot 10^{-8}$
450	0.3	4.16	20.8	3.3	0.59	$2.91 \cdot 10^{-3}$	$3.63 \cdot 10^{-7}$
450	0.2	5.04	24.7	3.8	0.39	$2.31 \cdot 10^{-3}$	$2.88 \cdot 10^{-7}$

Table E.6: *Calculated selectivity to benzene, cyclohexane, cyclohexene and methyl cyclopentane of the MoP/SiO_2 catalyst. Temperature ranged between 350^oC and 450^oC, and flow rate between 0.2 and 0.3 mL/min. Pressure was set to 25 bar and H_2 flow to 100 mL/min.*

		Selectivity to [%]			
Temperature [C]	**Flow rate [ml/min]**	**Benzene**	**Cyclohexane**	**Cyclohexene**	**Methyl cyclopentane**
350	0.3	100	0	0	0
350	0.2	100	0	0	0
400	0.2	100	0	0	0
400	0.3	100	0	0	0
450	0.3	100	0	0	0
450	0.2	99.4	0	0	0.6

MoP/TiO_2

Table E.7: *Results from the activity measurement of the MoP/TiO_2 catalyst. Temperature ranged between 350^oC and 450^oC, and flow rate between 0.2 and 0.3 mL/min. Pressure was set to 25 bar and H_2 flow to 100 mL/min. TOF is based on total dispersion,*

Temperature [C]	**Flow rate [mL/min]**	**Time on stream [h]**	**Conversion [%]**	**Carbon balance [%]**	**WHSV** $[g_{fenol}/g_{cat} \cdot h]$	**TOF** $[s^{-1}]$	**Reaction rate** $[mol/g_{cat} \cdot s]$
350	0.3	0.31	3.6	7.5	0.49	$6.94 \cdot 10^{-4}$	$5.31 \cdot 10^{-8}$
350	0.2	1.20	6.8	3.5	0.33	$8.63 \cdot 10^{-4}$	$6.60 \cdot 10^{-8}$
400	0.2	2.37	74.7	4.9	0.33	$9.53 \cdot 10^{-3}$	$7.28 \cdot 10^{-7}$
400	0.3	3.10	48.0	10.6	0.49	$9.18 \cdot 10^{-3}$	$7.02 \cdot 10^{-7}$
450	0.3	4.14	95.2	2.5	0.49	$1.82 \cdot 10^{-2}$	$1.39 \cdot 10^{-6}$
450	0.2	5.04	93.1	-6.0	0.33	$1.19 \cdot 10^{-2}$	$9.08 \cdot 10^{-7}$

Table E.8: *Calculated selectivity to benzene, cyclohexane, cyclohexene and methyl cyclopentane of the MoP/TiO_2 catalyst. Temperature ranged between 350^oC and 450^oC, and flow rate between 0.2 and 0.3 mL/min. Pressure was set to 25 bar and H_2 flow to 100 mL/min.*

		Selectivity to [%]			
Temperature [C]	**Flow rate [ml/min]**	**Benzene**	**Cyclohexane**	**Cyclohexene**	**Methyl cyclopentane**
350	0.3	100	0	0	0
350	0.2	89.2	0	10.8	0
400	0.2	91.4	3.0	4.3	1.3
400	0.3	93.2	1.6	5.2	0
450	0.3	90.5	2.9	0	6.6
450	0.2	88.8	3.5	0	7.6

MoP/ZrO_2

Table E.9: *Results from the activity measurement of the MoP/ZrO_2 catalyst. Temperature ranged between 350^oC and 450^oC, and flow rate between 0.2 and 0.3 mL/min. Pressure was set to 25 bar and H_2 flow to 100 mL/min. TOF is based on total dispersion.*

Temperature [C]	**Flow rate [mL/min]**	**Time on stream [h]**	**Conversion [%]**	**Carbon balance [%]**	**WHSV** $[g_{fenol}/g_{cat} \cdot h]$	**TOF** $[s^{-1}]$	**Reaction rate** $[mol/g_{cat} \cdot s]$
350	0.3	0.34	0.6	18.6	0.42	$6.19 \cdot 10^{-5}$	$6.86 \cdot 10^{-9}$
350	0.2	1.21	1.2	23.0	0.29	$8.83 \cdot 10^{-5}$	$9.80 \cdot 10^{-9}$
400	0.2	2.34	23.1	2.2	0.29	$1.80 \cdot 10^{-3}$	$1.83 \cdot 10^{-7}$
400	0.3	3.08	13.2	10.6	0.42	$1.48 \cdot 10^{-3}$	$1.64 \cdot 10^{-7}$
450	0.3	4.09	56.6	-0.2	0.42	$6.34 \cdot 10^{-3}$	$7.03 \cdot 10^{-7}$
450	0.2	4.58	69.7	-1.6	0.29	$5.20 \cdot 10^{-3}$	$5.77 \cdot 10^{-7}$

Table E.10: *Calculated selectivity to benzene, cyclohexane, cyclohexene and methyl cyclopentane of the MoP/TiO_2 catalyst. Temperature ranged between 350^oC and 450^oC, and flow rate between 0.2 and 0.3 mL/min. Pressure was set to 25 bar and H_2 flow to 100 mL/min.*

		Selectivity to [%]			
Temperature [C]	**Flow rate [ml/min]**	**Benzene**	**Cyclohexane**	**Cyclohexene**	**Methyl cyclopentane**
350	0.3	100	0	0	0
350	0.2	100	0	0	0
400	0.2	96.5	1.0	2.5	0
400	0.3	97.3	0	2.7	0
450	0.3	95.4	0.2	0.9	3.4
450	0.2	93.2	0.9	0.8	5.1

E.4.2 Additional results from deactivation measurement

Deactivation of MoP/TiO_2, 0.2 mL/min

Table E.11: *Results from the deactivation measurement of the MoP/TiO_2 catalyst at 0.2 mL/min, 350^oC, 100 mL/min H_2 and 25 bar. TOF is based on total dispersion*

Temperature [C]	**Flow rate [mL/min]**	**Time on stream [h]**	**Conversion [%]**	**Carbon balance [%]**	**WHSV** $[g_{fenol}/g_{cat} \cdot h]$	**TOF** $[s^{-1}]$	**Reaction rate** $[mol/g_{cat} \cdot s]$
350	0.3	0.32	11.4	6.0	0.56	$2.99 \cdot 10^{-3}$	$1.89 \cdot 10^{-7}$
350	0.2	1.29	9.4	5.5	0.37	$1.63 \cdot 10^{-3}$	$1.03 \cdot 10^{-7}$
350	0.2	2.16	7.1	-18.3	0.37	$1.23 \cdot 10^{-3}$	$7.78 \cdot 10^{-8}$
350	0.2	3.05	6.4	2.3	0.37	$1.11 \cdot 10^{-3}$	$7.01 \cdot 10^{-8}$
350	0.2	3.54	5.7	1.9	0.37	$9.94 \cdot 10^{-4}$	$6.28 \cdot 10^{-8}$
350	0.2	4.42	5.0	2.6	0.37	$8.71 \cdot 10^{-4}$	$5.50 \cdot 10^{-8}$

Table E.12: *Calculated selectivity to benzene, cyclohexane, cyclohexene and methyl cyclopentane in the deactivation measurement of the MoP/TiO_2 catalyst at 0.2 mL/min, 350^oC, 100 mL/min H_2 and 25 bar*

		Selectivity to [%]			
Temperature [C]	**Flow rate [ml/min]**	**Benzene**	**Cyclohexane**	**Cyclohexene**	**Methyl cyclopentane**
350	0.3	71.9	14.4	9.6	4.1
350	0.2	79.1	6.6	14.3	0
350	0.2	78.9	3.5	17.6	0
350	0.2	80.9	0.0	19.1	0
350	0.2	80.0	0	20.0	0
350	0.2	79.4	0	20.6	0

Deactivation of MoP/TiO_2, 0.3 mL/min

Table E.13: *Results from the deactivation measurement of the MoP/TiO_2 catalyst at 0.3 mL/min, 350^oC, 100 mL/min H_2 and 25 bar. TOF is based on total dispersion.*

Temperature [C]	**Flow rate [mL/min]**	**Time on stream [h]**	**Conversion [%]**	**Carbon balance [%]**	**WHSV** $[g_{fenol}/g_{cat} \cdot h]$	**TOF 1** $[s^{-1}]$	**Reaction rate** $[mol/g_{cat} \cdot s]$
350	0.3	0.29	1.5	3.2	0.43	$3.03 \cdot 10^{-4}$	$1.91 \cdot 10^{-8}$
350	0.3	0.59	1.0	-1.1	0.43	$2.04 \cdot 10^{-4}$	$1.29 \cdot 10^{-8}$
350	0.3	1.31	0.8	4.0	0.43	$1.58 \cdot 10^{-4}$	$9.96 \cdot 10^{-9}$
350	0.3	2.00	0.7	10.1	0.43	$1.33 \cdot 10^{-4}$	$8.42 \cdot 10^{-9}$
350	0.3	2.30	0.5	1.6	0.43	$9.76 \cdot 10^{-5}$	$6.16 \cdot 10^{-9}$
350	0.3	3.00	0.4	0.8	0.43	$8.87 \cdot 10^{-5}$	$5.60 \cdot 10^{-9}$
350	0.3	3.35	0.4	-13.5	0.43	$8.22 \cdot 10^{-5}$	$5.19 \cdot 10^{-9}$

Table E.14: *Calculated selectivity to benzene, cyclohexane, cyclohexene and methyl cyclopentane in the deactivation measurement of the MoP/TiO_2 catalyst at 0.3 mL/min, 350^oC, 100 mL/min H_2 and 25 bar*

		Selectivity to [%]			
Temperature [C]	**Flow rate [ml/min]**	**Benzene**	**Cyclohexane**	**Cyclohexene**	**Methyl cyclopentane**
350	0.3	100	0	0	0
350	0.3	100	0	0	0
350	0.3	100	0	0	0
350	0.3	100	0	0	0
350	0.3	100	0	0	0
350	0.3	100	0	0	0
350	0.3	100	0	0	0

E.4.3 Additional results with different H_2/oil ratio

Effect of H_2 flow with 0.3 mL/min

Table E.15: *Results from the measurement of the MoP/TiO_2 catalyst with varying H_2-flow, 370^{o}C, 0.3 mL/min feed and 25 bar. TOF is based on total dispersion.*

Temperature [C]	**Flow rate [mL/min]**	**Time on stream [h]**	**H_2/Oil ratio** $[Nm^3/m^3]$	**Conversion [%]**	**Carbon balance [%]**	**WHSV** $[g_{fenol}/g_{cat} \cdot h]$	**TOF 1** $[s^{-1}]$	**Reaction rate** $[mol/g_{cat} \cdot s]$
370	0.3	0.31	333	6.0	-3.6	0.46	$1.31 \cdot 10^{-3}$	$8.25 \cdot 10^{-8}$
370	0.3	1.07	300	5.0	-3.6	0.46	$1.09 \cdot 10^{-3}$	$6.89 \cdot 10^{-8}$
370	0.3	1.46	266	3.7	0.3	0.46	$7.99 \cdot 10^{-4}$	$5.05 \cdot 10^{-8}$
370	0.3	2.28	233	3.3	-3.8	0.46	$7.12 \cdot 10^{-4}$	$4.49 \cdot 10^{-8}$
370	0.3	3.10	200	2.9	-6.0	0.46	$6.35 \cdot 10^{-4}$	$4.01 \cdot 10^{-8}$
370	0.3	3.50	166	2.6	-6.4	0.46	$5.73 \cdot 10^{-4}$	$3.62 \cdot 10^{-8}$

Table E.16: *Calculated selectivity to benzene, cyclohexane, cyclohexene and methyl cyclopentane in measurement with varying H_2 flow for the MoP/TiO_2 catalyst, 370^{o}C, 0.3 mL/min feed and 25 bar*

			Selectivity to [%]			
Temperature [C]	**Flow rate [ml/min]**	**H_2/Oil ratio** $[Nm^3/m^3]$	**Benzene**	**Cyclohexane**	**Cyclohexene**	**Methyl cyclopentane**
370	0.3	333	97.5	0	2.5	0
370	0.3	300	93.4	0	6.6	0
370	0.3	266	100	0	0	0
370	0.3	233	100	0	0	0
370	0.3	200	100	0	0	0
370	0.3	166	100	0	0	0

Effect of H_2 flow with 0.2 mL/min

Table E.17: *Results from the measurement of the MoP/TiO_2 catalyst with varying H_2-flow, 370^{o}C, 0.2 mL/min feed and 25 bar. TOF is based on total dispersion.*

Temperature [C]	**Flow rate [mL/min]**	**Time on stream [h]**	**H_2/Oil ratio** $[Nm^3/m^3]$	**Conversion [%]**	**Carbon balance [%]**	**WHSV** $[g_{fenol}/g_{cat} \cdot h]$	**TOF 1** $[s^{-1}]$	**Reaction rate** $[mol/g_{cat} \cdot s]$
370	0.2	0.49	500	9.6	-3.2	0.46	$1.39 \cdot 10^{-2}$	$8.75 \cdot 10^{-7}$
370	0.2	1.51	300	6.3	-3.7	0.46	$9.07 \cdot 10^{-3}$	$5.73 \cdot 10^{-7}$
370	0.2	2.47	500	6.1	-0.1	0.46	$8.90 \cdot 10^{-3}$	$5.62 \cdot 10^{-7}$
370	0.2	3.32	200	4.5	-2.8	0.46	$6.51 \cdot 10^{-3}$	$4.11 \cdot 10^{-7}$
370	0.2	4.01	500	4.7	-1.1	0.46	$6.84 \cdot 10^{-3}$	$4.32 \cdot 10^{-7}$
370	0.2	4.55	350	4.3	15.7	0.46	$6.23 \cdot 10^{-3}$	$3.94 \cdot 10^{-7}$

Table E.18: *Calculated selectivity to benzene, cyclohexane, cyclohexene and methyl cyclopentane in measurement with varying H_2 flow for the MoP/TiO_2 catalyst, 370^{o}C, 0.2 mL/min feed and 25 bar*

			Selectivity to [%]			
Temperature [C]	**Flow rate [ml/min]**	**H_2/Oil ratio** $[Nm^3/m^3]$	**Benzene**	**Cyclohexane**	**Cyclohexene**	**Methyl cyclopentane**
370	0.2	500	93.7	0	6.3	0
370	0.2	300	98.3	0	1.7	0
370	0.2	500	92.1	0	7.9	0
370	0.2	200	100	0	0	0
370	0.2	500	100	0	0	0
370	0.2	350	100	0	0	0

E.4.4 Additional results with different pressure

Table E.19: *Results from the measurement of the MoP/Al_2O_3 catalyst with pressure varying from 10-50 bar, 370^oC, 0.2 mL/min feed and 100 mL/min H_2 flow. TOF is based on total dispersion.*

Temperature [C]	**Flow rate [mL/min]**	**Time on stream [h]**	**Pressure [bar]**	**Conversion [%]**	**Carbon balance [%]**	**WHSV** $[g_{fenol}/g_{cat} \cdot h]$	**TOF 1** $[s^{-1}]$	**Reaction rate** $[mol/g_{cat} \cdot s]$
370	0.2	1.23	25	16.7	4.6	0.35	$2.19 \cdot 10^{-3}$	$1.73 \cdot 10^{-7}$
370	0.2	2.16	35	13.3	0.7	0.35	$1.74 \cdot 10^{-3}$	$1.37 \cdot 10^{-7}$
370	0.2	3.21	50	14.6	3.7	0.35	$1.92 \cdot 10^{-3}$	$1.52 \cdot 10^{-7}$
370	0.2	4.19	25	11.0	1.8	0.35	$1.44 \cdot 10^{-3}$	$1.14 \cdot 10^{-7}$
370	0.2	5.07	10	11.8	1.1	0.35	$1.55 \cdot 10^{-3}$	$1.22 \cdot 10^{-7}$
370	0.2	6.53	25	7.8	2.2	0.35	$1.03 \cdot 10^{-3}$	$8.11 \cdot 10^{-8}$

Table E.20: *Calculated selectivity to benzene, cyclohexane, cyclohexene and methyl cyclopentane in measurement with varying pressure for the MoP/Al_2O_3 catalyst, 370^oC, 0.2 mL/min feed and 100 mL/min H_2 flow*

			Selectivity to [%]			
Temperature [C]	**Flow rate [ml/min]**	**Pressure [bar]**	**Benzene**	**Cyclohexane**	**Cyclohexene**	**Methyl cyclopentane**
370	0.2	25	93.0	0	7.0	0
370	0.2	35	90.8	0	9.2	0
370	0.2	50	88.7	0	11.3	0
370	0.2	25	90.3	0	9.7	0
370	0.2	10	93.6	0	6.4	0
370	0.2	25	88.4	0	11.6	0

E.4.5 Additional results with conversion at 350^oC

Conversion at 350C, for MoP/TiO_2

Table E.21: *Results from the measurement with conversion of the MoP/TiO_2 catalyst at 350^oC, 100 mL/min H_2 and 25 bar. TOF is based on total dispersion.*

Temperature [C]	**Flow rate [mL/min]**	**Time on stream [h]**	**Conversion [%]**	**Carbon balance [%]**	**WHSV** $[g_{fenol}/g_{cat} \cdot h]$	**TOF 1** $[s^{-1}]$	**Reaction rate** $[mol/g_{cat} \cdot s]$
330	0.2	0.48	1.7	6.1	0.31	$2.48 \cdot 10^{-4}$	$1.57 \cdot 10^{-8}$
340	0.25	1.49	1.8	8.1	0.39	$3.35 \cdot 10^{-4}$	$2.11 \cdot 10^{-8}$
350	0.3	2.36	2.2	13.3	0.47	$4.84 \cdot 10^{-4}$	$3.06 \cdot 10^{-8}$
360	0.35	3.11	2.7	7.6	0.54	$6.83 \cdot 10^{-4}$	$4.31 \cdot 10^{-8}$
370	0.4	3.39	3.7	6.6	0.62	$1.09 \cdot 10^{-3}$	$6.86 \cdot 10^{-8}$
350	0.3	4.34	1.6	4.4	0.47	$3.41 \cdot 10^{-4}$	$2.15 \cdot 10^{-8}$

Table E.22: *Calculated selectivity to benzene, cyclohexane, cyclohexene and methyl cyclopentane in measurement conversion at 350^oC for the MoP/TiO_2 catalyst 100 mL/min H_2 and 25 bar*

		Selectivity to [%]			
Temperature [C]	**Flow rate [ml/min]**	**Benzene**	**Cyclohexane**	**Cyclohexene**	**Methyl cyclopentane**
330	0.2	100	0	0	0
340	0.25	100	0	0	0
350	0.3	100	0	0	0
360	0.35	100	0	0	0
370	0.4	100	0	0	0
350	0.3	100	0	0	0

Conversion at 350C for MoP/Al_2O_3

Table E.23: *Results from the measurement with conversion of the MoP/Al_2O_3 catalyst at 350^oC, 100 mL/min H_2 and 25 bar. TOF is based on total dispersion.*

Temperature [C]	**Flow rate [mL/min]**	**Time on stream [h]**	**Conversion [%]**	**Carbon balance [%]**	**WHSV** $[g_{fenol}/g_{cat} \cdot h]$	**TOF 1** $[s^{-1}]$	**Reaction rate** $[mol/g_{cat} \cdot s]$
330	0.2	0.49	5.2	1.6	0.38	$7.49 \cdot 10^{-4}$	$5.92 \cdot 10^{-8}$
340	0.25	1.51	7.1	-0.1	0.48	$1.27 \cdot 10^{-3}$	$1.01 \cdot 10^{-7}$
350	0.3	2.47	9.0	-18.4	0.57	$1.93 \cdot 10^{-3}$	$1.52 \cdot 10^{-7}$
360	0.35	3.32	15.0	1.3	0.67	$3.78 \cdot 10^{-3}$	$2.99 \cdot 10^{-7}$
370	0.4	4.01	15.7	1.3	0.76	$4.49 \cdot 10^{-3}$	$3.55 \cdot 10^{-7}$
350	0.3	4.55	9.1	-1.1	0.57	$1.95 \cdot 10^{-3}$	$1.54 \cdot 10^{-8}$

Table E.24: *Calculated selectivity to benzene, cyclohexane, cyclohexene and methyl cyclopentane in measurement conversion at 350^oC for the MoP/Al_2O_3 catalyst 100 mL/min H_2 and 25 bar*

		Selectivity to [%]			
Temperature [C]	**Flow rate [ml/min]**	**Benzene**	**Cyclohexane**	**Cyclohexene**	**Methyl cyclopentane**
330	0.2	96.5	0	3.5	0
340	0.25	92.3	0	7.7	0
350	0.3	92.9	0	7.1	0
360	0.35	94.1	0	5.9	0
370	0.4	94.4	0	5.6	0
350	0.3	93.5	0	6.5	0

Conversion at 370C for MoP/Al_2O_3

Table E.25: *Results from the measurement with conversion of the MoP/Al_2O_3 catalyst at 370^oC, 100 mL/min H_2 and 25 bar. TOF is based on total dispersion.*

Temperature [C]	**Flow rate [mL/min]**	**Time on stream [h]**	**Conversion [%]**	**Carbon balance [%]**	**WHSV** $[g_{fenol}/g_{cat} \cdot h]$	**TOF 1** $[s^{-1}]$	**Reaction rate** $[mol/g_{cat} \cdot s]$
350	0.2	0.49	4.3	7.5	0.38	$6.08 \cdot 10^{-4}$	$4.81 \cdot 10^{-8}$
360	0.25	1.45	4.5	9.9	0.47	$8.04 \cdot 10^{-4}$	$6.35 \cdot 10^{-8}$
370	0.3	2.32	5.6	20.2	0.57	$1.20 \cdot 10^{-3}$	$9.45 \cdot 10^{-8}$
380	0.35	3.10	8.6	8.3	0.66	$2.13 \cdot 10^{-3}$	$1.68 \cdot 10^{-7}$
390	0.4	3.39	14.5	8.6	0.76	$4.11 \cdot 10^{-3}$	$3.25 \cdot 10^{-7}$
370	0.3	4.34	6.9	16.0	0.57	$1.47 \cdot 10^{-3}$	$1.17 \cdot 10^{-7}$

Table E.26: *Calculated selectivity to benzene, cyclohexane, cyclohexene and methyl cyclopentane in measurement conversion at 370^oC for the MoP/Al_2O_3 catalyst 100 mL/min H_2 and 25 bar*

		Selectivity to [%]			
Temperature [C]	**Flow rate [ml/min]**	**Benzene**	**Cyclohexane**	**Cyclohexene**	**Methyl cyclopentane**
350	0.2	88.4	0	11.6	0
360	0.25	87.2	0	12.8	0
370	0.3	90.1	0	9.9	0
380	0.35	91.8	0	8.2	0
390	0.4	93.0	0	7.0	0
370	0.3	90.1	0	9.9	0

E.4.6 Additional results from the repeatability measurement

Table E.27: *Additional results from the repeatability measurement with the MoP/TiO_2 catalyst made during spring 2013. The temperature varied between 350^oC-450^oC, flow rate was set to 0.2 and 0.3 mL/min, pressure was 25 bar and the H_2 flow rate was 100 mL/min. TOF is based on total dispersion.*

Temperature [C]	**Flow rate [mL/min]**	**Time on stream [h]**	**Conversion [%]**	**Carbon balance [%]**	**WHSV** $[g_{fenol}/g_{cat} \cdot h]$	**TOF 1** $[s^{-1}]$	**Reaction rate** $[mol/g_{cat} \cdot s]$
350	0.3	0.29	3.0	1.4	0.42	$6.05 \cdot 10^{-4}$	$3.82 \cdot 10^{-8}$
350	0.2	1.19	3.4	1.3	0.28	$4.49 \cdot 10^{-4}$	$2.84 \cdot 10^{-8}$
400	0.2	2.36	19.2	-5.7	0.28	$2.54 \cdot 10^{-3}$	$1.60 \cdot 10^{-7}$
400	0.3	2.57	12.6	-4.1	0.42	$2.49 \cdot 10^{-3}$	$1.57 \cdot 10^{-7}$
450	0.3	3.56	55.6	-1.7	0.42	$1.10 \cdot 10^{-2}$	$6.96 \cdot 10^{-7}$
450	0.2	4.46	66.2	-4.9	0.28	$8.75 \cdot 10^{-3}$	$5.53 \cdot 10^{-7}$

Table E.28: *Calculated selectivity to benzene, cyclohexane, cyclohexene and methyl cyclopentane in the repeatability measurement with the MoP/Al_2O_3 catalyst made during spring 2013, 350^oC-450^oC, 0.2-0.3 mL/min feed, 100 mL/min H_2 flow and 25 bar*

		Selectivity to [%]			
Temperature [C]	**Flow rate [ml/min]**	**Benzene**	**Cyclohexane**	**Cyclohexene**	**Methyl cyclopentane**
350	0.3	80.0	0	20.0	0
350	0.2	81.3	0	18.7	0
400	0.2	95.4	0	4.6	0
400	0.3	95.1	0	4.9	0
450	0.3	99.0	0	1.0	0
450	0.2	98.1	0	0.6	1.2

E.5 GC-calibration

Table E.29 and Table E.30 show the calibration tables for the liquid GC and gas GC, respectively, used in the activity measurement. The calibration was done by post doc. Sara Boullosa Eiras.

Table E.29: *Calibration table for liquid GC*

Nr.	**Retention time**	**Signal**	**Compund**
1	4.677	FID1 A	n-hexane
2	5.690	FID1 A	methylcyclopentane
3	6.570	FID1 A	benzene
4	6.900	FID1 A	cyclohexane
5	7,700	FID1 A	cyclohexene
6	7.950	FID1 A	1-pentanol
7	12.454	FID1 A	toluene
8	24.307	FID1 A	hexanol
9	25.900	FID1 A	cyclohexanone
10	26.673	FID1 A	cyclohexanol
11	27.969	FID1 A	anisole
12	29.800	FID1 A	phenol
13	31.480	FID1 A	n-decane
14	32.089	FID1 A	guaiacol

Table E.30: *Calibration table for gas GC*

Nr.	**Retention time**	**Signal**	**Compund**
1	2.012	TCD2 B	H_2
2	3.040	FID1 A	methane
3	3.543	FID1 A	ethane
4	4.809	FID1 A	ethylene
5	5.961	TCD2 B	N_2
6	6.200	TCD2 B	O_2
7	6.458	TCD2 B	propane
8	7.609	TCD2 B	CO
9	9.132	FID1 A	i-butane
10	9.590	FID1 A	propene
11	9.952	FID1 A	n-butane
12	11.339	FID1 A	i-butene
13	11.681	FID1 A	n-pentane
14	12.779	FID1 A	trans-2-butene
15	13.099	FID1 A	1-butene
16	13.514	FID1 A	3-methyl-1-butanol
17	13.520	FID1 A	n-hexane
18	13.758	TCD2 B	CO_2
19	15.002	FID1 A	i-pentane
20	15.300	FID1 A	cis-2-butene
21	16.093	FID1 A	i-pentene

F Risk assessment

NTNU HMS	Hazardous activity identification process	Risikovurdering	Nummer	Dato
		HMS-avd.	HMSRV2601	
		Godkjent av	Side	Erstatter

Unit: *Kjemisk prosessteknologi* **Date:** 09.01.2013

Line manager: *Øyvind Gregersen*

Participants in the identification process (including their function): Sindre Asphaug, student

Short description of the main activity/main process: Preparation and characterization of catalyst

ID no.	Activity/process	Responsible person	Laws, regulations etc.	Existing documentation	Existing safety measures	Comment
1	Crushing and sieving of support pellets	Sindre Asphaug	Working environment act	HSE data sheet	Protective equipment, fume hoods	
2	Calcination at 500C	Sindre Asphaug	Working environment act	User's intruction book	Protective equipment, fume hoods	
3	Handling of molybdenum and phosphor precursor	Sindre Asphaug	Working environment act	HSE data sheet	Protective equipment, fume hoods	Includes diluting of precursor and incipient wetness impregnation
4	TPR	Sindre Asphaug	Working environment act	User's intruction book	Protective equipment, gas detector	
5	BET	Sindre Asphaug	Working environment act	User's intruction book	Protective equipment	
6						
7	Catalyst reduction with hydrogen and passivation with oxygen in argon	Sindre Asphaug	Working environment act	User's intruction book	Protective equipment, fume hoods, gas detectors	
8	TGA	Sindre Asphaug	Working environment act	User's intruction book	Protective equipment, gas detector	
9	XRD	Sindre Asphaug	Working environment act	User's intruction book	Protective equipment	
10	Chemisorption	Sindre Asphaug	Working environment act	User's intruction book	Protective equipment, gas detector	
11						
12						
13						
14						
15						
16						
17						
18						

NTNU HMS /KS	Risk assessment	Utarbeidet av	Nummer	Dato
		HMS-avd.	HMSRV2603	04.02.2011
		Godkjent av	Side	Erstatter

Unit: *Kjemisk prosessteknologi* **Date:** 09.01.2013

Line manager: *Øyvind Gregersen*

Participants in the identification process (including their function): *Sindre Asphaug, student*

Signatures:

ID no.	Activity from the identification process form	Potential undesirable incident/strain	Likelihood:	Consequence:				Risk value	Comments/status Suggested measures
			Likelihood (1-5)	Human (A-E)	Environment (A-E)	Economy/ material (A-E)	Reputation (A-E)	Human	
1	Crushing and sieving of support pellets	Inhalation of support particles	1	A					Use protective equipment, fume hood and particle mask
2	Calcination at 500C	Heat treatment, possible leakage of ammonium	1	A					Use protective equipment, fume hood
3	Handling of molybdenum and phosphor precursor	Inhalation and spill of chemicals	2	B					Use protective equipment, fume hood
4	TPR	Heat treatment, gas leakage, frost injury from dry ice	3	C					Use protective equipment, gas detector
5	BET	Frost injury from liquid nitrogen, heat treatment of degassed samples	3	A					Use protective equipment
6									
7	Catalyst reduction with hydrogen and passivation with oxygen in argon	Heat treatment, fire, gas leakage	3	A					Use protective equipment, fume hood, gas detector, fire alarm
8	TGA	Gas leakage, heat treatment	2	A					Use protective equipment, gas detector
9	XRD	Spill of chemicals	1	A					Use protective equipment
10	Chemisorption	Gas leakage, heat treatment	2	B					Use protective equipment, gas detector
11									
12									
13									
14									
15									
16									
17									
18									

NTNU HMS	Hazardous activity identification process	Risikovurdering	Nummer	Dato
		HMS-avd.	HMSRV2601	
		Godkjent av	Side	Erstatter

Unit: *Kjemisk prosessteknologi* **Date:** 09.01.2013

Line manager: *Øyvind Gregersen*

Participants in the identification process (including their function): Sindre Asphaug, student

Short description of the main activity/main process: Activity testing of catalyst

ID no.	Activity/process	Responsible person	Laws, regulations etc.	Existing documentation	Existing safety measures	Comment
1	Preparation of reactor	Sindre Asphaug	Working environment act	HSE datasheet	Protective equipment, fume hoods, particle mask	
2	Diluting phenol in decane	Sindre Asphaug	Working environment act	HSE datasheet	Protective equipment, fume hoods, particle mask	Phenol is highly carciogenic
3	Activation of catalyst	Sindre Asphaug	Working environment act	User's instruction book	Gas detectors, protective equipment, protective mask	Warm equipment
4	Take out samples from reactor	Sindre Asphaug	Working environment act	User's instruction book	Protective equipment	
5	Preparation of GC samples	Sindre Asphaug	Working environment act	HSE datasheet	Protective equipment, fume hoods	
6	Cleaning the reactor	Sindre Asphaug	Working environment act	HSE datasheet	Protective equipment, fume hoods	
7						
8						
9						
10						
11						
12						
13						
14						
15						
16						
17						
18						

NTNU HMS /KS	Risk assessment	Utarbeidet av	Nummer	Dato
		HMS-avd.	HMSRV2603	04.02.2011
		Godkjent av	Side	Erstatter

Unit: *Kjemisk prosessteknologi* **Date:** 09.01.2013
Line manager: *Øyvind Gregersen*
Participants in the identification process (including their function): *Sindre Asphaug, student*

Signatures:

ID no.	Activity from the identification process form	Potential undesirable incident/strain	Likelihood:	Consequence:				Risk value	Comments/status Suggested measures
			Likelihood (1-5)	Human (A-E)	Environment (A-E)	Economy/ material (A-E)	Reputation (A-E)	Human	
1	Preparation of reactor	Spill of chemicals, inhalation of quartz wool	2	B					Use protective equipment, particle mask, fume hoods
2	Diluting phenol in decane	Spill of chemicals, inhalation decane and phenol,	3	C					Use protective equipment, particle mask, fume hoods. Wash equipment with ethanol
3	Activation of catalyst	Gas leakage, spill of chemicals	1	A					Test for gas leakage
4	Take out samples from reactor	Spill of chemicals	1	A					Use protective equipment, fasten the bottle when collecting sample to avoid spill
5	Preparation of GC samples	Spill of chemicals, inhalation of organic liquids	3	B					Use protective equipment, fume hoods. Waste in special bottle for organic waste
6	Cleaning the reactor	Spill of chemicals	2	A					Use protective equipment, waste in specal waste basket
7									
8									
9									
10									
11									
12									
13									
14									
15									
16									
17									
18									

Potential undesirable incident/strain

Identify possible incidents and conditions that may lead to situations that pose a hazard to people, the environment and any materiel/equipment involved.

Criteria for the assessment of likelihood and consequence in relation to fieldwork

Each activity is assessed according to a worst-case scenario. Likelihood and consequence are to be assessed separately for each potential undesirable incident.
Before starting on the quantification, the participants should agree what they understand by the assessment criteria:

Likelihood

Minimal 1	Low 2	Medium 3	High 4	Very high 5
Once every 50 years or less	Once every 10 years or less	Once a year or less	Once a month or less	Once a week

Consequence

Grading	Human	Environment	Financial/material
E Very critical	May produce fatality/ies	Very prolonged, non-reversible damage	Shutdown of work >1 year.
D Critical	Permanent injury, may produce serious serious health damage/sickness	Prolonged damage. Long recovery time.	Shutdown of work 0.5–1 year.
C Dangerous	Serious personal injury	Minor damage. Long recovery time	Shutdown of work < 1 month
B Relatively safe	Injury that requires medical treatment	Minor damage. Short recovery time	Shutdown of work < 1 week
A Safe	Injury that requires first aid	Insignificant damage. Short recovery time	Shutdown of work < 1 day

The unit makes its own decision as to whether opting to fill in or not consequences for economy/materiel, for example if the unit is going to use particularly valuable equipment.

It is up to the individual unit to choose the assessment criteria for this column.

Risk = Likelihood x Consequence

Please calculate the risk value for "Human", "Environment" and, if chosen, "Economy/materiel", separately.

About the column "Comments/status, suggested preventative and corrective measures": Measures can impact on both likelihood and concequences. Prioritise measures

that can prevent the incident from occurring; in other words, likelihood-reducing measures are to be prioritised above greater emergency preparedness,

i.e. voncequence-reducing measures.